NASA CR-2276

NASA CONTRACTOR REPORT

NASA CR-2276

STOL RIDE CONTROL FEASIBILITY STUDY

Technical Report

by C. K. Gordon and R. O. Dodson

Prepared by
THE BOEING COMPANY
Wichita, Kansas 67210
for Langley Research Center

NATIONAL AERONAUTICS AND SPACE ADMINISTRATION • WASHINGTON, D. C. • JULY 1973

1. Report No.	2. Government Accession No.	3. Recipient's Catalog No.
NASA CR - 2276		

4. Title and Subtitle	5. Report Date
STOL RIDE CONTROL FEASIBILITY STUDY - TECHNICAL REPORT	July 1973
	6. Performing Organization Code

7. Author(s)	8. Performing Organization Report No.
C. K. Gordon and R. O. Dodson	D3-9052-1
	10. Work Unit No.
	741-86-99-01

9. Performing Organization Name and Address	11. Contract or Grant No.
The Boeing Company Wichita Division Wichita, KS 67210	NAS1-11683

12. Sponsoring Agency Name and Address	13. Type of Report and Period Covered
National Aeronautics and Space Administration Washington, D.C. 20546	Contractor report
	14. Sponsoring Agency Code

15. Supplementary Notes

16. Abstract

The feasibility of developing a ride-smoothing control system for a 20-passenger turboprop STOL transport was assessed. Five different ride-control system configurations with varying degrees of complexity, performance, and cost were investigated. Results indicate that a satisfactory ride-control system can be practically implemented on the aircraft with minimum flight performance degradation.

17. Key Words (Suggested by Author(s))	18. Distribution Statement
STOL Ride smoothing Ride quality Active controls	Unclassified - unlimited

19. Security Classif. (of this report)	20. Security Classif. (of this page)	21. No. of Pages	22. Price*
Unclassified	Unclassified	103	$3.00

*For sale by the National Technical Information Service, Springfield, Virginia 22151

TABLE OF CONTENTS

TABLE OF CONTENTS (CONT'D.)

LIST OF FIGURES

LIST OF FIGURES (CONT'D.)

LIST OF TABLES

STOL RIDE CONTROL FEASIBILITY STUDY

TECHNICAL REPORT

By C. K. GORDON and R. O. DODSON
THE BOEING COMPANY, WICHITA DIVISION

SUMMARY

Development of ride-smoothing systems is an important part of advancing STOL transport technology. A study of the feasibility of developing and certificating a ride-smoothing system for a passenger STOL aircraft has been performed by Boeing-Wichita, with de Havilland Aircraft of Canada, Limited, as the principal subcontractor. The de Havilland DHC-6 Twin Otter was selected for the feasibility study as it is the only STOL vehicle presently certificated and in use by a number of air carriers in this country.

Five different ride control system configurations with varying degrees of complexity, performance and cost were investigated. The total system provides symmetrical aileron, elevator, rudder and spoiler ride control surfaces, with accelerometers and rate gyros for motion sensors. The lesser systems eliminate the spoiler, rudder and elevator surfaces respectively. An alternate total system was synthesized utilizing a boom-mounted angle-of-attack sensor instead of an accelerometer.

The feasibility study has indicated that an acceptable ride control system can be practically implemented on a DHC-6 Twin Otter with minimum airplane performance degradation. Vertical and lateral accelerations can be significantly reduced using split aileron and split rudder control surfaces. A split elevator may be required to provide adequate handling qualities. Further, spoiler control surfaces must be added if significant acceleration reductions are desired during landing approach.

1.0 INTRODUCTION

1.1 Objective

The overall objective is the advancement of the technology of STOL aircraft ride-smoothing systems. Such systems will probably be required for passenger acceptance of any low- to moderate-wing-loading STOL vehicle due to its operational environment and flight dynamic characteristics. The immediate objective is examination of the feasibility of developing and certificating a ride-smoothing control system for a STOL aircraft currently in airline use. The de Havilland DHC-6 Twin Otter was selected for the feasibility study as it is the only STOL vehicle presently certificated and in use by a number of air carriers in this country.

1.2 Background

Concern over the unwanted response of aircraft to atmospheric turbulence dates back to the initial NACA reports by Hunsaker and Wilson in 1915.[1] Indepth research regarding the use of active control systems for ride smoothing did not begin until the late 1940's and early 1950's when the United States commercial airline fleet started expanding rapidly. The work at Langley Aeronautical Laboratory, NACA, by Phillips and Kraft[2] exemplifies this research. The introduction of the jet transport, with its higher wing loading and cruise altitude, led to an improved ride without an active ride control system and thus greatly reduced the immediate need for ride smoothing research. However, recent and proposed extensive future use by feeder airlines of STOL aircraft, which fly low, and with low to moderate wing loading, has resulted in a ride environment inferior to conventional aircraft, and has thus renewed interest in ride smoothing efforts. Development of a ride smoothing system is therefore an important step in the accomplishment of NASA's goal of advancing STOL transport technology.

1.3 Feasibility Study

A five month feasibility and planning study was conducted by the Wichita Division of The Boeing Company under NASA Langley Research Contract NAS1-11683 during the second half of CY-1972. The de Havilland Aircraft of Canada, Limited, assisted as the principal subcontractor. Results of the study are contained in this report.

Synthesis and preliminary design were accomplished to modify the existing DHC-6 Twin Otter flight control system by incorporating a control system for ride improvement in the vertical and lateral axes.

Several system configurations were designed to provide trade studies of ride quality, airplane handling, and complexity. Initially turbulence response in all six motion degrees of freedom were examined and compared with tentative criteria proposed as goals for the ride-smoothing system performance. Only vertical and lateral aircraft motions were found to need ride smoothing to meet these tentative criteria.

1.4 De Havilland DHC-6 Twin Otter Characteristics

The Series 300 Twin Otter has a maximum gross weight of 55,600 N (12,500 lbs.) and carries 20 passengers and a crew of two. It has a nominal wing loading of 1436 N/m^2 (30 lb/ft^2), making it susceptible to ride quality degradation in severe turbulence. The Twin Otter is powered by two Pratt and Whitney PT6A-27 turboprop engines. Maximum cruising speed is 92.6 m/sec (180 KTAS), while the maximum altitude is 3049 m (10,000 ft), due to the unpressurized cabin. Maximum range is 1399 km (755 n.m.). However, the average flight time is less than 45 minutes for normal commuter service in the United States. Approximately 90 of the 366 Twin Otters in service operate in the United States under FAA Part 135 rules. A three-view illustration of the Twin Otter is shown as Figure 1.

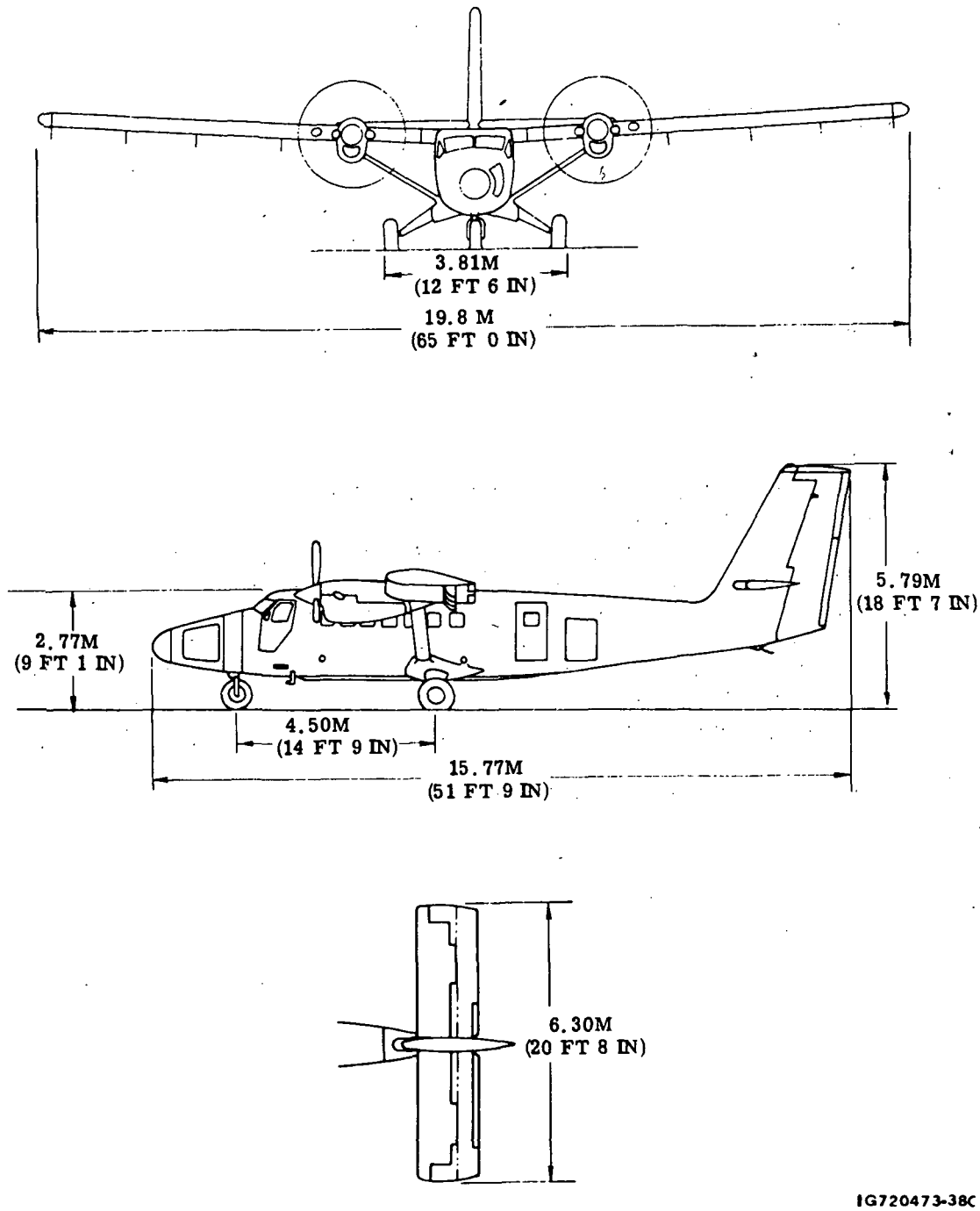

Figure 1: de Havilland DHC-6 Twin Otter - 300 Series

2.0 SYMBOLS

b	wing span, m (ft)
$\bar{c}$	mean aerodynamic chord, m (ft)
C_D	drag coefficient, dimensionless
C_L	lift coefficient, dimensionless
(C_ℓ, C_M, C_N)	aerodynamic moment coefficients about the (x, y, z) body axes, dimensionless
C_T	thrust coefficient, dimensionless
(C_X, C_Y, C_Z)	force coefficients along the (x, y, z) body axes, dimensionless
g	normalized acceleration
(I_{xx}, I_{yy}, I_{zz})	moments of inertia with respect to (x, y, z) body axes, kg-m^2 (slug-ft^2)
I_{xz}	product of inertia with respect to x and z axes, kg-m^2 (slug-ft^2)
j	$\sqrt{-1}$, unit imaginary number
K	gain constant
L	turbulence scale length, m (ft)
p, q, r	perturbation angular velocity vectors along (x, y, z) body axes, rad/sec
$\bar{q}$	dynamic pressure, N/m^2 (lb/ft^2)
$\bar{S}$	reference wing area, m^2 (ft^2)
S	LaPlace operator
U_o	steady flight velocity along x body axis, m/sec (ft/sec)
(u, v, w)	perturbation linear velocities along (x, y, z) body axes, m/sec (ft/sec)
V	total airplane velocity, m/sec (ft/sec)
v_g	component of gust velocity along body y axis, m/sec (ft/sec)
W	weight, N (lb)
w_g	component of gust velocity along body z axis, m/sec (ft/sec)
X_{sensor}	body station of sensor, m(ft)
$X_{c.g.}$	body station of center of gravity, m(ft)
$\ddot{Y}$	inertial acceleration along y body axis, g or m/sec^2 (ft/sec^2)
$\ddot{Z}$	Inertial acceleration along z body axis, g or m/sec^2 (ft/sec^2)
α	airplane angle of attack, rad
β	airplane sideslip, rad
δ_A	aileron deflection, rad
δ_E	elevator deflection, rad

δ_F	flap deflection, rad
δ_R	rudder deflection, rad
δ_{sp}	spoiler deflection, rad
(ϕ, θ, ψ)	roll, pitch, and yaw Euler angles (Reference 8), rad
ϕw_g	power spectral density of vertical turbulence, $\frac{(m/sec)^2}{rad/sec}$
ξ	damping ratio
Δ	incremental
σ	root mean squared
ω	frequency, rad/sec
ω_N	undamped natural frequency, rad/sec

SUBSCRIPTS:

AIL	aileron
C	command
FUS	fuselage
g	gust
max	maximum
SS	steady state
tot	total

3.0 DESIGN CRITERIA

3.1 Flight Conditions

A survey was conducted of existing data on operational profiles of the DHC-6 Twin Otter. Typical climb, cruise and landing approach conditions were selected for design flight conditions and are tabulated in Table I, below. Performance polars are presented in Appendix A.

TABLE I
FEASIBILITY STUDY FLIGHT CONDITIONS

Condition	Climb	Cruise	Landing Approach
Airspeed, m/s (KIAS)	51.5 (100)	77.2 (150)	36.0 (70)
Altitude, m (ft)	914.4 (3,000)	1 829 (6,000)	152.4 (500)
Gross weight, N (lb)	50 040 (11 250)	50 040 (11 250)	50 040 (11 250)
Flap position, rad (deg)	0 (0)	0 (0)	.698 (40)
CG location, % MAC	30	30	30
Rate of climb, m/s (ft/min)	2.54 (500)	– –	– –
Glide slope, rad (deg)	– –	– –	-.1309 (-7.5)

The cruise condition is representative of both cruise and descent for a ride control study, since airspeeds are similar and the cruise altitude is relatively low. The DHC-6 altitude ceiling is 3048 m (10,000 ft), and the typical cruise altitude is 1829 m (6,000 ft).

Typical flight durations are approximately 45 minutes, and therefore the constant weight and center-of-gravity locations are representative of all flight phases.

3.2 Design Turbulence Conditions

A random turbulence intensity with an exceedance probability of 0.01 was selected as a design condition for this study. Figure 2 shows rms gust velocity with 0.01 exceedance

probability, as a function of altitude[3,4]. This probability level corresponds to an rms gust velocity of 2.1 m/sec (7.0 ft/sec) for all the design flight conditions, since the altitude is 1829 m (6,000 ft) or less for all conditions.

Atomospheric turbulence was modeled with a von Karman spectrum having the following spectral density for digital computation of airplane response power spectra.

$$\phi_{w_g} = \frac{\sigma_{w_g}^2 L}{\pi U_o} \frac{1 + \frac{8}{3}\left(1.339 \frac{L}{U_o}\omega\right)^2}{\left[1 + \left(1.339 \frac{L}{U_o}\omega\right)^2\right]^{11/6}} \frac{(\text{m/sec})^2}{\text{rad/sec}} \qquad (1)$$

where σ_{w_g} = rms gust velocity, m/sec.

U_o = airplane forward velocity, m/sec.

L = turbulence scale length, m.

ω = frequency, rad/sec.

A scale length (L) of 762 m (2500 ft) was used for the climb and cruise conditions, and 152 m (500 ft) for the landing condition.[5]

For hybrid simulation, an analog of random turbulence velocity was generated by filtering the output of a random white noise source so that the power spectral density of the filter output approximated the von Karman spectrum. The LaPlace transform of the von Karman gust filter is:

$$F(S) = \frac{\sigma_{w_g} \sqrt{U_o}\ 2.229 \left(S + .317 \frac{U_o}{L}\right)\left(S + 11.54 \frac{U_o}{L}\right)\left(S + 166.3 \frac{U_o}{L}\right)}{\sqrt{L}\left(S + .372 \frac{U_o}{L}\right)\left(S + 1.372 \frac{U_o}{L}\right)\left(S + 17.79 \frac{U_o}{L}\right)\left(S + 264.8 \frac{U_o}{L}\right)} \qquad (2)$$

3.3 Performance Goals

Positive, well-defined ride-quality criteria for aircraft do not presently exist. However, a Symposium on Vehicle Ride Quality held at the NASA Langley Research Center, July 6 and 7, 1972, did produce indications of approximate human comfort motion boundaries. Motion levels felt to be conservative based on the symposium discussions were suggested by NASA to the contractor for use as ride-smoothing performance goals, rather than as precise performance requirements. Several ride-smoothing systems with varying degrees of complexity were to be examined with the intent that performance of these various systems bracket the given performance goals.

3.3.1 Ride qualities. – The primary ride quality goals were to reduce vertical acceleration in each flight condition to 0.030 g rms or less and lateral acceleration to 0.015 g rms or less, at all crew and passenger stations, while subjecting the airplane to the design random turbulence.

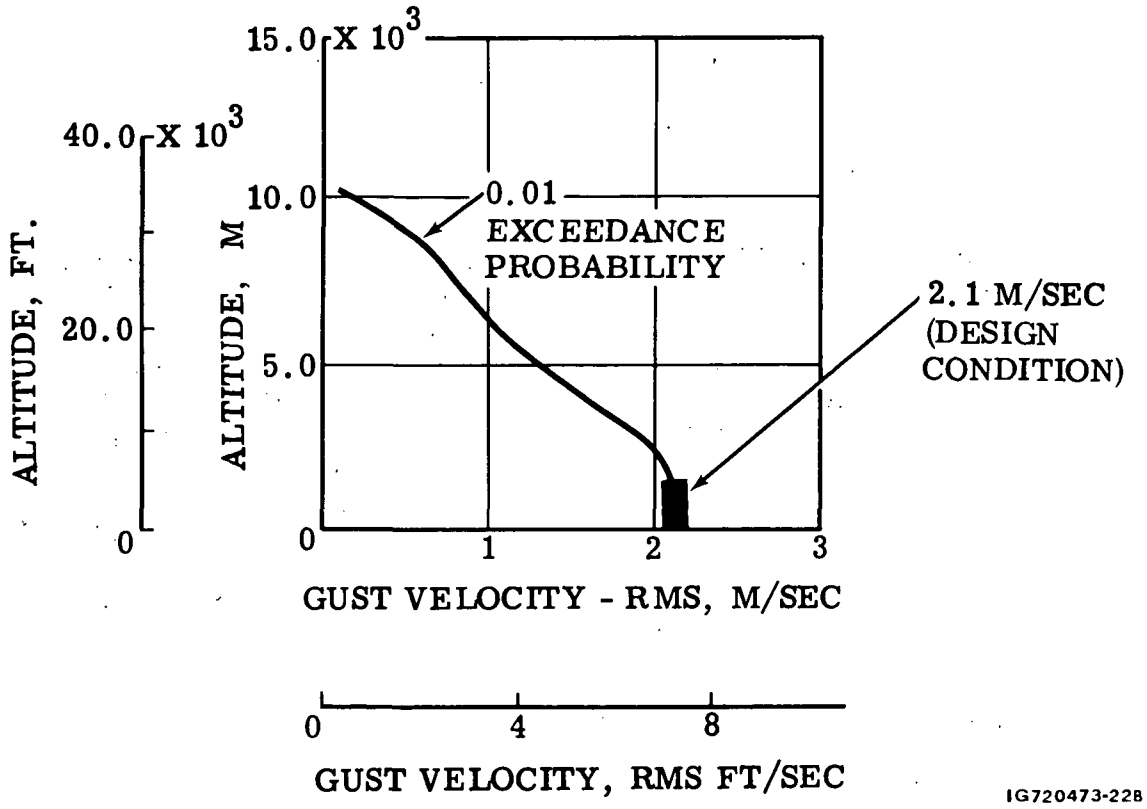

Figure 2: Design turbulence condition

In addition, angular accelerations and rates were not to exceed existing free airplane values. Specific maximum angular rates of 4 deg/sec for pitch and yaw and 7 deg/sec for roll were suggested by NASA; however, the existing values were used as goals since they were smaller for all conditions.

3.3.2 Handling qualities. – Pitch short period handling qualities were evaluated qualitatively by comparing pitch rate and normal acceleration of the aircraft plus ride control system with those of the free airplane in response to control column step inputs. A minimum damping ratio of 0.04 was selected as a design goal for the phugoid mode.

Lateral-directional handling qualities from MIL-F-8785B (Reference 7, Level 1 for light airplanes) or existing values, whichever were less, were used as design goals. In general, the quantities specified are dependent upon characteristic root locations. Specific values are tabulated and compared with actual performance in Paragraph 5.4.2.2

3.4 Safety Criteria

The ride control system was designed to provide (1) adequate handling qualities and safety for continued flight following a single engine failure, total hydraulic or electrical power failure or a single ride control surface hardover, and (2) safe maneuvering and landing capability following two engine failures.

4.0 CONTROL SURFACE CONFIGURATIONS

For this feasibility study, the ailerons, elevators and rudder were each split spanwise into two segments for ride control and manual flight control, as follows:

	Manual Flight Control Segment — Percent Span —	Ride Control Segment — Percent Span —
Aileron	60	40
Elevator	80	20
Rudder	70	30

Manual segments are controlled through existing mechanisms. Ride control segments are controlled by electrohydraulic power actuators that receive electrical position command signals from both pilot manual and ride control commands.

Spoiler control surfaces, operating from a biased position, were added to augment the ailerons for direct lift control during landing approach.

Figure 3 defines five surface/sensor combination options that were selected to provide performance, complexity and cost trade data to aid in selecting a specific configuration for subsequent implementation and demonstration phases. The cross hatched areas are electrohydraulically actuated surfaces that accomplish both ride control and manual control functions (spoilers excluded). The remaining control surfaces are manually actuated. Under normal operation, the control authority for the modified airplane is the same as the basic airplane.

Option II uses an angle of attack feed forward sensor while the other options use an accelerometer as the primary motion feedback sensor.

The aileron and spoiler configurations are illustrated in Figure 4. The existing aileron trim tab is retained on the left wing and the present geared tabs are moved to the manual portions of the ailerons. The geared tabs are adjustable to achieve aerodynamic balance of the manual aileron.

The selected configurations of the elevator and rudder surface are compared to the existing configurations in Figures 5 and 6, respectively. The split configurations require aerodynamic balancing of the manual portion of the surface since the ride control portion eliminates the horn balance. Aerodynamic balance is achieved with more overhang area in front of the hinge line and adjustable geared tabs. This requires addition of a gear tab on the right elevator. The present elevator trim tab and flap interconnect tab are retained. A portion of the present rudder geared tab is retained. The rudder trim tab is moved to the manual rudder surface.

Aerodynamic analyses supporting the choice of spoilers to supplement the ailerons and the areas allowed for the ride control surfaces are discussed in Paragraph 7.

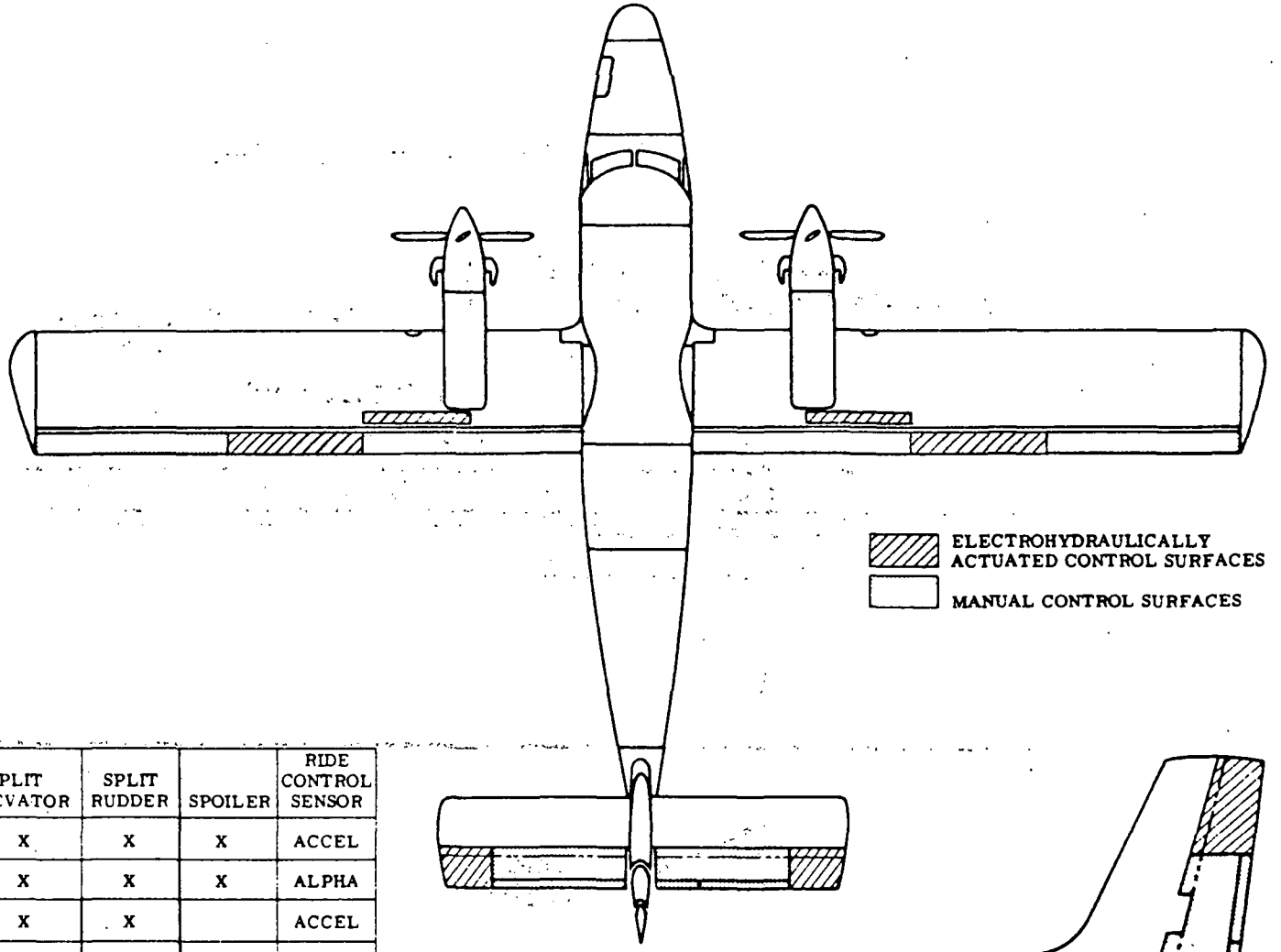

OPTION	SPLIT AILERON	SPLIT ELEVATOR	SPLIT RUDDER	SPOILER	RIDE CONTROL SENSOR
I	X	X	X	X	ACCEL
II	X	X	X	X	ALPHA
III	X	X	X		ACCEL
IV	X	X			ACCEL
V	X				ACCEL

Figure 3: Ride control surfaces

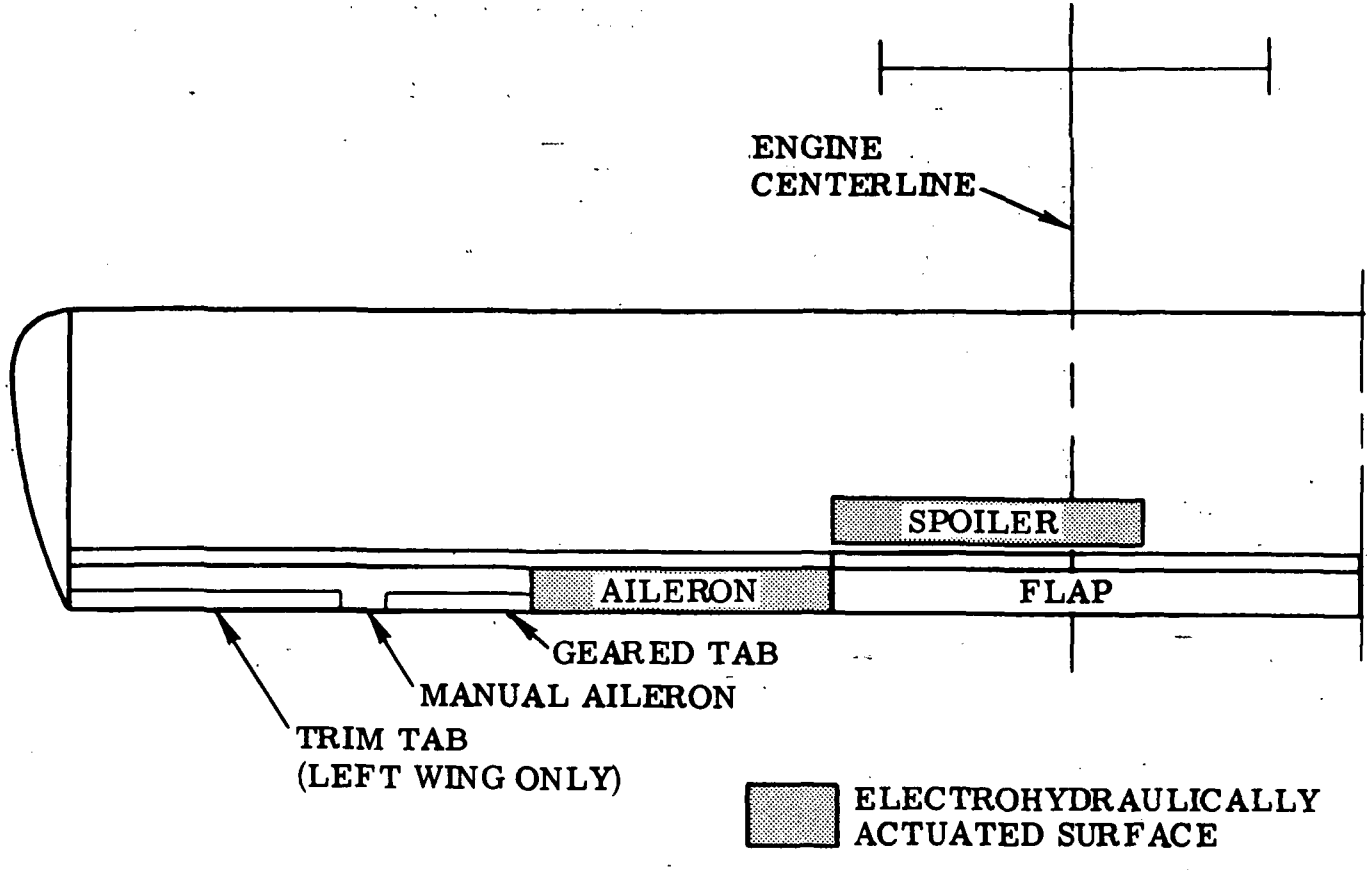

Figure 4: Wing control surfaces

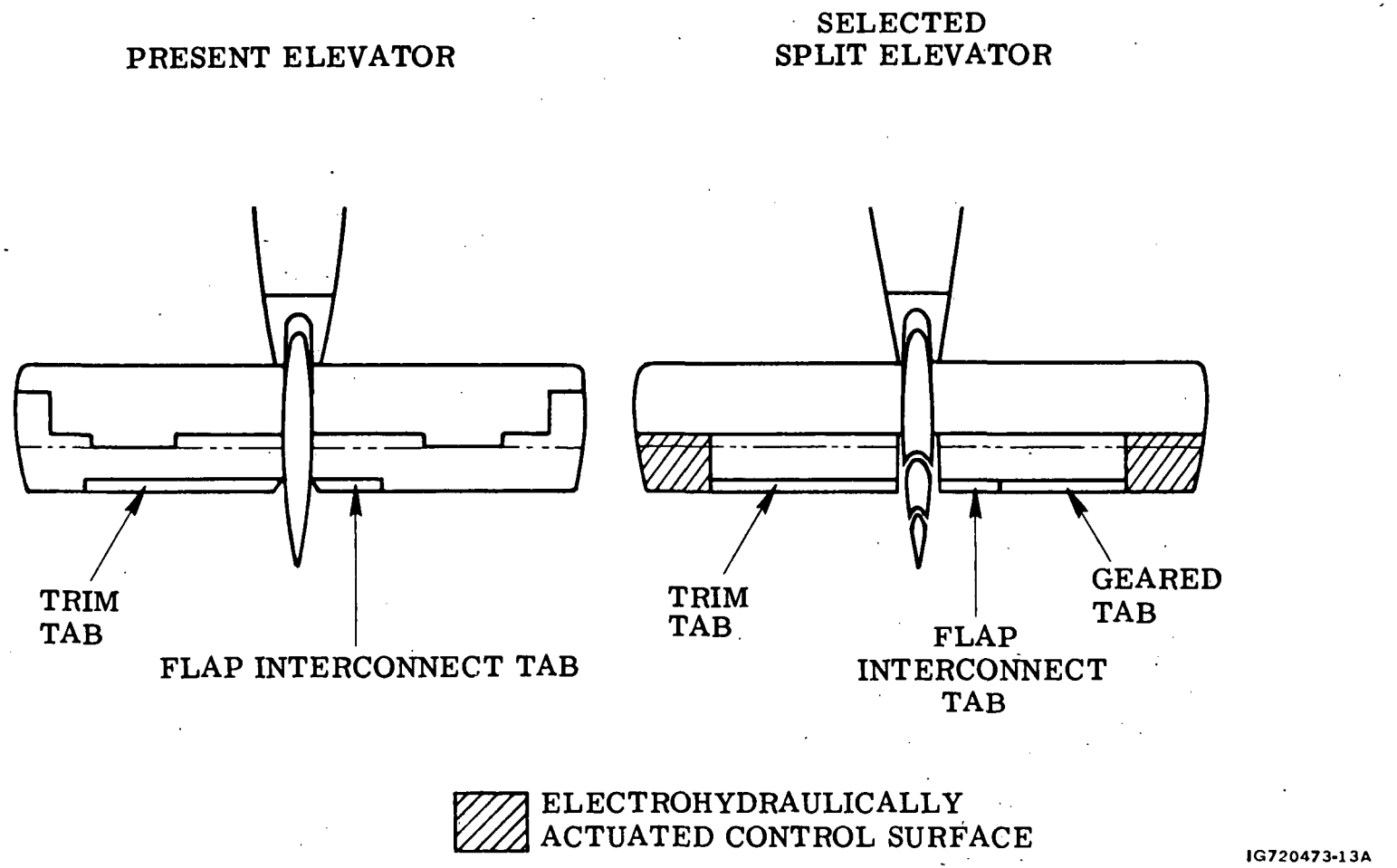

Figure 5: Elevator surfaces

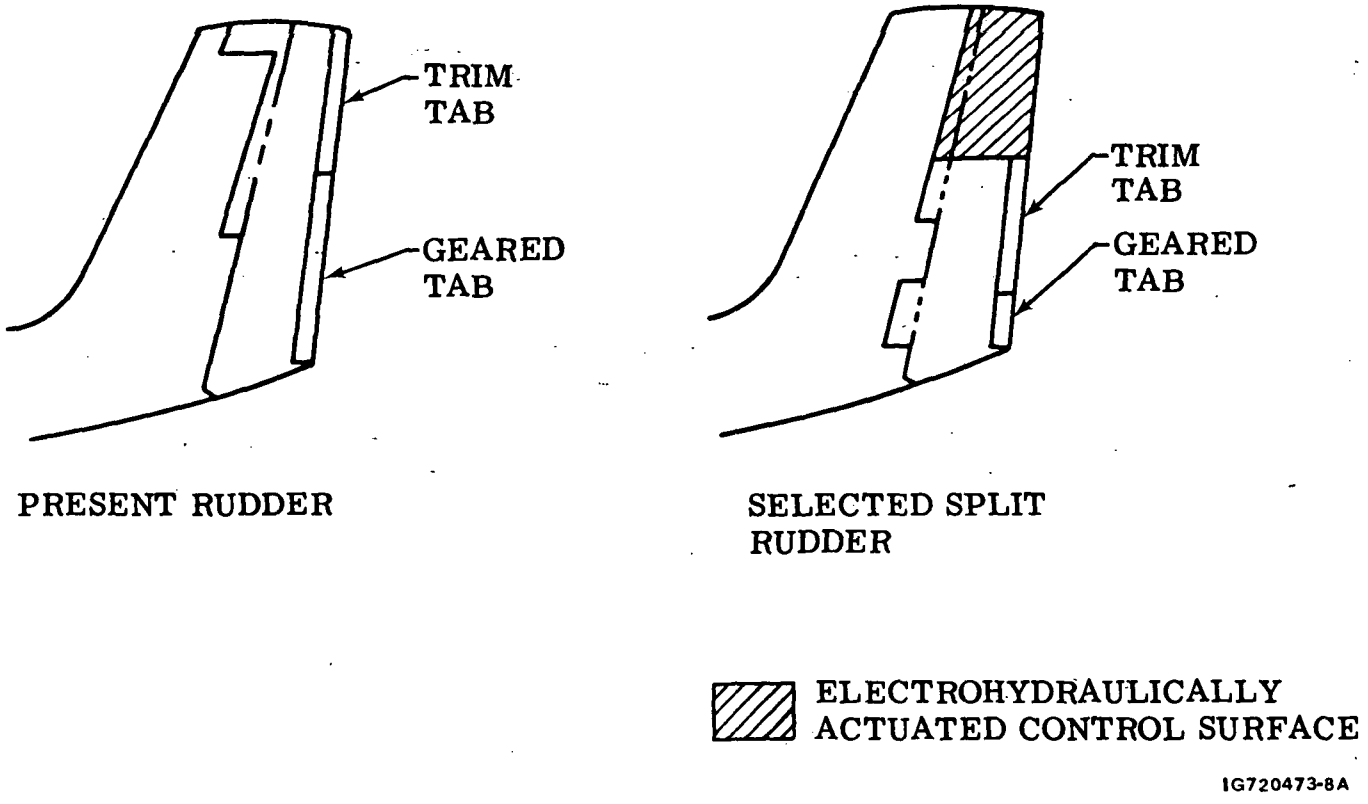

Figure 6: Rudder surfaces

5.0 CONTROL SYSTEM SYNTHESIS AND PERFORMANCE ANALYSIS

Ride control system synthesis was accomplished by digital computation with the linear equations presented in the Appendices, without lift growth effects. Actuator bandpass, position limit, and rate limit studies, and final ride quality performance evaluations were accomplished by hybrid computation with lift growth included.

5.1 Mathematical Models

Small perturbation, linear, rigid-body equations of motion were used for the airplane mathematical model. A statement of the equations and tabulations of stability and control derivatives, inertial properties, and geometric properties are contained in the Appendices B and C. The general form of the equations is derived in Reference 8, in stability axes. Conditions and assumptions required to derive linear, small perturbation equations are stated in the referenced manual. Sign convertions are presented in Appendix C.

The function used to simulate lift growth of the circulatory aerodynamic forces resulting from airplane positions and rates is given in Equation 3. The functions is in LaPlace form and is derived from the Wagner function[9,10].

$$W(S) = 1 - \frac{.165S}{S+g} - \frac{.335\,S}{S+f} \tag{3}$$

where $g = .0455\,\frac{2U_o}{\bar{c}}$, $f = .3\,\frac{2U_o}{\bar{c}}$

Similarly, the function below, derived from Kussner's function, simulates the lift growth of circulatory lift resulting from gusts.

$$\psi(S) = 1 - \frac{.500}{S + .130\,B_o} - \frac{.500}{S + B_o} \tag{4}$$

where $B_o = \frac{2U_o}{\bar{c}}$

Airplane motion variables were filtered, one at a time, through W(S) before multiplying by the aerodynamic coefficients in the hybrid simulation. The effect of the Wagner function filter on acceleration responses was negligible, except when applied to the symmetrical aileron deflections for vertical ride control. The Wagner function filter was employed only on the aileron deflections to obtain the acceleration data presented.

The turbulence generated using the turbulence model (Paragraph 3.2) was passed through the Kussner filter, $\psi(S)$, and then multiplied by each of the gust coefficients in the hybrid simulation. The gust coefficients include fuselage effects, which are noncirculatory. However, fuselage forces are small relative to wing and tail forces.

5.2 Longitudinal Synthesis and Performance Analysis – Acceleration Feedback

5.2.1 Longitudinal synthesis – acceleration feedback. – Control surfaces available for vertical ride control are shown in Figure 3. Ride control systems were synthesized utilizing the three combinations of vertical control surfaces with acceleration feedback listed in that figure. Configuration numbers referred to in the following paragraphs are defined in Figure 3.

Figure 7 is a block diagram of the vertical RCS configuration I. Symmetrical ailerons and spoilers are driven by cg vertical acceleration, and the elevators are commanded by pitch rate.

The primary concept was essentially to reduce translational acceleration with feedback cg acceleration to control surfaces near the cg, and to control angular acceleration and pitch handling qualities with pitch rate feedback to the elevators.

Effectiveness of cg acceleration feedback to the ailerons was determined for each flight condition as shown in Figure 8 for the cruise condition. The figure presents vertical rms acceleration at the cg as a function of acceleration feedback gain. The data was digitally computed by power spectral methods for acceleration feedback, without feedback filter or actuator dynamics. A gain of 96.6 deg/g (3 deg/ft/sec^2) was selected for the cruise condition. This work was accomplished for full span aft flaps and ailerons. Later, when the configuration was changed to partial span ailerons, the gain was increased appropriately for the decrease in control surface lift authority.

The acceleration gain for climb was set by the acceleration goal also. However, the gain for landing was set to prevent frequent and prolonged saturation of the ailerons and spoilers, since they are not effective enough in the landing condition to meet the acceleration goal.

The spoilers, active only in the landing phase, are commanded by the same sensor and filters as the ailerons. The feedback gain to the spoilers is half of that to the ailerons, since the spoilers have only about half as much deflection available from their biased position.

Feeding back acceleration decreases the natural frequency and increases the damping ratio of the short period mode as shown in the root locus plot in Figure 9, closing only the acceleration loop at the cruise condition. This feecback makes the airplane response to pilot commands sluggish. Angular rate feedback is required to restore handling qualities. Angular rate feedback through a lag filter (pseudo integration) essentially accomplishes a blend of rate and position feedback, the conventional methods of controlling damping ratio and frequency, respectively.

Figure 10 is a short period root locus with the acceleration gain fixed, and closing the pitch rate feedback loop to the elevator through a 2/(S + 2) lag filter. With $K_{\dot{\theta}}$ = 11.5 deg/rad/sec, the ride control system short period root location was made almost coincident with the free airplane root. Again, $K_{\dot{\theta}}$ was appropriately adjusted when the system configuration was changed to partial span elevators. A high pass (washout) filter

GAIN	FLIGHT CONDITION		
	CLIMB	CRUISE	LANDING
$K_{\dot{\theta}}$	.98	.98	.98
$K_{\ddot{Z}_A}$	43.6	35.1	13.1
$K_{\ddot{Z}_{SP}}$	0	0	6.5

GAIN SCHEDULING

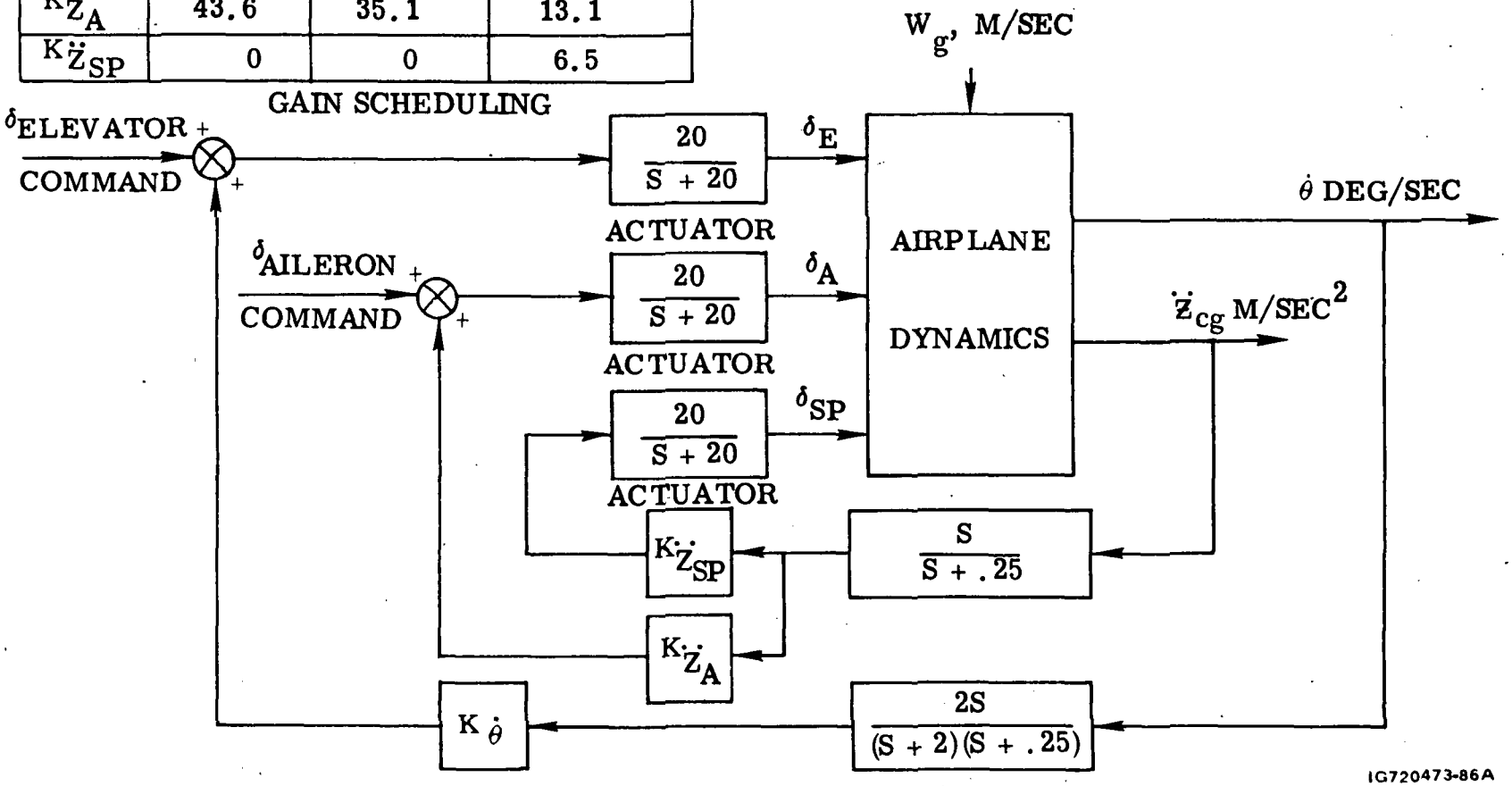

Figure 7: Vertical ride control system block diagram

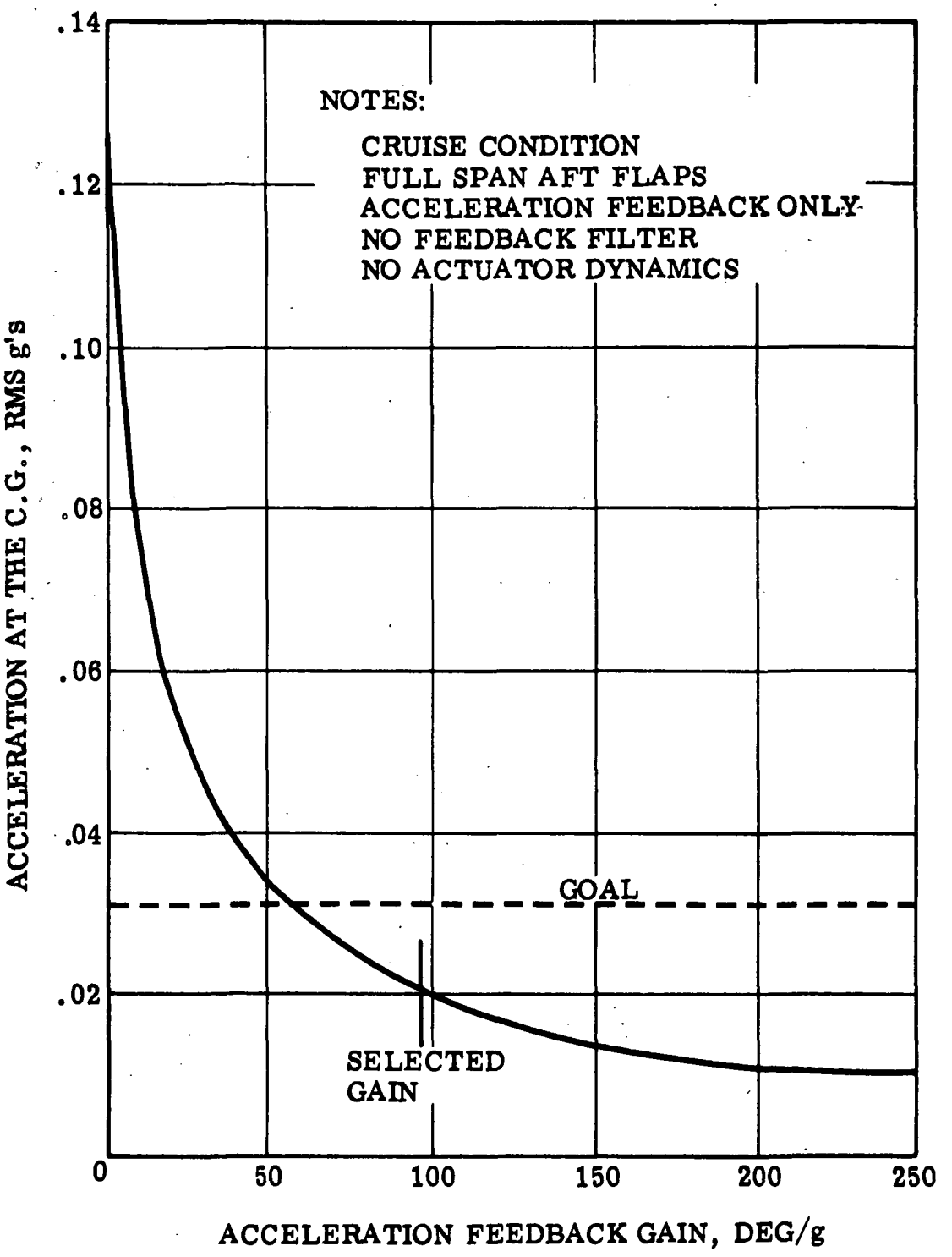

Figure 8: The effect of acceleration feedback on vertical acceleration at the c.g.

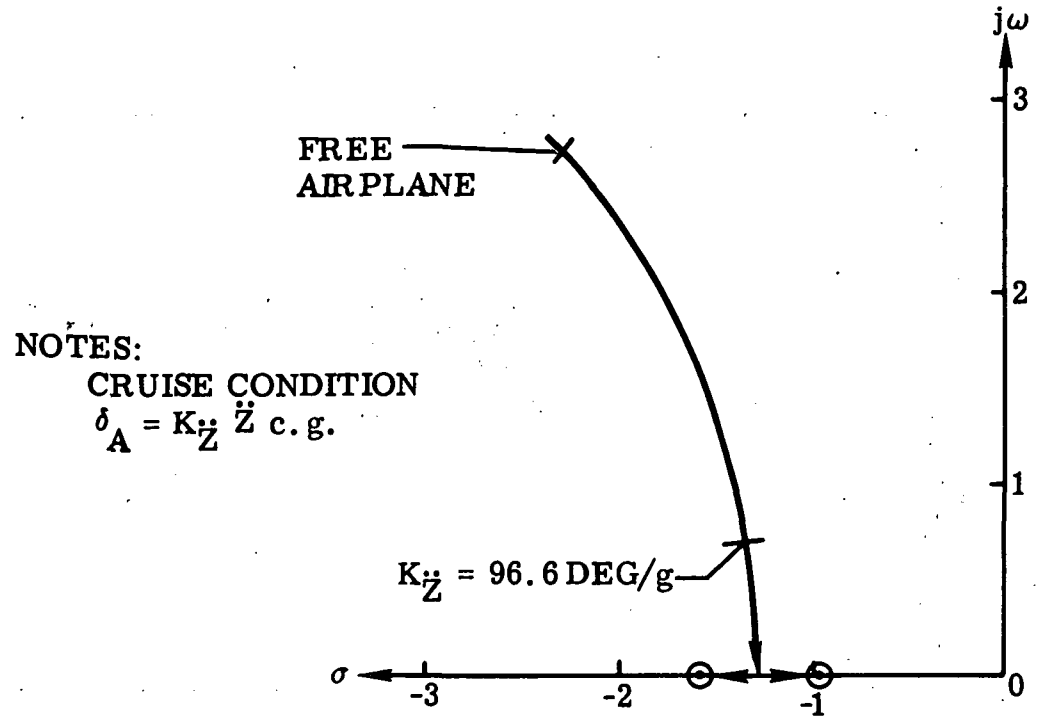

Figure 9: Short period root locus, closing acceleration loop only

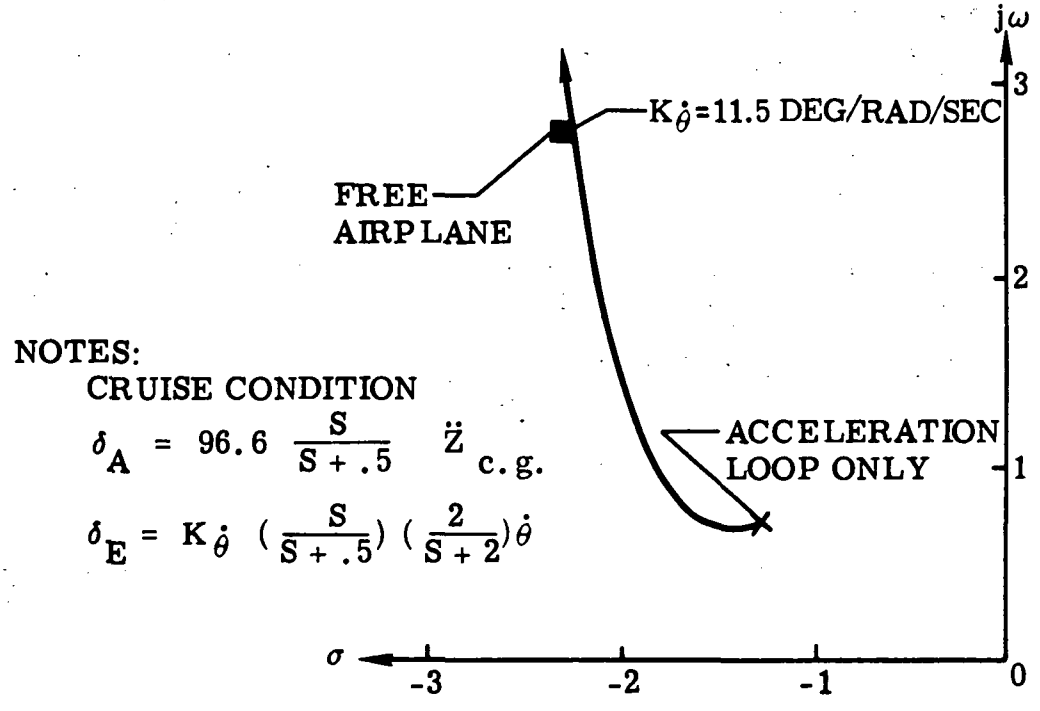

Figure 10: Short period root locus, closing pitch rate loop around fixed acceleration gain

was included in each feedback to eliminate feedback of steady state acceleration or pitch rate. The washout break frequency was later changed to 0.25 rad/sec to accommodate landing approach and climb condition phugoid stability requirements.

Vertical RCS Configuration III is identical to Configuration I, except that the spoilers are omitted. This affects the landing condition only. Gains and filters in the aileron and elevator loops are identical to Configuration I.

Vertical RCS Configuration V utilizes only the aileron control surfaces. The acceleration feedback gain was increased only to a point where the short period root location was still acceptable (reference Figure 9) without pitch rate feedback. The same high pass filter was used, with a feedback gain of 13.1 deg/m/sec^2 (4 deg/ft/sec^2) at all flight conditions.

5.2.2 Longitudinal Performance Analysis – Acceleration Feedback

5.2.2.1 Longitudinal ride qualities – acceleration feedback: For the landing approach and climb conditions rms accelerations of the phugoid mode alone exceed the 0.03 g rms goal and cannot be effectively reduced by pitch rate or acceleration feecback. Figure 11 shows that the rms acceleration resulting from the free airplane phugoid mode in the landing condition is approximately 0.006 g's, for a 0.3049 m/sec (1 ft/sec) rms turbulence intensity. The rms acceleration would be approximately 0.042 g's for the design turbulence of 2.1 m/sec (7 ft/sec).

Attempting to control the very low frequency phugoid mode with acceleration or pitch rate feedback interferes with even long term pilot commands. It was felt that passengers would not be sensitive to such low frequencies (30 seconds or more per cycle). Boeing and NASA agreed to exclude the phugoid contribution to rms acceleration for comparison with the ride quality goal.

Referring to Figure 11, the cumulative rms at a frequency, ω_1, is the square root of the integral of the PSD from $\omega = 0$ to $\omega = \omega_1$. The rms acceleration to be compared with the goal is then $\sqrt{\sigma_{tot}^2 - \sigma_{phu}^2}$, where σ_{tot} is the cumulative rms over the total frequency range, and σ_{phu} is the cumulative rms over the phugoid range. The value of σ_{phu} is taken at the plateau in cumulative rms at the frequency where the PSD returns to zero from the spike resulting from the phugoid mode.

Figure 12 shows rms vertical accelerations computed digitally by power spectral methods. The PSD's were generated from linear equations, without lift growth effects. Accelerations at the pilot, cg and aft passenger (fwd, mid,aft) stations are shown for the three flight conditions for a 2.1 m/sec (7.0 ft/sec) rms gust velocity. The linear analysis indicated that the ride quality goal of 0.03 g's or less would be met with partial span ailerons and elevators for cruise and climb conditions at all stations. In the landing condition acceleration at the aft passenger station is reduced by 42 percent with spoilers added and 20 percent without spoilers. A major part of the reduction accomplished by RCS ailerons and elevators can be accomplished with RCS ailerons alone on the DHC-6 as defined for this study.

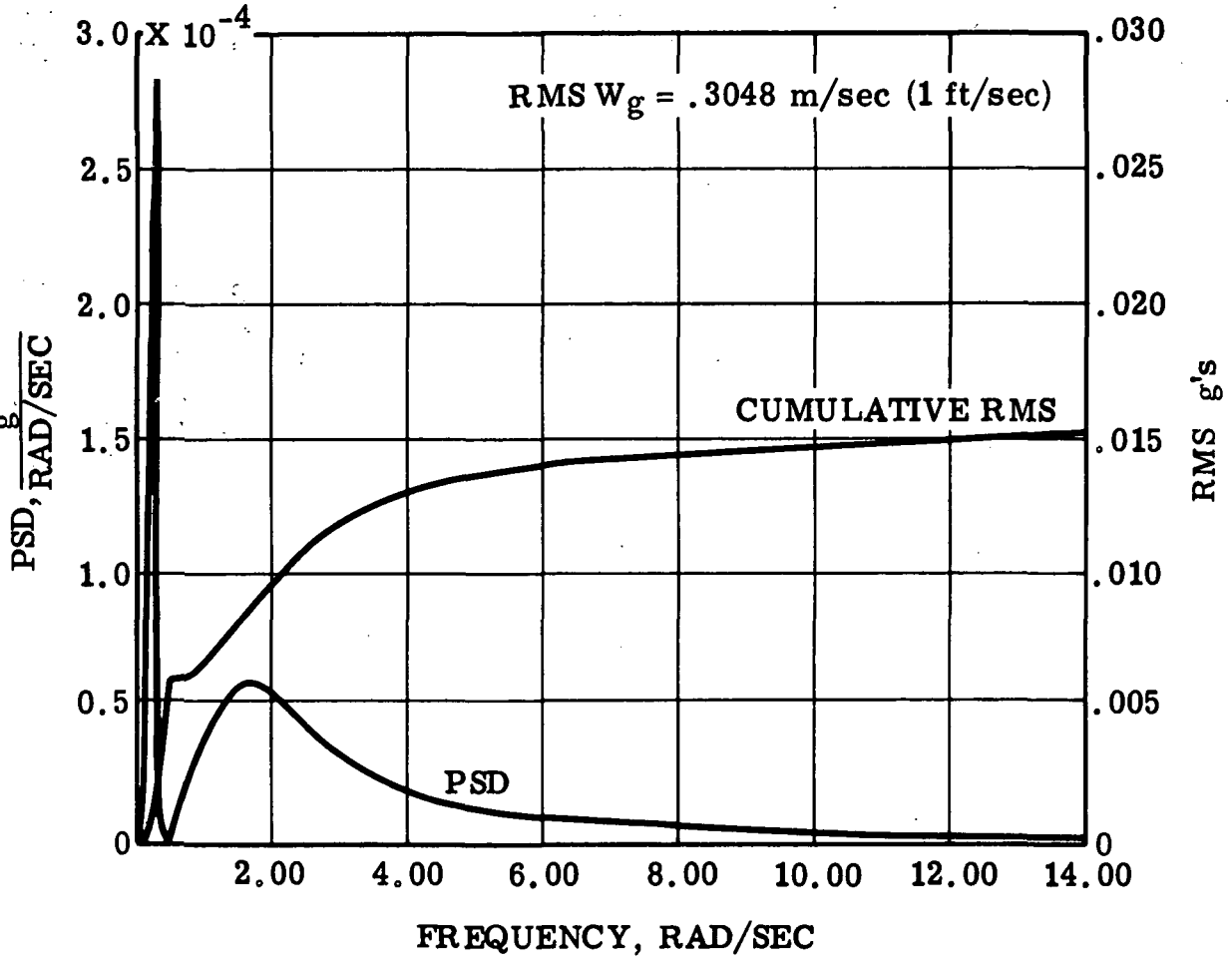

Figure 11: PSD/RMS of c.g. vertical acceleration for the free airplane at landing condition

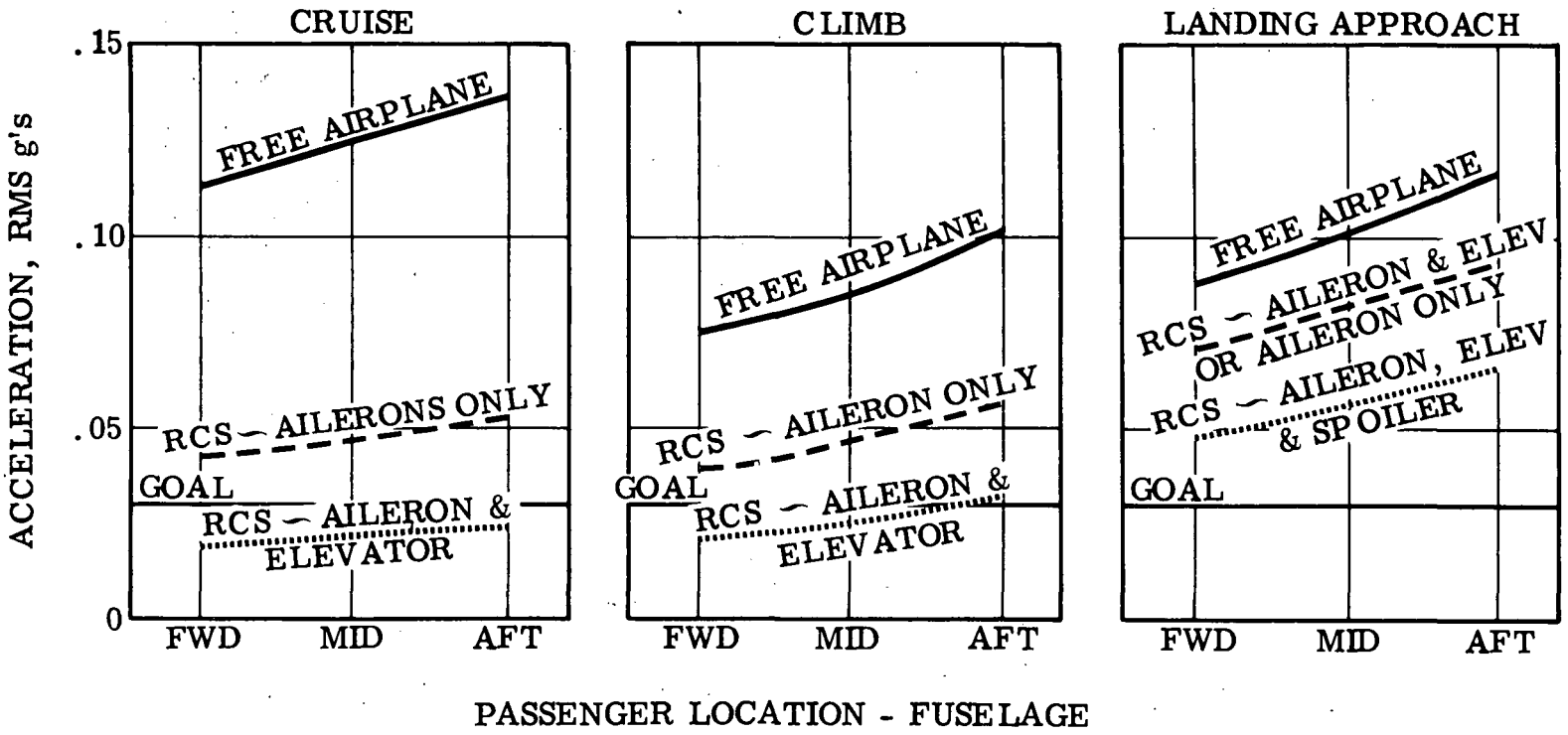

Figure 12: Vertical acceleration - linear analysis

The PSD and cumulative rms of vertical RCS accelerations are compared with those for the free airplane in Figure 13. The accelerations are aft passenger station responses to 0.3048 m/sec (1 ft/sec) rms turbulence at the cruise condition. The ride control surfaces are ailerons and elevators. Cumulative rms at a frequency, ω_1, is equal to the square root of the areas under the corresponding PSD from $\omega = 0$ to $\omega = \omega_1$. In addition to reducing the power (or rms) of the response, the power is concentrated at very low frequencies, which is typical of the RCS at all flight conditions. Practically all of the power exists below 0.20 Hertz.

Performance analyses were conducted with a hybrid computer simulation that included lift growth as described in Paragraph 5.1 and actuator dynamics and limits as described in the following paragraphs. Only two rigid body degrees of freedom were included in the hybrid simulation. Effects of the phugoid mode were omitted.

The effect of aileron actuator bandpass on acceleration reduction was evaluated by the hybrid simulation at the cruise condition and is illustrated in Figure 14. Actuator bandpass is defined as the break frequency of the first order lay simulating actuator dynamics. An aileron actuator break frequency of 20 radians per second or more provides adequate performance. This value was selected as the design break frequency and was used in all further analyses. This data was produced without actuator rate or position limits. Aft station accelerations is presented in these parametric studies because it is the maximum acceleration among the various stations.

The effect of aileron actuator rate limit on acceleration reduction, shown in Figure 15, was evaluated at the cruise condition also. Data was obtained with the aileron actuator bandbpass set at 20 radians per second and the aileron deflection limit at 20 degrees. One hundred degrees per second provides satisfactory performance and was used in all further control analyses.

Development and maintenance of actuators with this relative high rate may be difficult and expensive. Increasing aileron authority would reduce this rate in direct proportion to the aileron area increase. The split surface approach was selected as the most practical initial design. The scope of this feasibility study did not allow aileron authority design trades. Using the full aileron for both ride control and manual flight control should be considered in future work.

Similar analyses were conducted to determine the elevator actuator requirements, which were found to be quite low. The elevator actuator bandpass and rate limit were rather arbitrarily set at twenty rad/second and fifty deg/second, respectively, for the following performance analyses. These were considered practical to implement, and would not affect the performance.

The effect of lift growth was determined with the actuator dynamics and limits set as discussed above. The simulation of lift growth is discussed in Paragraph 5.1. Figure 16 shows that the Kussner filter applied to the turbulence decreases acceleration, and the Wagner filter applied to the aileron deflection increases acceleration. Stated differently, the Kussner function makes the gusts less effective and the Wagner function makes the ailerons less effective (at high frequencies). The data discussed below reflects the effect

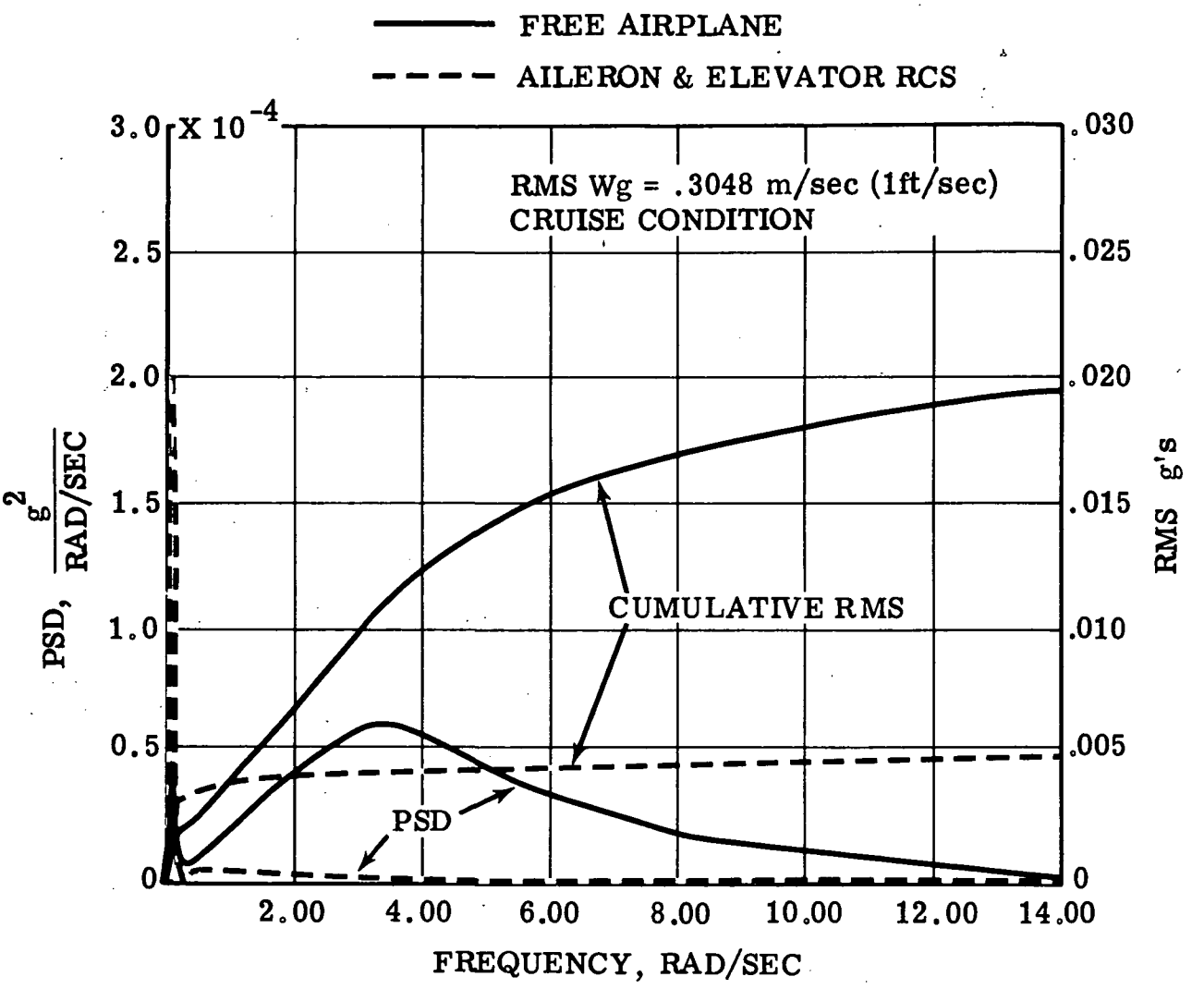

Figure 13: Comparison of free airplane and RCS power spectra of vertical acceleration - aft passenger station

NOTES:

CRUISE CONDITION

AILERON & ELEVATOR SURFACES

TURBULENCE INTENSITY, 2.1 M/SEC (7.0 FT/SEC) RMS

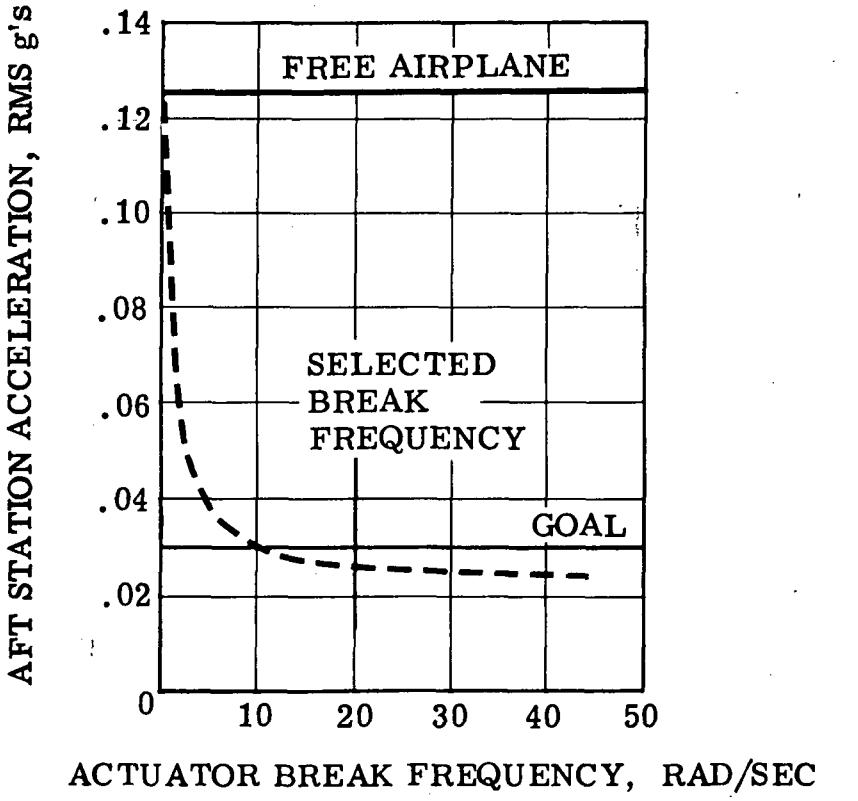

Figure 14: Effect of aileron actuator bandpass on vertical acceleration

NOTES:

CRUISE CONDITION

AILERON & ELEVATOR SURFACES

TURBULENCE INTENSITY, 2.1 M/SEC (7.0 FT/SEC) RMS

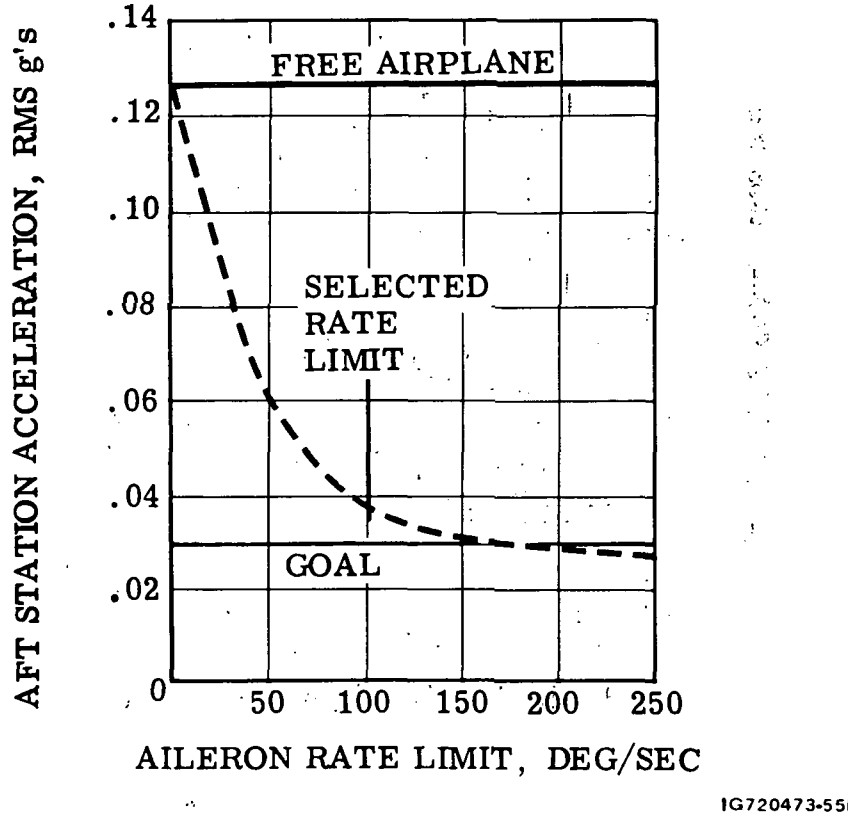

Figure 15: Effect of aileron rate limit on vertical acceleration

NOTES:

CRUISE CONDITION
AILERON & ELEVATOR RCS
TURBULENCE INTENSITY, 2.1 M/SEC (7.0 FT/SEC) RMS

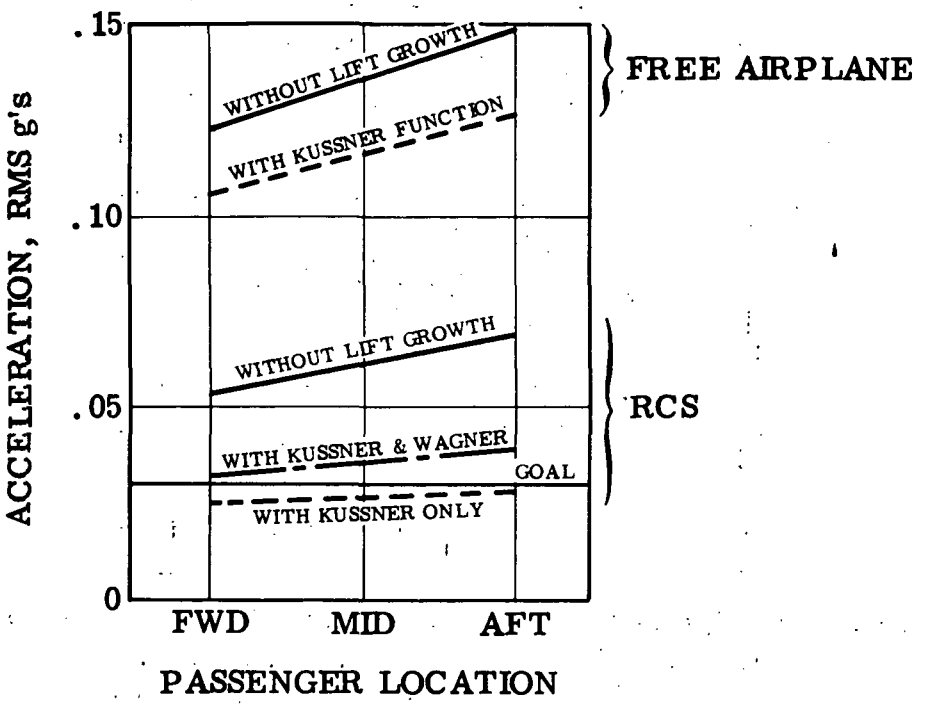

Figure 16: Effect of lift growth on vertical accelerations

of both functions. Actually, control deflections result in somewhat noncirculatory forces, the noncirculatory portion not being subject to lift growth. Consequently the data are conservative in this respect.

Vertical accelerations at the forward, mid and aft passenger stations are shown in Figure 17 for three flight conditions for a 2.1 m/sec (7.0 ft/sec) rms gust velocity. At cruise, climb and the landing approach conditions, aft passenger accelerations for the aileron-elevator ride control system were reduced to 31, 44 and 84 percent, respectively, of the free airplane accelerations. With spoiler feedback in the landing condition, aft acceleration is reduced to 64 percent of the free airplane level.

The ride quality goal of 0.03 g's rms is achieved at the forward passenger station for the cruise condition and at the mid to forward stations for the climb condition.

Actuator break frequencies were 20 radians per second. Aileron and spoiler rate limits were 100 deg/sec, and position limits were $\pm$ 20 degrees and $\pm$ 10 degrees, respectively. Reasonable elevator limits had no effect on the results.

As previously discussed, linear analysis indicated that the vertical ride quality goal would be met. Nonlinearities degrade performance slightly, exceeding the desired maximum acceleration. However, Figure 18 shows that the system meets the vertical ride quality goal of 0.03 g's rms at the cruise condition for all turbulence intensities up to approximately 6.2 feet per second, which has a probability of exceedance of only 0.012.

Table II compares the RCS pitch angular responses with those of the free airplane. All design goals were met at the cruise and climb conditions. At the landing condition pitch angular acceleration and angular rates were approximately 15 to 20 percent more than existing airplane values. However, the accelerations and rates are very small, and this slight increase is considered insignificant.

The ride control system is designed to reduce relatively small accelerations, much less than structural limit load levels. However, the system does reduce large gust-induced accelerations, as shown by the 1-cos transient response in Figure 19, and no instability is caused by system saturation. In this particular case, the gust frequency was selected to maximize free airplane acceleration. The nonlinear simulation included actuator rate and position limits.

5.2.2.2 Longitudinal handling qualities – acceleration feedback: Short period handling qualities were evaluated at all flight conditions by comparing ride control system vertical acceleration and pitch rate responses for column step inputs to free airplane responses. The comparison is shown for Configuration I at the cruise condition in Figure 20, for a two-degree deflection of the full span elevator (manual and RCS). The ride control system causes a loss of effectiveness of the elevator for relatively sharp inputs. A crossfeed from column input to ailerons corrects the problem. Initially, the crossfeed signal cancels the ride control signal opposing the acceleration and then washes out at the same rate as the ride control signal. The crossfeed transfer function is:

$$\delta_A = -16 \frac{S}{S+.25} \frac{2}{S+2} \delta_{E_{Command}} \quad (5)$$

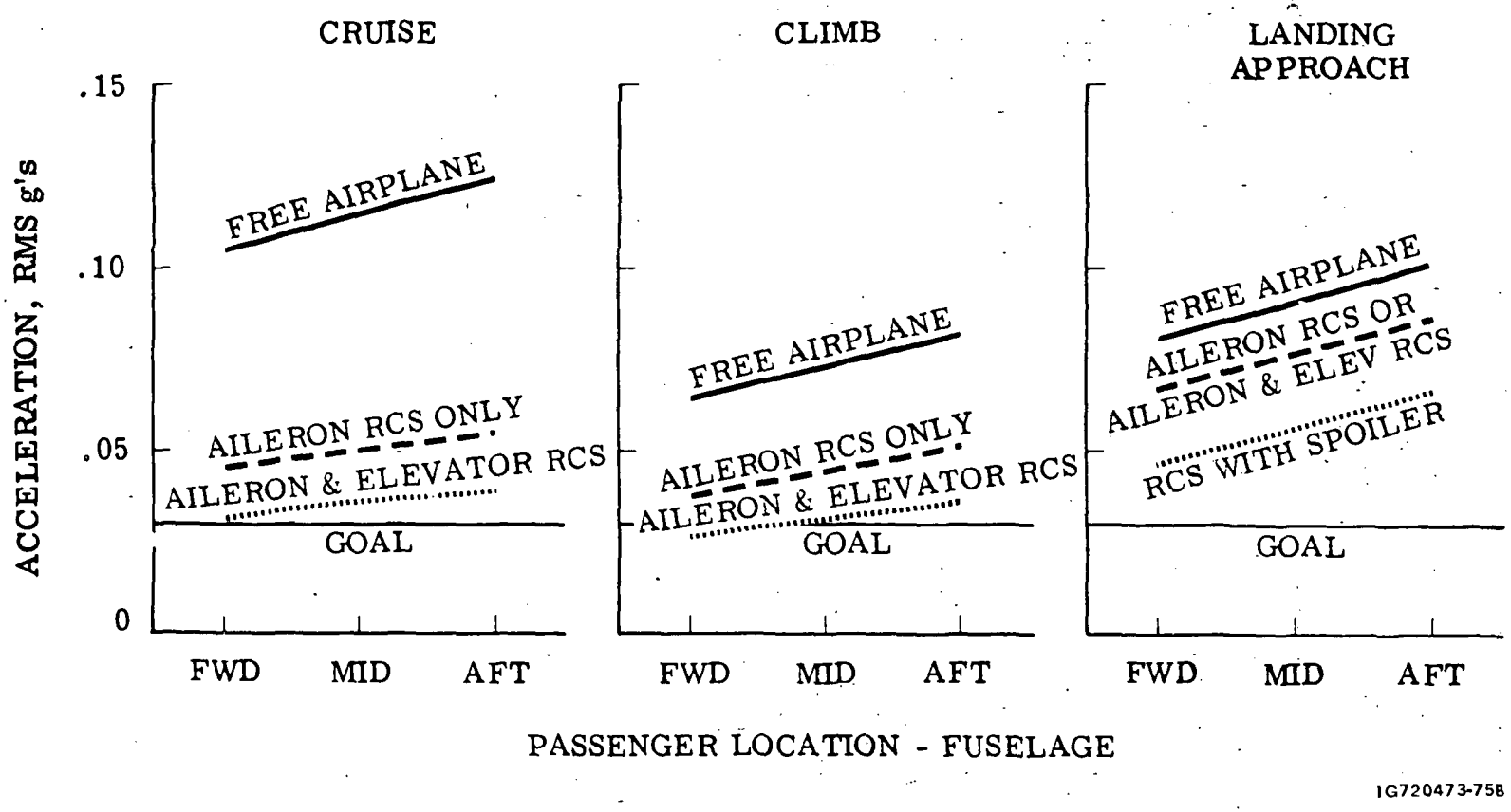

Figure 17: Vertical acceleration

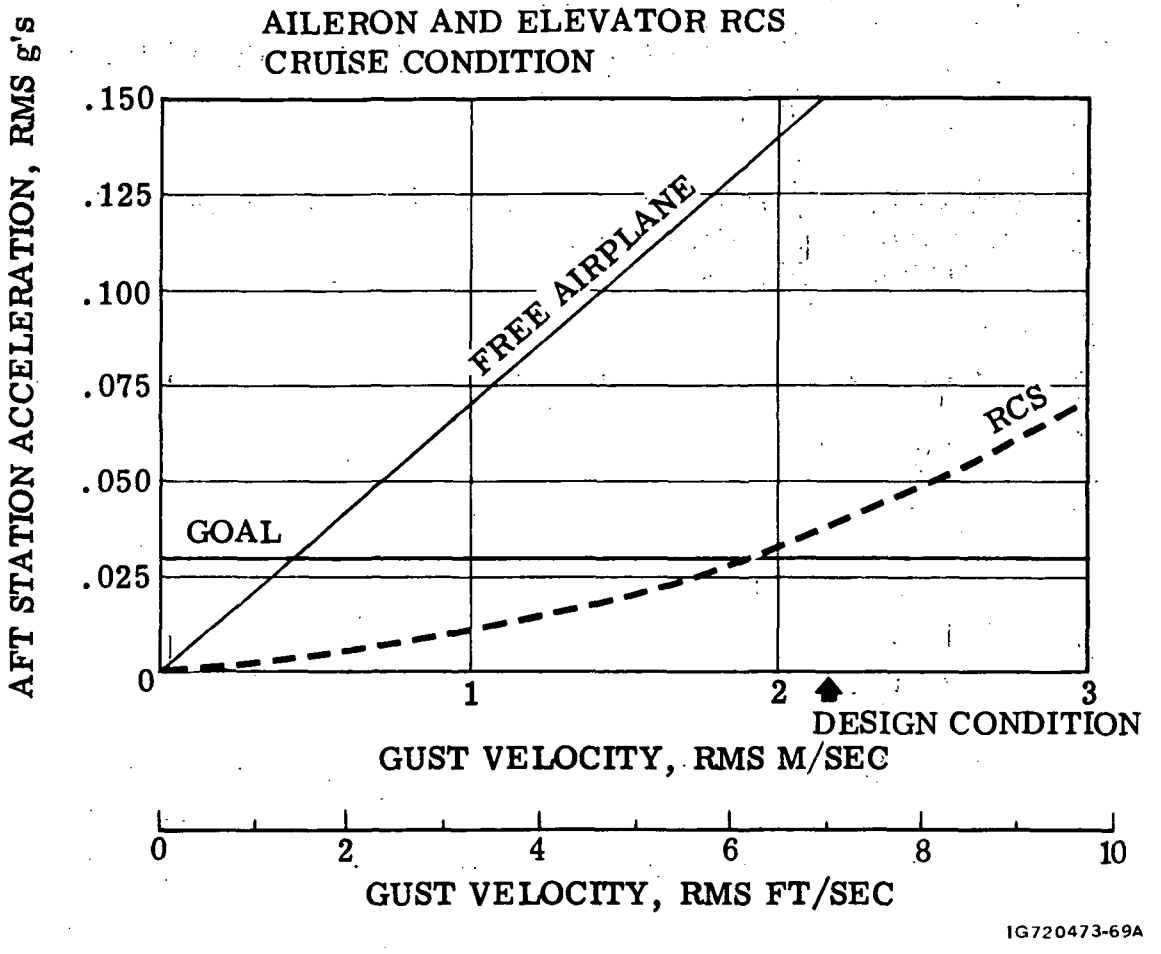

Figure 18: Effect of nonlinearities on vertical acceleration

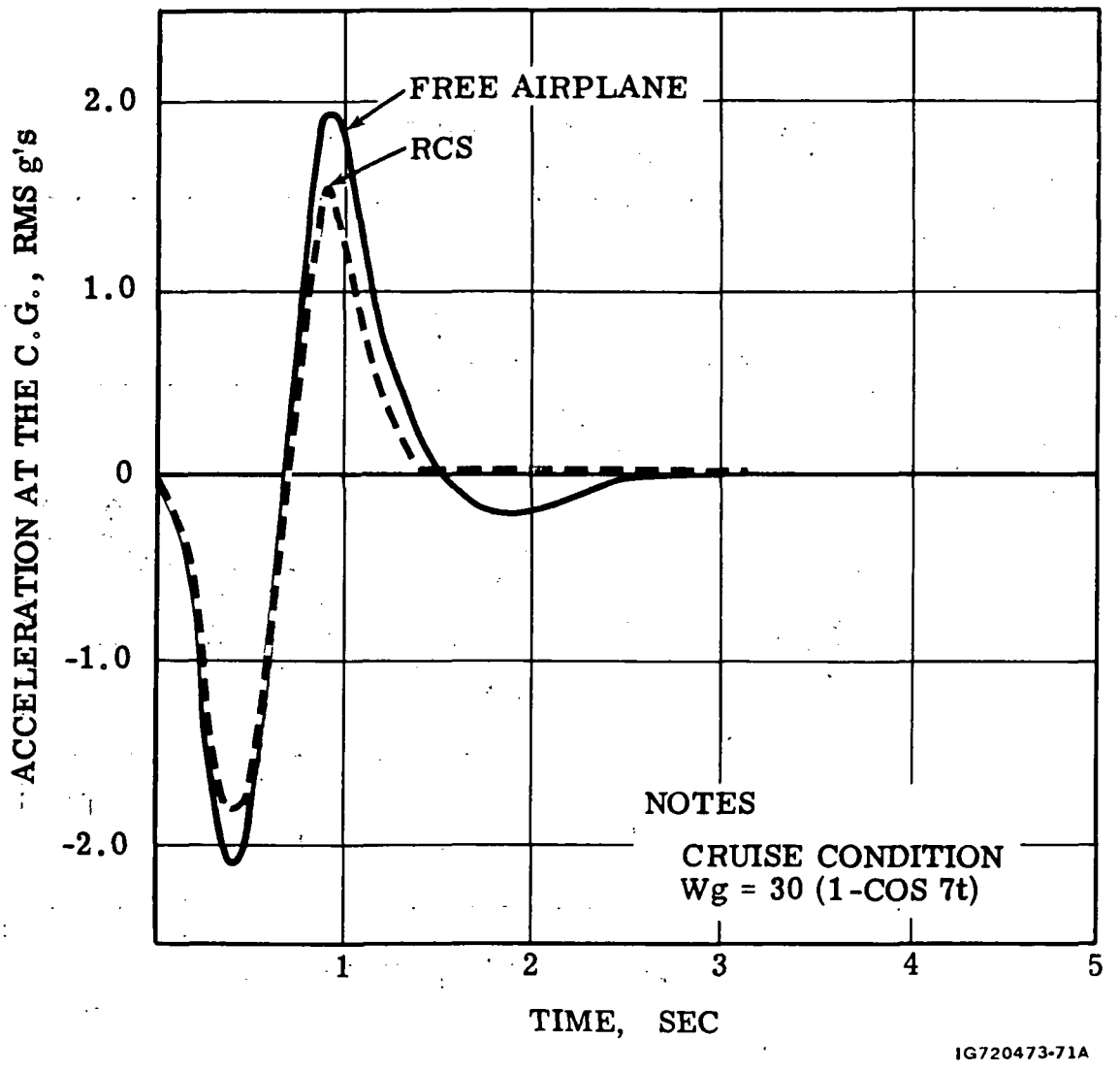

Figure 19: Vertical acceleration response to 1-cos gust

NOTES: CRUISE CONDITION
STEP COLUMN INPUT – 2° ELEVATOR

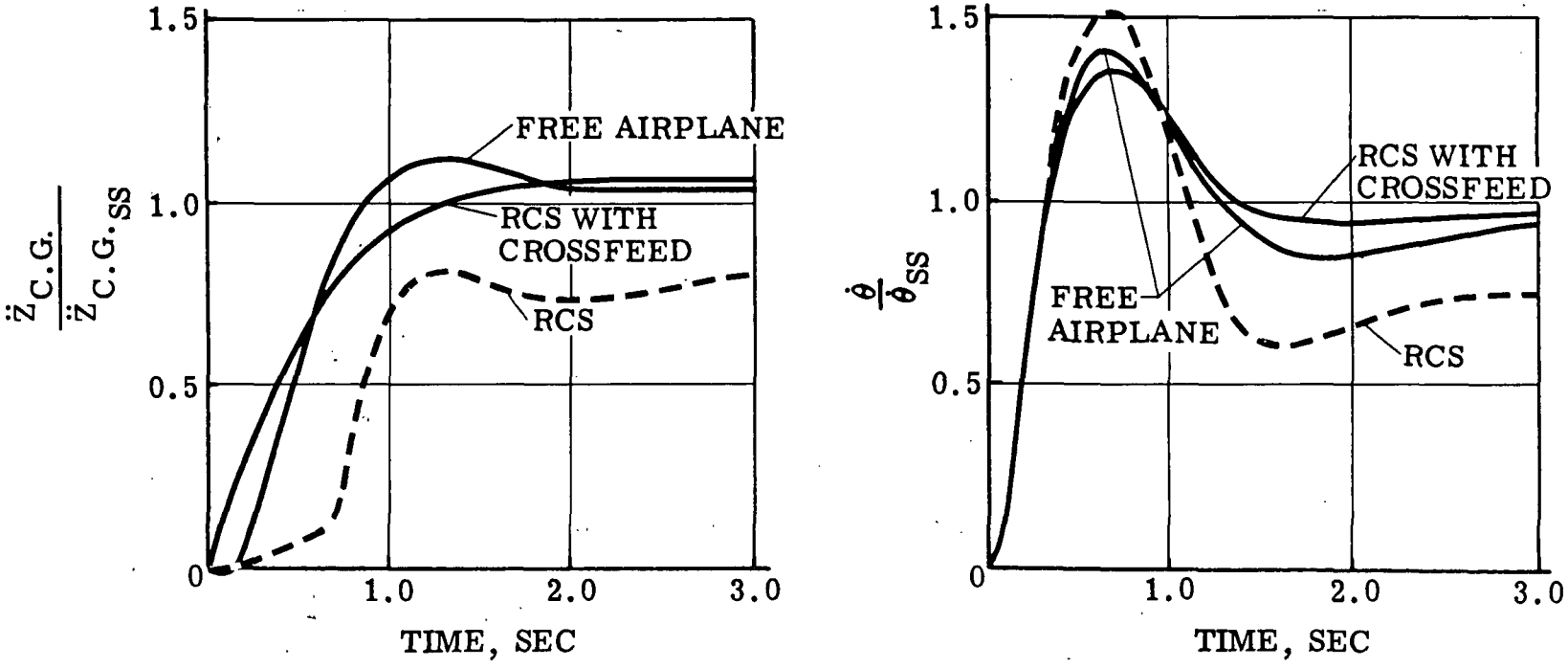

Figure 20: Pitch handling qualities

1G720473-73A

TABLE II
ANGULAR ACCELERATION AND RATE PERFORMANCE – LONGITUDINAL CONTROL SYSTEM

Condition – Mode	Free Airplane	RIDE CONTROL SYSTEM OPTION		
		I Ailerons Elevator Spoilers	III or IV Ailerons Elevator	V Ailerons
Angular Accel-Pitch, deg/sec^2				
• Cruise	2.6	1.2	1.2	1.5
• Climb	2.2	1.7	1.7	1.9
• Landing Approach	7.7	8.7	7.6	7.7
Angular Rate-Pitch, deg/sec				
• Cruise	.7	.4	.4	.5
• Climb	.8	.8	.8	.8
• Landing Approach	1.3	1.5	1.2	1.3

Whether the loss of elevator effectiveness for sharp inputs would present a problem, requiring the crossfeed, should be determined by piloted simulation in Phase II.

The damping ratio of the phugoid mode was also evaluated and was kept greater than 0.04 at all flight conditions.

5.2.2.3 Longitudinal control surface requirements – acceleration feedback: Figure 21 shows the RCS control surface rms deflections required by a 2.1 m/sec (7.0 ft/sec) turbulence intensity. Aileron deflections are approximately 8 degrees rms for climb and cruise conditions and 6 degrees for landing approach. Maximum deflections are approximately three times these levels.

The relatively small partial span elevator deflections indicate that the elevator may not be required to optimize short period root locations. The elevator feedback does not improve acceleration responses greatly, as shown in previous vertical acceleration data. Studies should be conducted during the Phase II design to investigate reducing, or possibly eliminating, the elevator segment used to improve handling qualities.

5.3 Longitudinal Synthesis and Performance Analysis – Angle of Attack Sensor

Synthesis and performance evaluation of the angle-of-attack system were accomplished completely by hybrid simulation, and for the cruise condition only. The angle-of-attack sensor was located on a boom on the nose of the airplane. The equation for the sensed parameter is:

$$\alpha_{tot} = \frac{w + w_g + (X_{sensor} - X_{cg})\,\dot{\theta}}{U_o} \qquad (6)$$

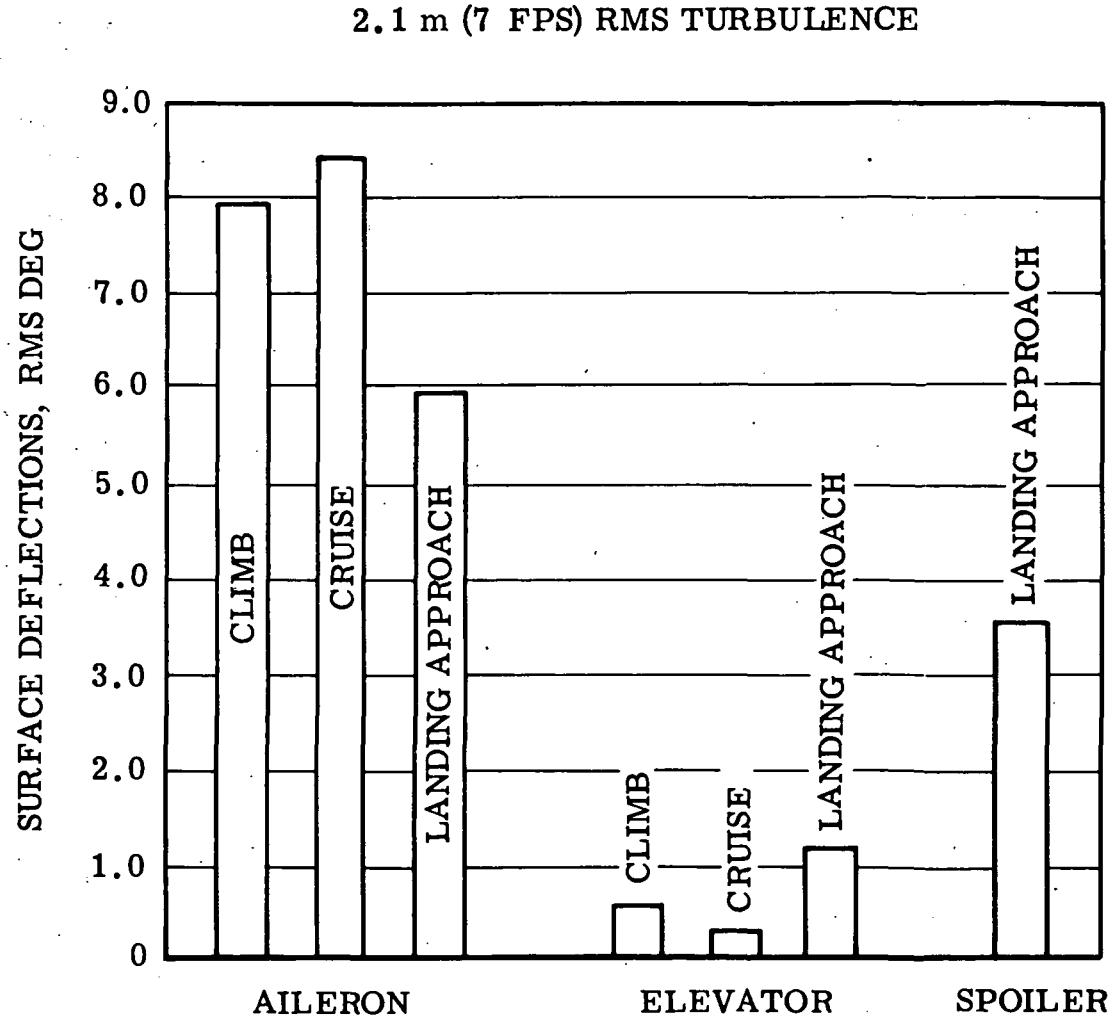

Figure 21: Surface deflections

Each term in the numerator is an increment of vertical velocity at the sensor: airplane velocity, gust velocity, and the velocity resulting from pitch rate. Sensed α_{tot} was then filtered and used as a feedforward command to symmetrically controlled ailerons. Figure 22 is a block diagram of the angle of attack system.

The time delay between sensing the gust and the resulting force on the wing was simulated. The second order portion of the RCS filter provides the required phasing, of ailerons relative to the time delay, to minimize acceleration response. The second order filter also attenuates high frequency gust signals which command unnecessarily high aileron actuator rates. The natural frequency and damping ratio were varied to optimize the filter regarding acceleration reduction. A Pade linear approximation for a time delay was tried in place of the second order filter, at a number of time delay periods. Acceleration reduction was as good, but it did not attenuate the high frequency commands as well. Several combinations of Pade approximations and second order filters were also tried, without improvement in performance. The filter would have to be tuned to the best compromise among the various flight conditions, if implemented, since the time delay between the angle of attack at the boom sensor and lift on the wings is a function of airplane velocity.

A high pass (washout) filter eliminates feedback of steady state angle of attack. Actuator dynamics are siulated with a first order lag 20/(S + 20). Pitch rate feedback to the elevators was tried, but it did not improve performance.

Ride quality performance for the system is shown in Figure 23. At the cruise condition the angle-of-attack ride control system reduces aft passenger acceleration to 36 percent of the free airplane level compared to 31 percent with acceleration feedback. The same actuator limits and bandpass were used for both systems.

5.4 Lateral-Directional Synthesis and Performance

5.4.1 Lateral-directional synthesis – The rudder is the only existing control surface that can be used for reduction of lateral accelerations. Forces applied by the rudder are not effective in reducing translational acceleration of the cg, although lateral accelerations aft of the c.g. resulting from angular acceleration can be reduced.

The rudder has much more rotational authority than translational. The problem is evidenced in a root locus as shown in Figure 24. The Dutch roll and spiral modes are shown, closing only the acceleration loop for the cruise condition. The spiral mode rapidly goes unstable as $K_{\ddot{Y}}$ is increased, and is highly unstable at $K_{\ddot{Y}}$ gains required to reduce translation acceleration significantly. The problem is even more severe at the othe; flight conditions. The spiral modes goes unstable faster if the washout frequency is decreased (or the washout is deleted), and slower if the frequency is increased. However, the washout begins to interfere with control of accelerations in the Dutch roll range of frequencies when the washout break frequency is increased above 0.50 rad/sec.

The criterion used for the spiral mode root location was a minimum time to double amplitude of 20 seconds[7]. State differently, the spiral mode root must be less than plus 0.035. The gains shown in Figure 24 reflect the authority of a full span rudder. In the final configuration, with a partial-span RCS rudder, the $K_{\ddot{Y}}$ used corresponds to approximately 1.57 deg/m/sec^2 (0.48 deg/ft/sec^2) in Figure 24. Feedback of yaw rate

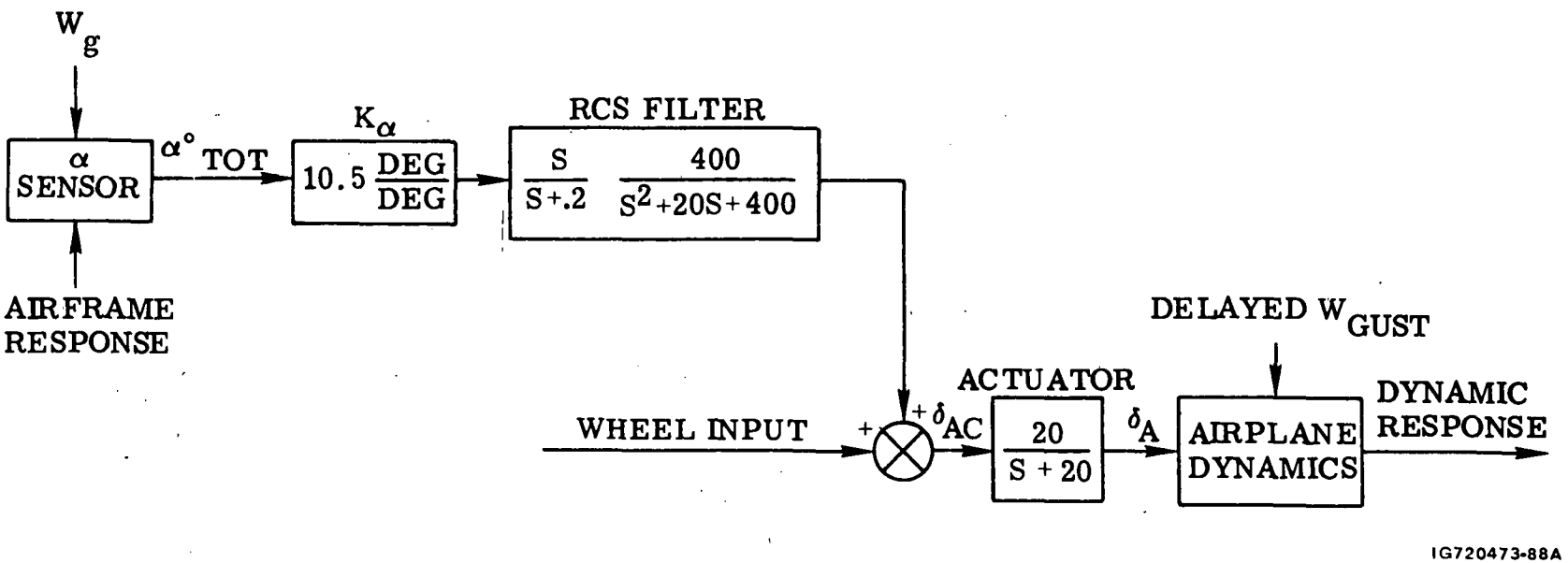

Figure 22: Vertical ride control system - angle of attack sensor

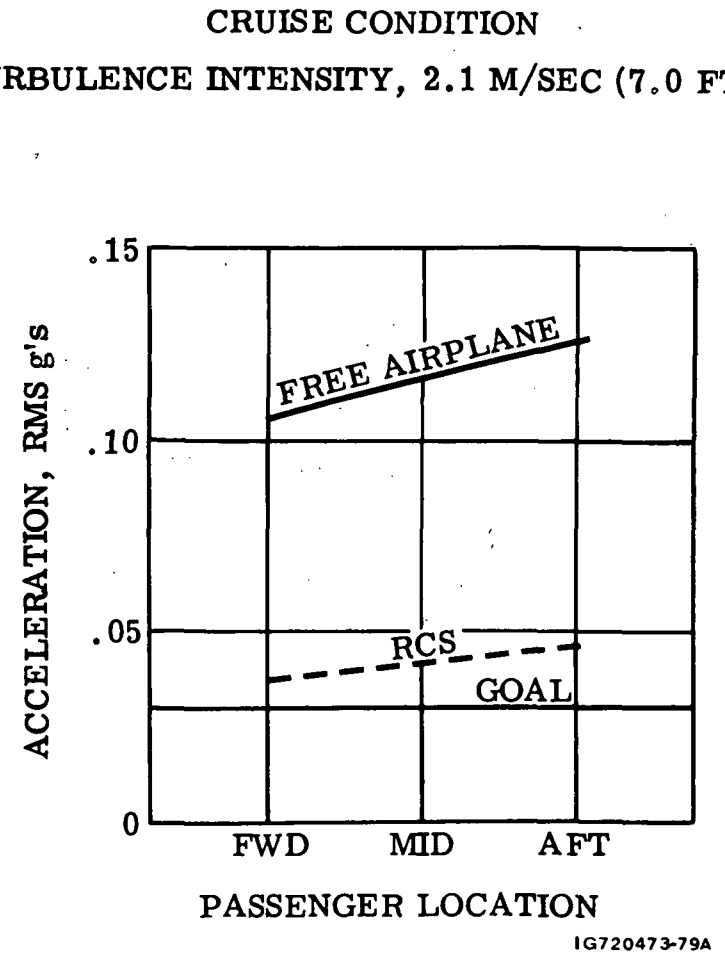

Figure 23: Vertical acceleration-angle of attack sensor

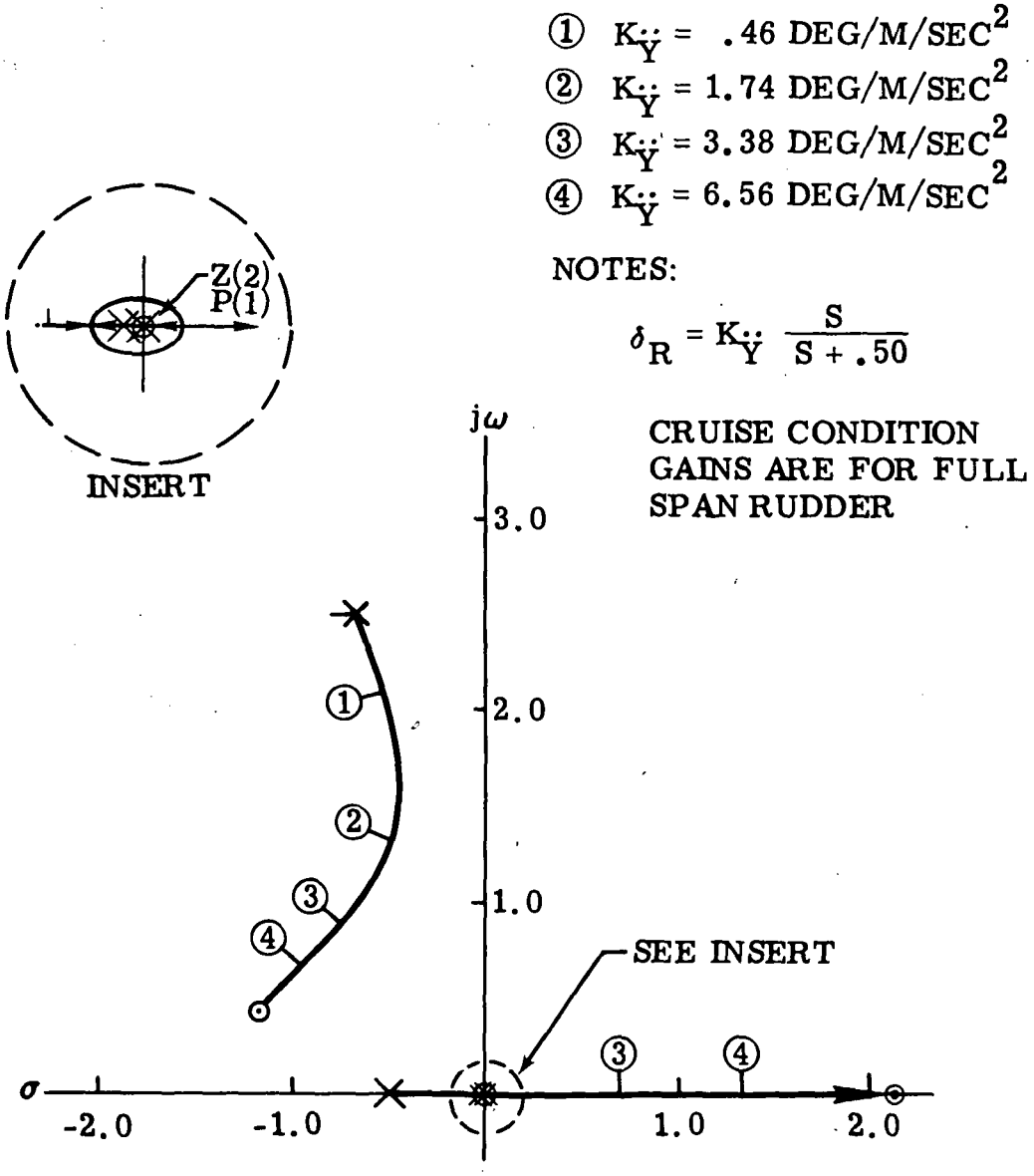

Figure 24: Dutch roll and spiral mode root loci, closing lateral acceleration only

(with proper filtering) tends to restore the spiral stability and increase Dutch roll frequency. However, all attempts to control the spiral mode at higher acceleration gains were unsuccessful. Figure 25 is a block diagram of the final lateral-directional ride control system.

A number of other combinations of feedback filters were tried, as well as feeding back roll attitude to the RCS ailerons, in order to achieve a higher acceleration gain. Generally, in making the spiral mode sufficiently stable with higher acceleration gains, a new, low frequency mode of oscillation is created. The rms accelerations for a full spectrum of frequencies may be increased from those of free the airplane for such systems. However, the power is concentrated at very low frequencies. The lateral acceleration goal could be met, or very nearly so, if accelerations below 0.10 Hertz were excluded. Since this artificially created low frequency mode is unconventional, and its effect on passenger comfort is unknown, the system was not recommended.

5.4.2 Lateral-Directional Performance. –

5.4.2.1 Lateral-directional ride qualities: Lateral acceleration responses to 2.1 m/sec (7.0 ft/sec) random turbulence are presented in Figure 26. The lateral ride control system significantly reduces aft passenger accelerations by reducing rotational acceleration. The cg cannot be translated effectively by a force introduced at the rudder, although translational accelerations are reduced somewhat in the landing condition. A lateral force surface located near the c.g. would be required to achieve the design goal of 0.015 g's. The additional complexity of such a surface was considered impractical for this program.

Figures 27 and 28 compare lateral accelerations for the free airplane and RCS. These figures show aft passenger and pilot station acceleration responses, respectively, to 0.3048 m/sec (1 ft/sec) rms turbulence at the cruise acceleration along with the reduction in rms. Even though the forward station acceleration is increased (reference Figure 26), the frequency is still shifted downward, which may be an improvement in comfort.

Angular acceleration and rate design goals were to maintain airplane responses with the ride control system below corresponding free airplane responses. Table III shows that the RCS roll and yaw rates and accelerations met the goal for all flight conditions.

5.4.2.2 Lateral-directional handling qualities: Existing handling qualities or the requirements of MIL-F-8785B[7] Level 1 for light airplanes, whichever were more stringent, were used as design goals for lateral handling qualities. Table IV presents the comparisons. All root locations meet the MIL-F-8785B levels except the spiral mode time-to-double at the landing condition, which meets existing values.

5.4.2.3 Lateral-directional control surface requirements: Figure 29 shows the RCS control surface rms deflections required by a 2.1 m/sec (7.0 ft/sec) turbulence intensity. The rms

rudder deflections are approximately 3.0 degrees at landing approach and approximately 1.5 degrees for cruise and climb. This indicates that the rudder ride control segment could be reduced, and should be investigated during Phase II.

TABLE III
ANGULAR ACCELERATION AND RATE PERFORMANCE LATERAL SYSTEM

CONDITION – MODE	FREE AIRPLANE	RUDDER RIDE CONTROL OPTION I, II & III
Angular Rate-Yaw, deg/sec^2		
• Cruise	4.0	1.0
• Climb	2.9	1.4
• Landing Approach	3.5	2.7
Angular Rate-Yaw, deg/sec		
• Cruise	1.5	.6
• Climb	1.4	.8
• Landing Approach	2.2	1.2
Angular Accel-Roll, deg/sec^2		
• Cruise	4.4	2.9
• Climb	2.9	2.1
• Landing Approach	3.0	2.3
Angular Rate-Roll, deg/sec		
• Cruise	1.0	.9
• Climb	.9	.6
• Landing Approach	1.5	.7

TABLE IV
LATERAL HANDLING QUALITIES

DESIGN GOALS: REFERENCE MIL-F-8785B

Flight Condition	Dutch Roll Mode				Roll Mode Time Constant (Sec)		Spiral Mode Time To Double (Sec)	
	Damping Ratio (ξ)		Damping Factor ($\xi\omega_n$)					
	Criteria	Actual	Criteria	Actual	Criteria	Actual	Criteria	Actual
Cruise	$\geq$.19	.49	$\geq$.35	1.01	<1.4	.124	>20	Convergent
Climb	$\geq$.19	.50	$\geq$.35	1.10	<1.4	.177	>20	99
Landing	$\geq$.08	.44	$\geq$.15	1.29	<1.0	.241	>Existing (5.24)	5.93

	CRUISE	CLIMB	LANDING APPROACH
$K_{\dot{Y}}$	5.23	5.23	0
$K_{\dot{\psi}}$	.87	1.74	5.23

GAIN SCHEDULING

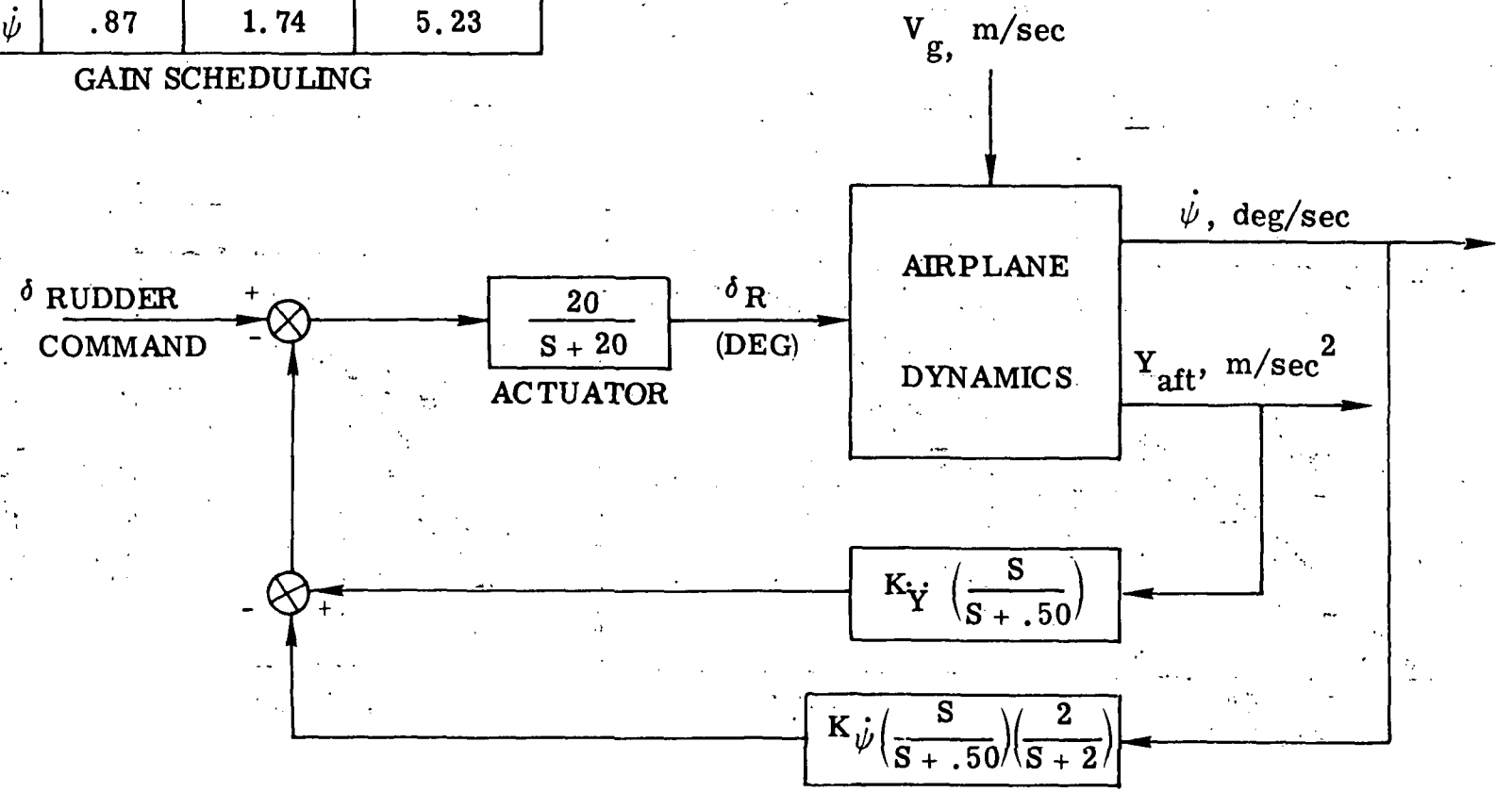

Figure 25: Lateral ride control system

IG720473-87A

TURBULENCE INTENSITY, 2.1 M/SEC (7.0 FT/SEC)RMS

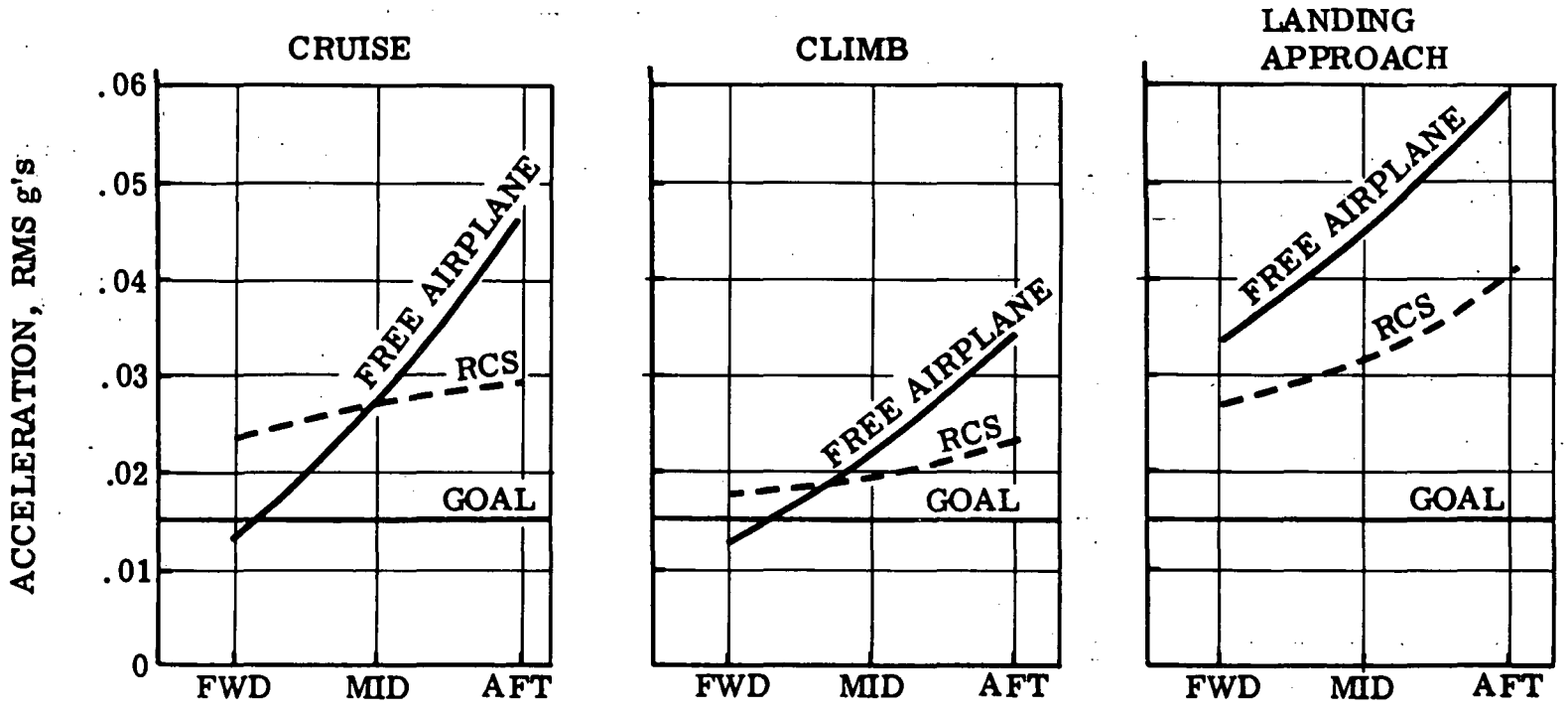

PASSENGER LOCATION - FUSELAGE

Figure 26: Lateral acceleration - rudder RCS

IG720473-85

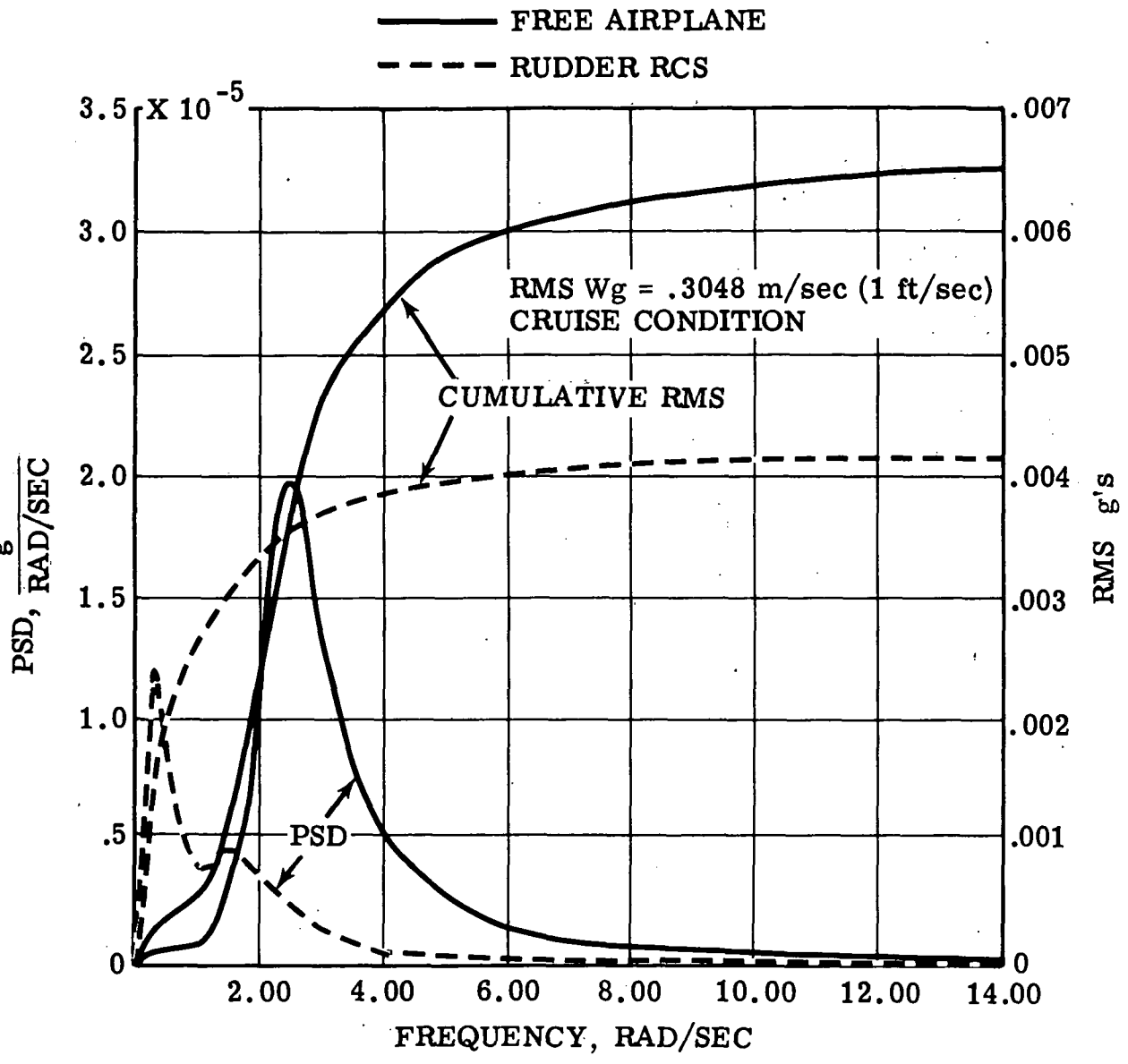

Figure 27: Comparison of free airplane and RCS power spectra of lateral acceleration - aft passenger station

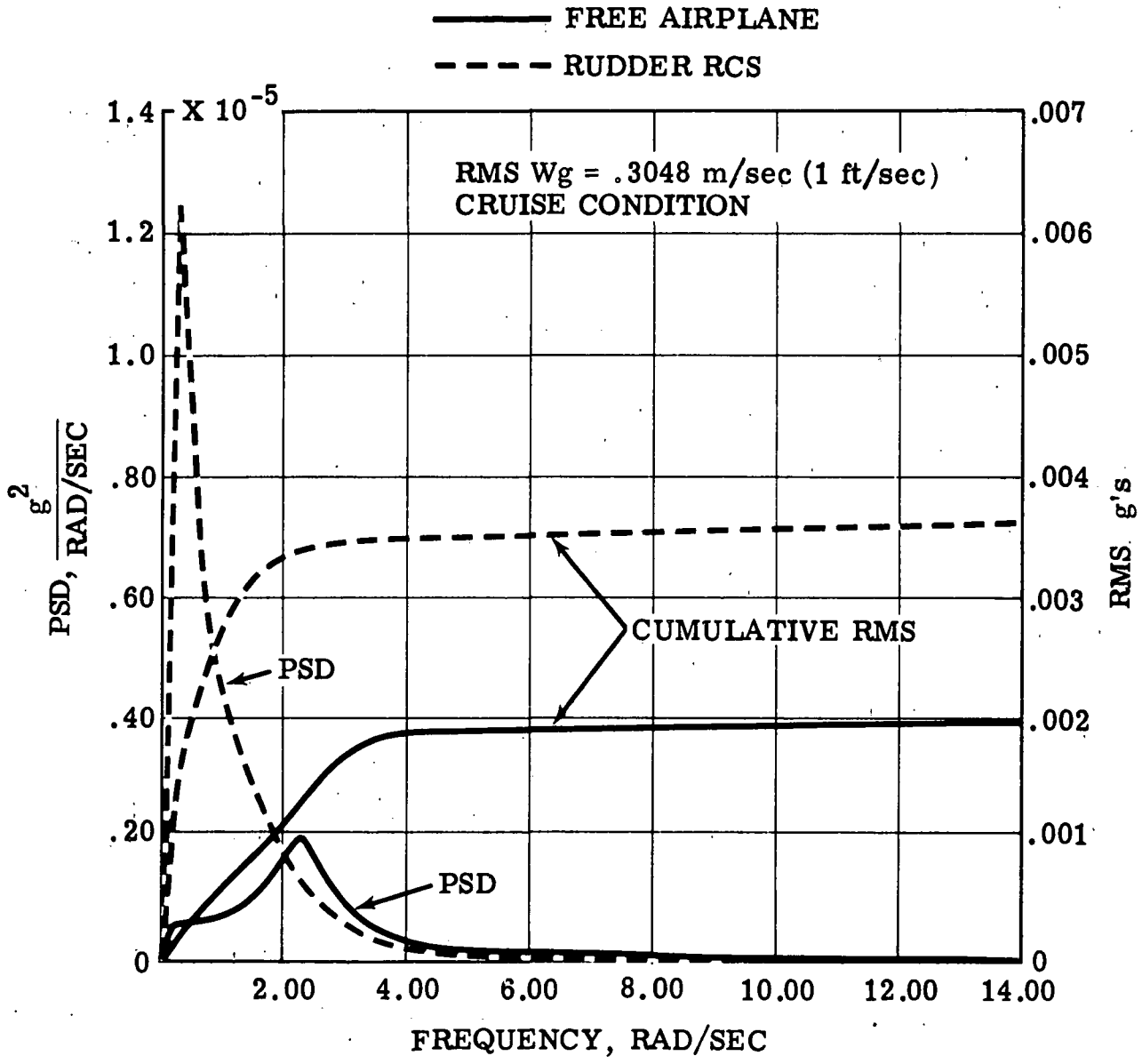

Figure 28: Comparison of free airplane and RCS power spectra of lateral acceleration - pilot station

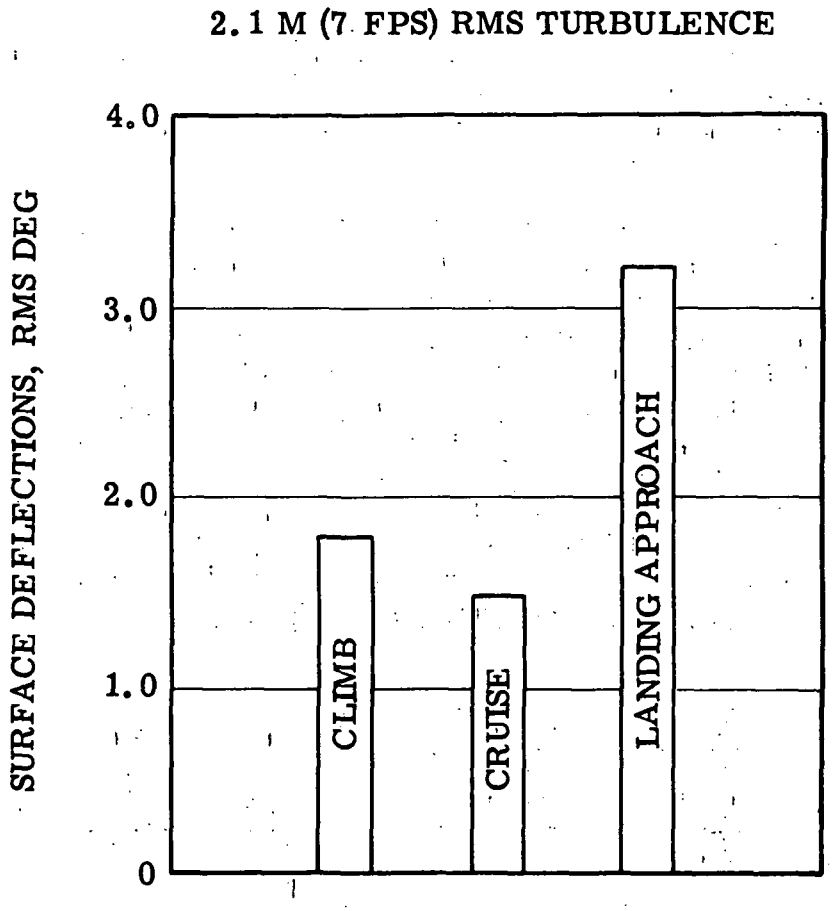

Figure 29: Rudder surface deflections

6.0 PRELIMINARY DESIGN

In addition to the control surface and control system synthesis, preliminary designs were initiated for utility systems, structural modifications, control system mechanisms and electronics.

6.1 Utility Systems

The utility system load requirements were based on those required to supply the more complex Option I configuration. The reduced supply requirements for the less complex configurations would not have a significant impact on the design or costs.

6.1.1 Hydraulic system. Hydraulic system flow rates and capacities were determined by actuator piston area, pressure, monent arm, surface loads, surface rates, number of actuators and number of servo valves. For the preliminary design, average rather than peak rates were utilized for the pump selection since the accumulator can make up short duration demands. The servo valve leakage was based on using an Abex SV2 valve on the aileron system since it requires the maximum rate. Pilot inputs were not included with the ride control inputs since they are expected to be relatively low and are not necessarily additive. The design requirements shown in Table V resulted in the selection of an Abex APO5V-7 engine driven pump. Two such pumps feeding a common reservoir through appropriate check valves will provide undegraded ride control performance following a single pump or engine failure at all but the flight idle power condition. The hydraulic pump capacities are shown on Figure 30.

TABLE V
HYDRAULIC SYSTEM DESIGN REQUIREMENTS

Design Characteristic	Aileron	Elevator	Rudder	Spoiler	SV Leakage	Total
Number of actuators or valves	2	2	1	2	7	–
Actuator area - $m^2 \times 10^6$	180.6	180.6	180.6	180.6	–	–
(in^2)	(0.28)	(0.28)	(0.28)	(0.28)	–	–
Moment arm - m	0.0889	8.0828	0.0889	0.066	–	–
(in)	(3.5)	(3.26)	(3.5)	(2.6)	–	–
Average rate - rad/s	0.873	0.262	0.436	0.524		
(deg/s)	(50)	(15)	(25)	(30)	–	–
Average flow - $m^3/s \times 10^6$	27.9	7.88	7.06	12.4	66.2	121.5
(gal/min)	(0.433)	(0.125)	(0.122)	(0.197)	(1.05)	(1.93)

6.1.2 Electrical system. The current DHC-6 electrical power requirements, exclusive of optional equipment, are shown with the estimated ride control requirements in Table VI. Ample DC power is available. However, there is no margin available on the AC power.

Two additional 75 volt-amp static inverters are required to provide redundant power for the ride control electronics.

TABLE VI
ELECTRICAL POWER REQUIREMENTS

Type	Existing	Present Requirements	RCS Requirement
28V DC	2-200 Amp Generators	150 Amps	1 Amp
115V AC	1-175 VA Inverter	126 VA	49 VA

6.2 Structural Modification

Preliminary structural modification in the form of layout drawings were completed for the aileron, elevator, rudder, and spoiler control surfaces. Surface splits were made at logical separation locations such as ribs and struts. Existing hardware was retained and utilized in the modified system as much as practical. Modified configurations are illustrated in Figures 4, 5, and 6.

6.3 Control System Mechanisms

The split surface control system concept minimizes changes to the flight control linkage and components. Principal features of the required changes have been incorporated into the structural design layouts. The split surfaces were chosen for the feasibility study to provide a simple inexpensive means of manual backup following a system failure.

6.4 Electronics and Control Implementation

The manual mechanical control authority is sufficient to counteract any electrical or hydraulic failure of the powered segment, including hardovers, without switching off the failed system. In addition, electrically separated dual channel electronics are included in this preliminary design to provide fail-soft capability. Trade studies including safety, system reliability, and cost should be accomplished during subsequent design activities to determine redundancy requirements.

Power surfaces will float to a neutral position following loss of hydraulic power, and will be flutter free. Negative structural feedback is provided for all actuators.

The ride control system is connected in series and therefore does not move the pilots' control. Trim systems, connected in parallel, move the primary controls, as in existing airplane configurations.

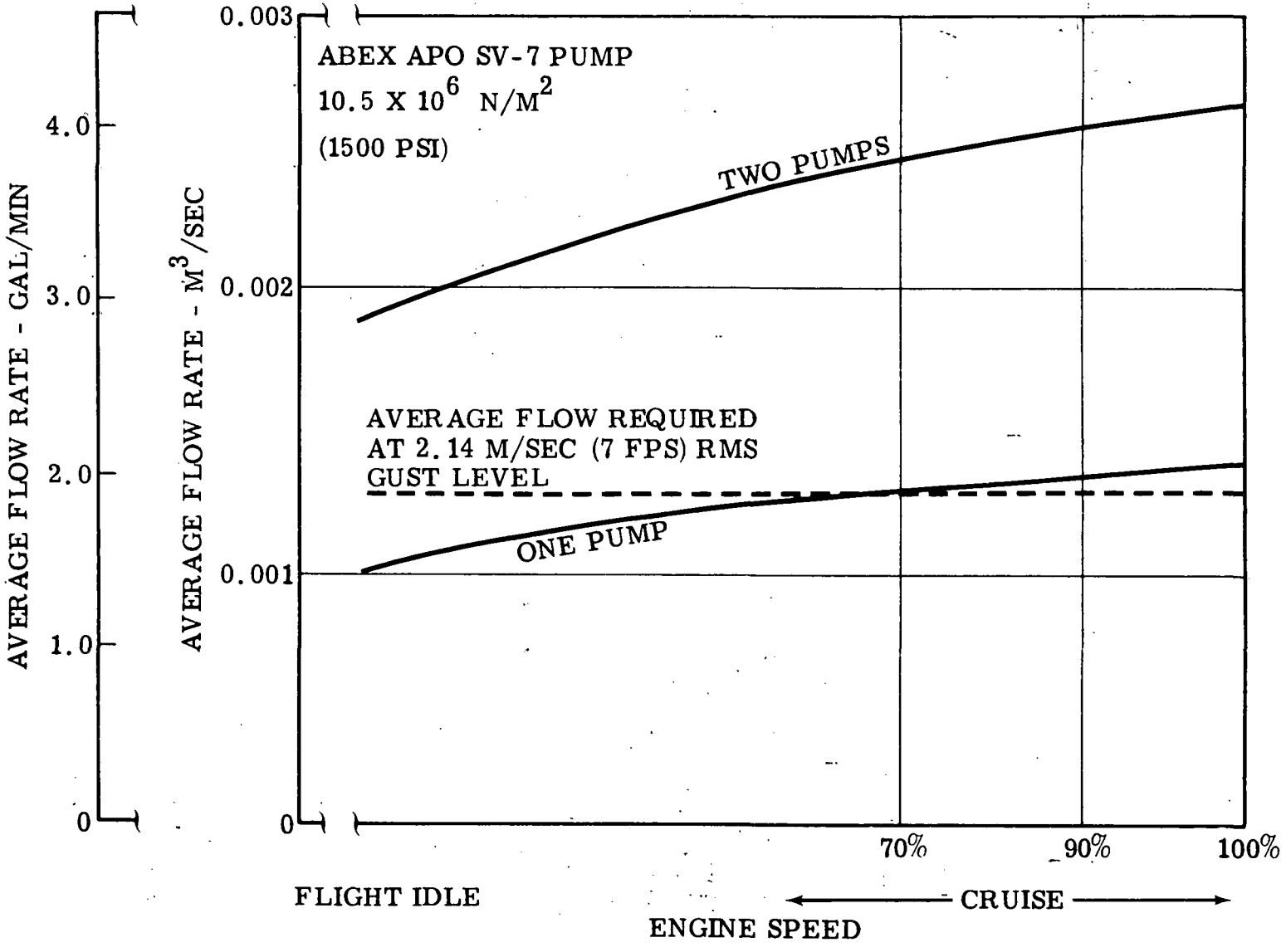

Figure 30: Hydraulic flow capacity

Figures 31 through 34 are implementation block diagrams of the rudder, elevator, aileron, and spoiler control systems, respectively. The primary control surfaces are split spanwise into two segments, with RCS feedback to one segment and with pilot authority over both. The manually controlled segments are controlled through existing mechanisms. Each RCS segment is controlled by an electrohydraulic actuator that receives electrical position command signals from two sources: pilot manual commands and ride control commands. These two signals are summed in the valve drive amplifier. Pilot manual commands to the RCS surfaces are sensed by LVDT's attached to manual control linkages.

Yaw rate and lateral acceleration, sensed at the aft passenger location, are gain scheduled, filtered and summed to form the lateral ride control command signal to the 30 percent RCS rudder segment. The fail-soft preliminary design control system contains dual signal channels with two stages of monitoring between channels for failure detection. An electronics monitor channel is compared to the primary channel, and an unfavorable comparison switches off the ride control signals. Following such a failure, the pilot retains control of both rudder segments.

A second logic circuit compares actuator position to an electronic model of the actuator dynamics. A failure detection in this circuit switches off hydraulic power to the actuator. The pilot then controls the airplane through the lower, 70 percent span rudder segment.

The inboard 80 percent segments of the elevators are bussed together are controlled through existing elevator mechanisms. The elevator control system, similar to the rudder control system, consists of the segmented surfaces, dual channel electronics, and two stages of failure detection. Pitch rate constitutes the ride control feedback to the elevators. Left and right hand powered segment positions are compared; therefore, an actuator model is not required.

The aileron control system is similar to the rudder and elevator systems with manual and ride control commands superimposed on the electrohydraulically powered segment. Manual inputs to the ailerons accomplish roll control with differential deflections. Vertical ride control is accomplished by symmetrical deflection of the 40 percent powered aileron segments commanded by vertical acceleration sensed at the cg. Manual inputs are subtracted for comparison of left and right hand actuator positions.

Spoiler control surfaces are added for vertical ride control in the landing approach flight phase. When active, the spoilers deflect from a biased position. Spoiler bias is commanded by the flap actuator, with a dead-zone between flap deflection and the bias. The specific amplitude of the dead-zone will be determined in subsequent work. An override activated by the throttles may be required to prevent spoiler bias during takeoff or "go-around". The spoilers are deflected symmetrically to augment the ailerons for direct lift ride control during landing approach and are commanded by the same feedback. Feedback gain is varied as a function of spoiler bias so that commanded deflections are smaller than the bias.

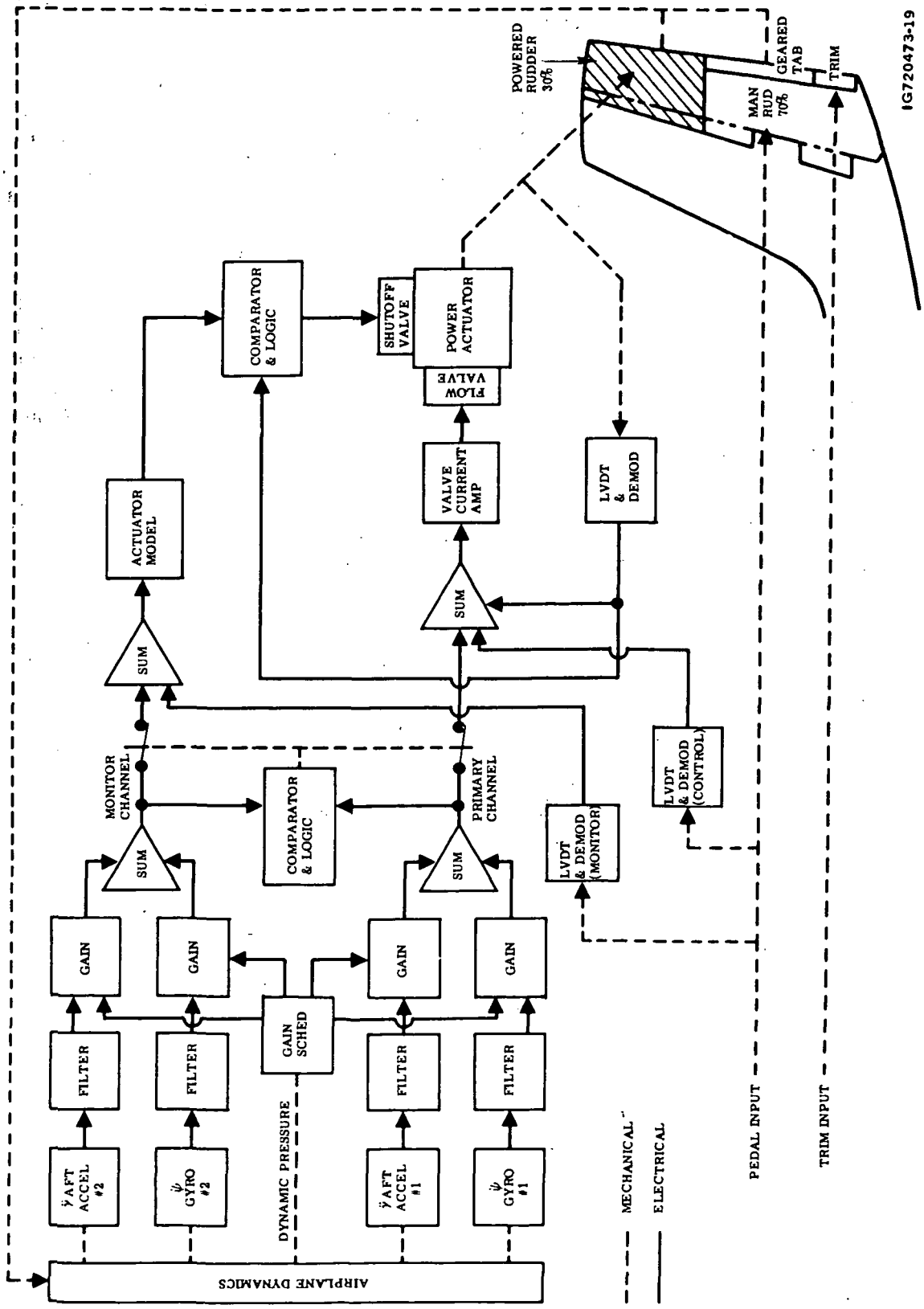

Figure 31: Rudder control system

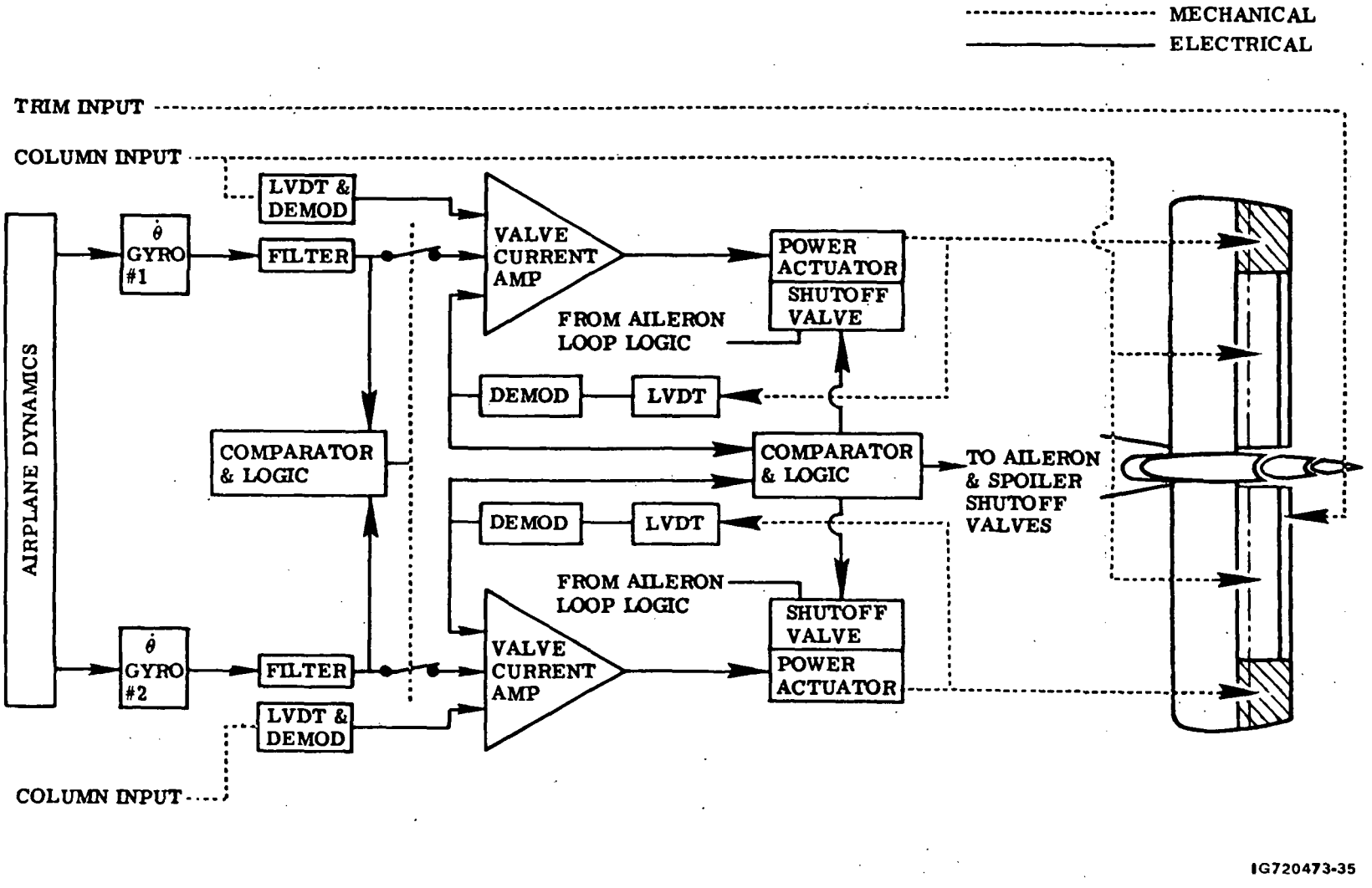

Figure 32: Elevator control system

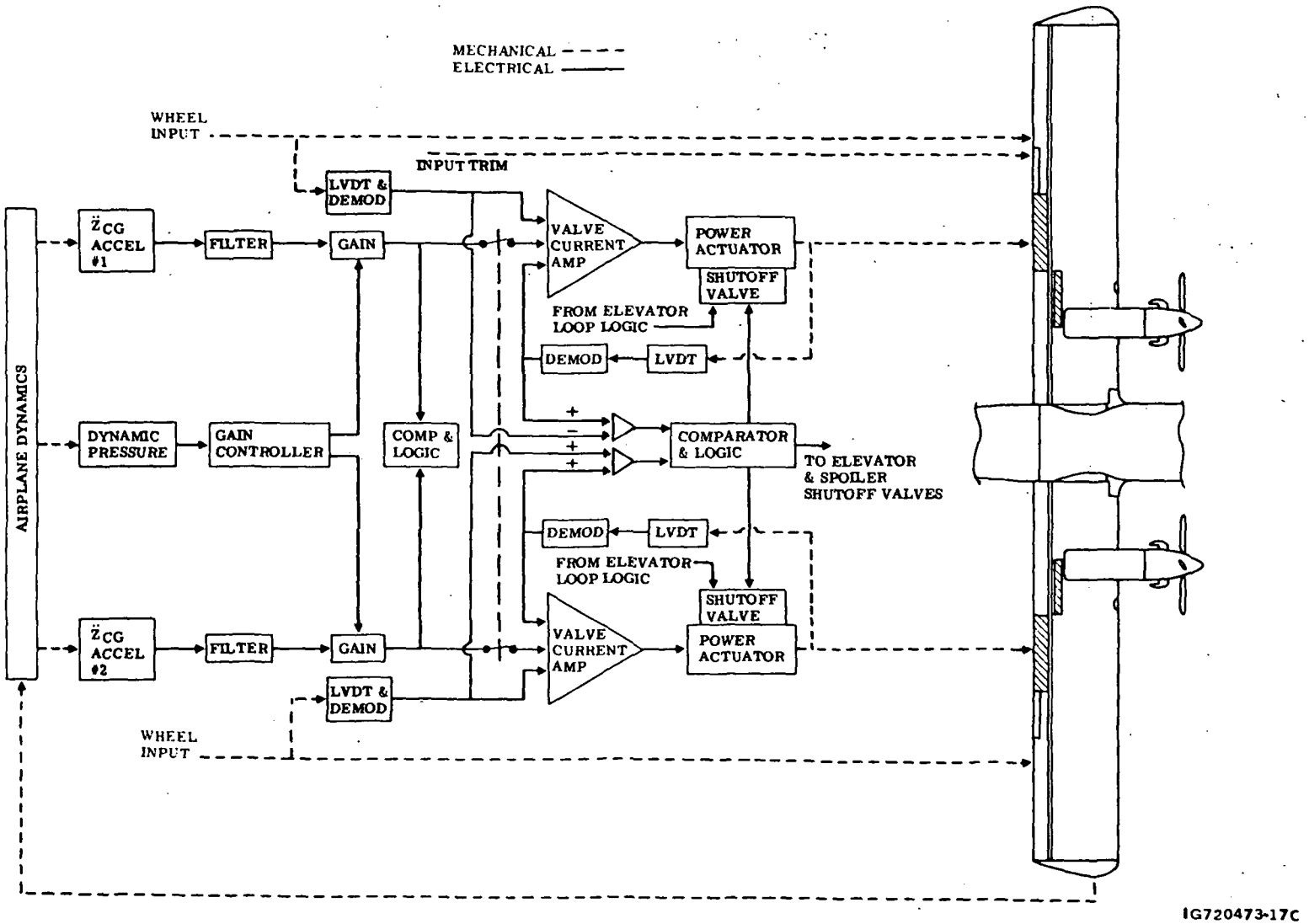

Figure 33: Aileron control system

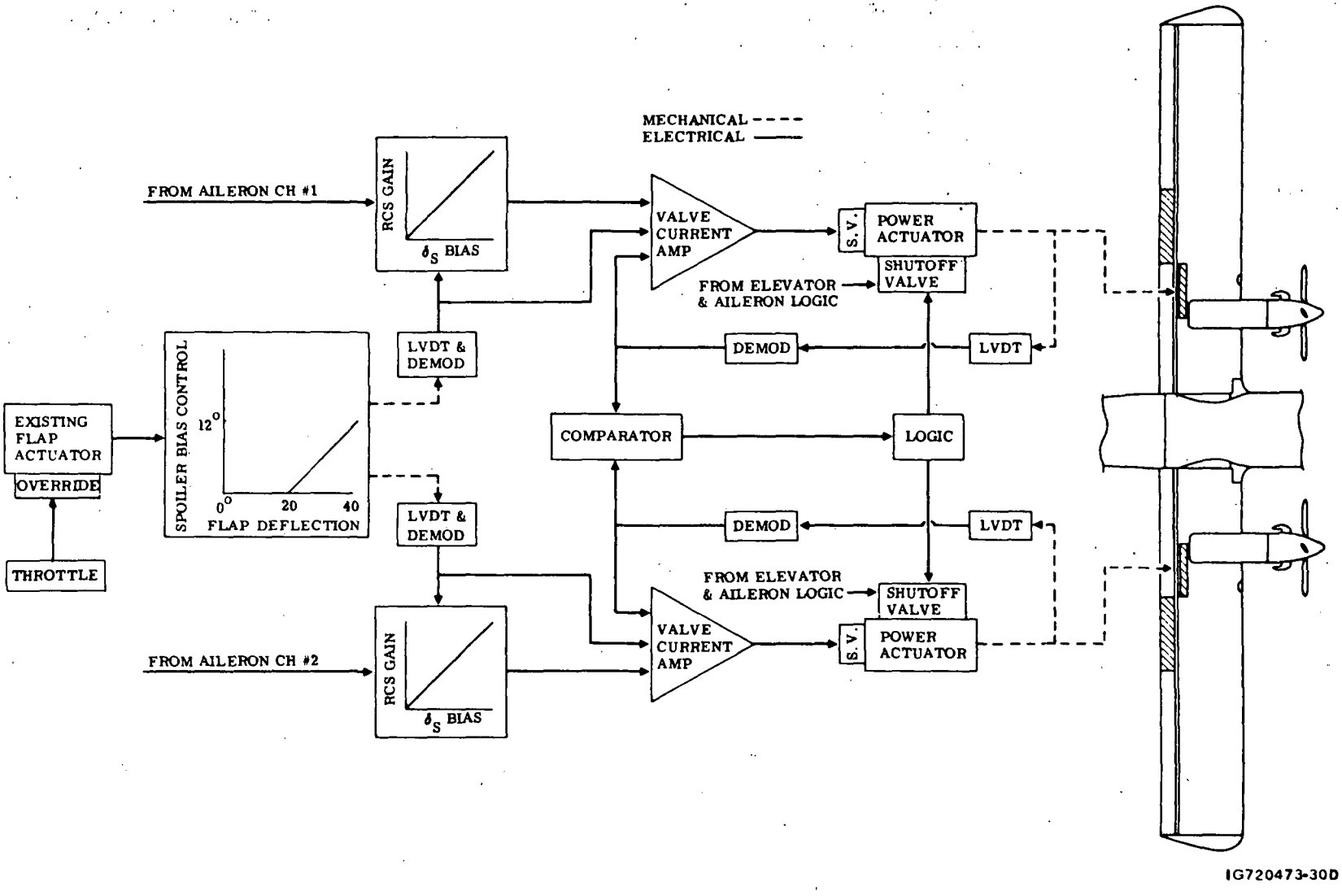

Figure 34: Spoiler control system

6.5 Hardware Location and Weight Distribution

The ride control hardware locations are shown in Figures 35 and 36. Conservative weight estimates for the ride control system are presented for the various options in Table VII.

TABLE VII
RIDE CONTROL SYSTEM WEIGHT ESTIMATES – NEWTONS (POUNDS)

OPTION	I	II	III	IV	V
Description	Aileron Elevator Rudder Spoiler	Same as I with α Sensor	Aileron Elevator Rudder	Aileron Elevator	Aileron
Structural	200 (45)	200 (45)	133 (30)	93.4 (21)	66.7 (15)
Actuators	311 (70)	311 (70)	222 (50)	178 (40)	89 (20)
Hydraulics	245 (55)	245 (55)	222 (50)	200 (45)	178 (40)
Electrical	142 (32)	142 (32)	133 (30)	116 (26)	98 (22)
Electronic & sensors	129 (29)	129 (29)	125 (28)	107 (24)	98 (22)
Angle of attack Boom	–	66.7 (15)	–	–	–
Total	1 029 (231)	1 094 (246)	835 (188)	694 (156)	530 (119)

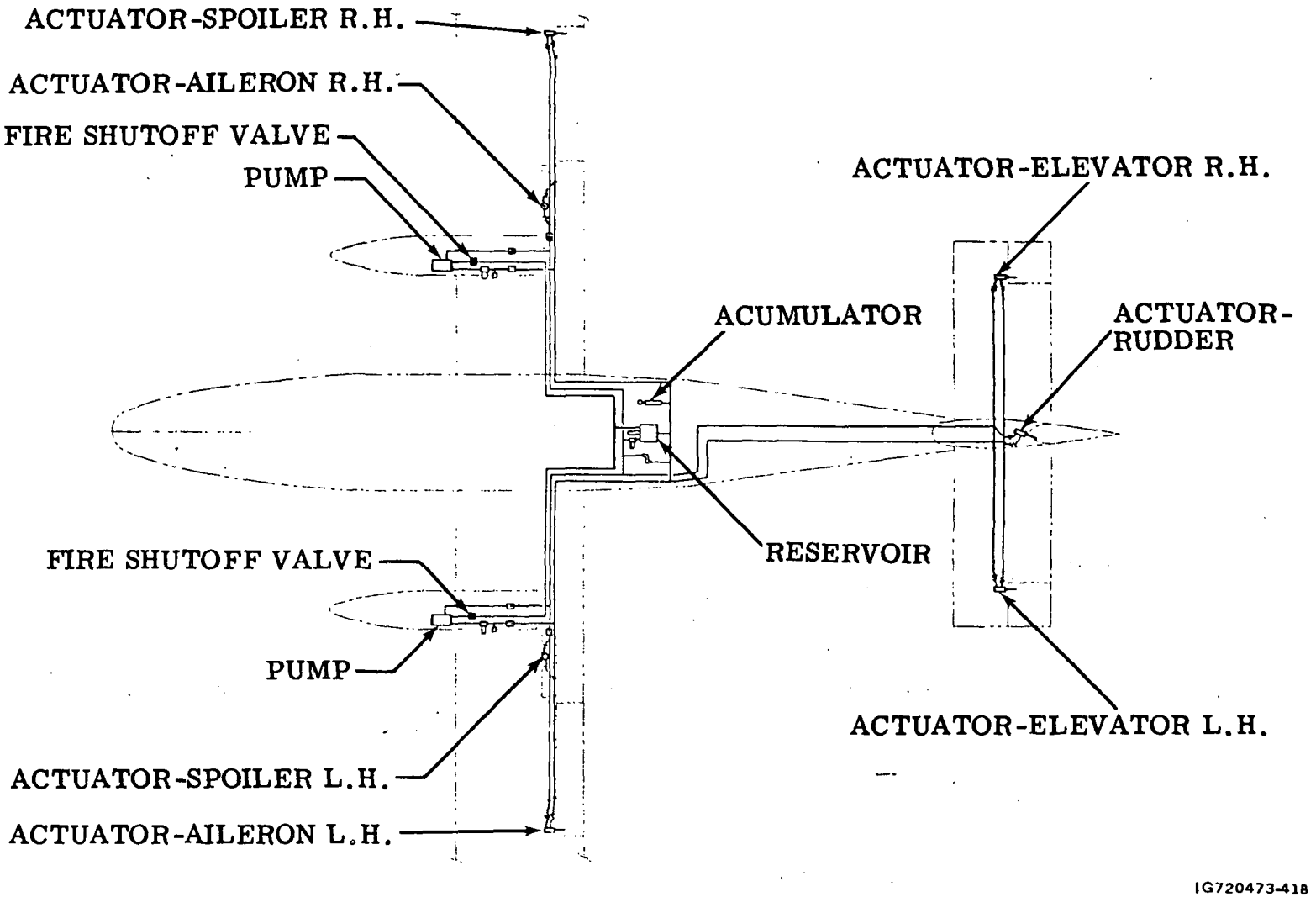

Figure 35: Major hydraulic component location

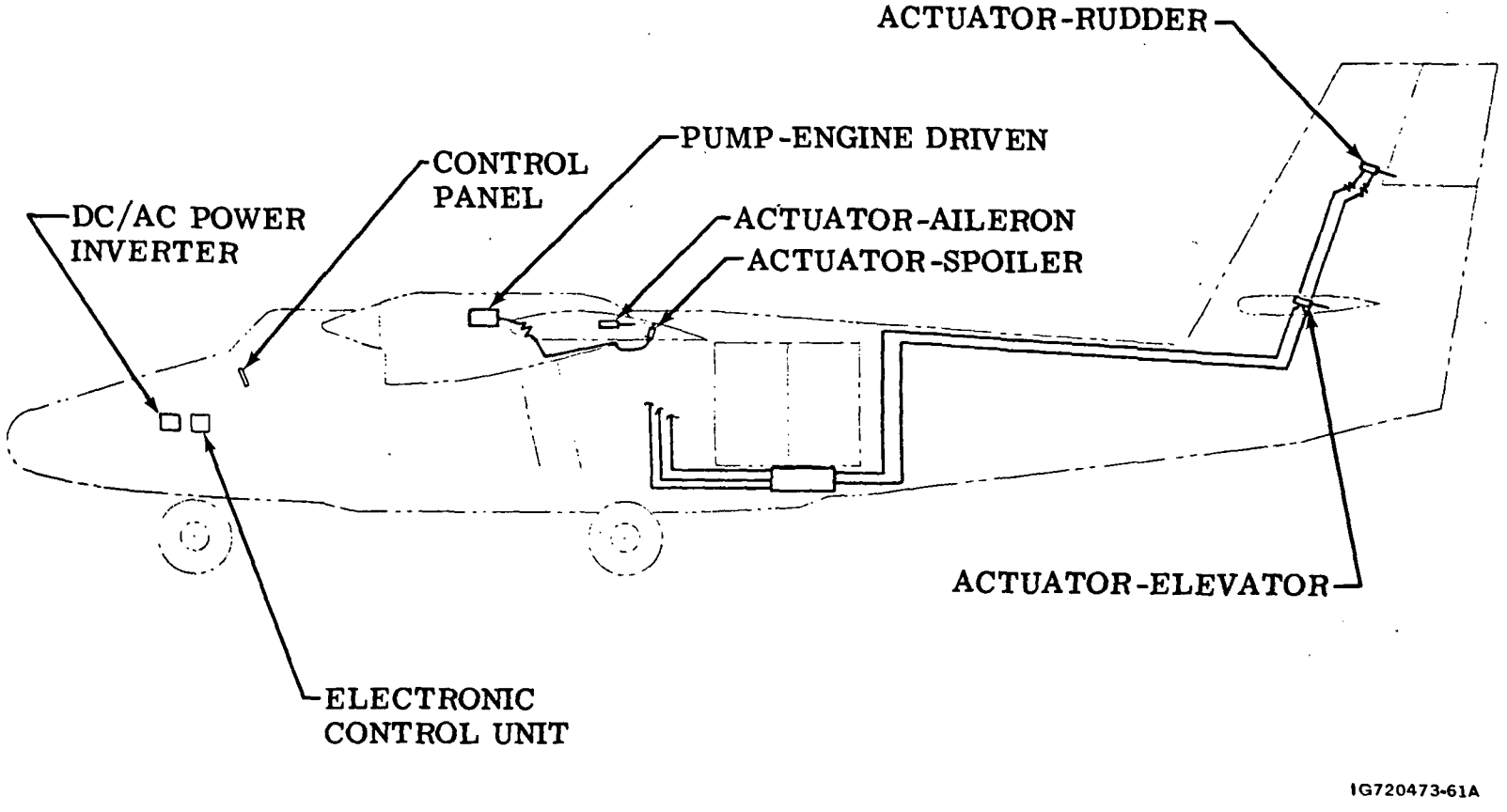

Figure 36: Ride control hardware locations

7.0 AERODYNAMIC ANALYSIS AND TRADES

The full span aft flap segment and aileron were initially considered for vertical ride control surfaces. However, the aft flap segment was ineffective as a ride control surface during the landing approach with 40 degrees of flap deflection. Preliminary estimates indicated that the authority of the ailerons was adequate to meet the acceleration goal during climb and cruise, but not during landing. Aerodynamic trade studies were conducted among methods of supplementing the ailerons during landing. Methods investigated were (1) increasing the aileron chord, (2) varying the fore flap gap and (3) addition of spoiler surfaces. Spoilers wwere chosen in the preliminary design.

The existing DHC-6 Twin Otter flap configuration is shown in Figure 37. The Twin Otter has double-slotted flaps extending to 44.2 percent semispan. Outboard of this station are the droop ailerons attached to a slotted fore-flap which deflects when the flaps are extended. In the extreme 40 degree flap position the inboard fore-flap is deflected 40 degrees and the aft flap segment about 60 degrees with respect to the wing chord plane. The outboard fore flap and aileron are deflected 26 degrees.

The inboard aft flap effectiveness, including effects of the propeller slip stream on the flap at the low thrust level during landing, is shown in Figure 38, for the landing condition.

When the flap deflects beyond the nominal position the incremental lift begins to decrease, so that this surface is unacceptable for ride control during this condition. Since the outboard aileron is deflected only 26 degrees at this condition, it does not have this characteristic. However, the effectiveness of the aileron is not sufficient to meet the ride quality goal during landing, so that an auxiliary ride control surface is required.

The effectiveness of a large chord on the outboard aileron was considered. The effect of an aileron chord extension is shown in Figure 39. The present aileron is a 17 percent chord surface. Increasing the aileron chord to 34 percent will gain about 20 percent effectiveness above the present aileron. To meet the vertical acceleration goal at landing will require two to three times the present aileron effectiveness.

The effect of varying the fore flap gap was also investigated as a possible auxiliary force producing method. Effectiveness of this method from reference 11 is illustrated in Figure 40. Varying the Twin Otter fore flap gap about the nominal does not produce appreciable incremental lift, so that this method was unacceptable for a ride control surface.

A biased hinged flap type spoiler was then considered for an auxiliary ride control surface. The spoiler has good effectiveness and incremental lift characteristics when deflected from a bias position. The incremental lift characteristics of the spoiler chosen for the Twin Otter ride control system is shown in Figure 41. During the landing approach condition the biased, 10 percent chord, 17 percent semispan, hinged flap type spoiler is required with the aileron to approach the 0.03 g vertical acceleration goal. The spoiler is biased at about 12 degrees and deflected $\pm$ 10 degrees for the ride control system inputs. During the climb and cruise conditions the spoiler is not required.

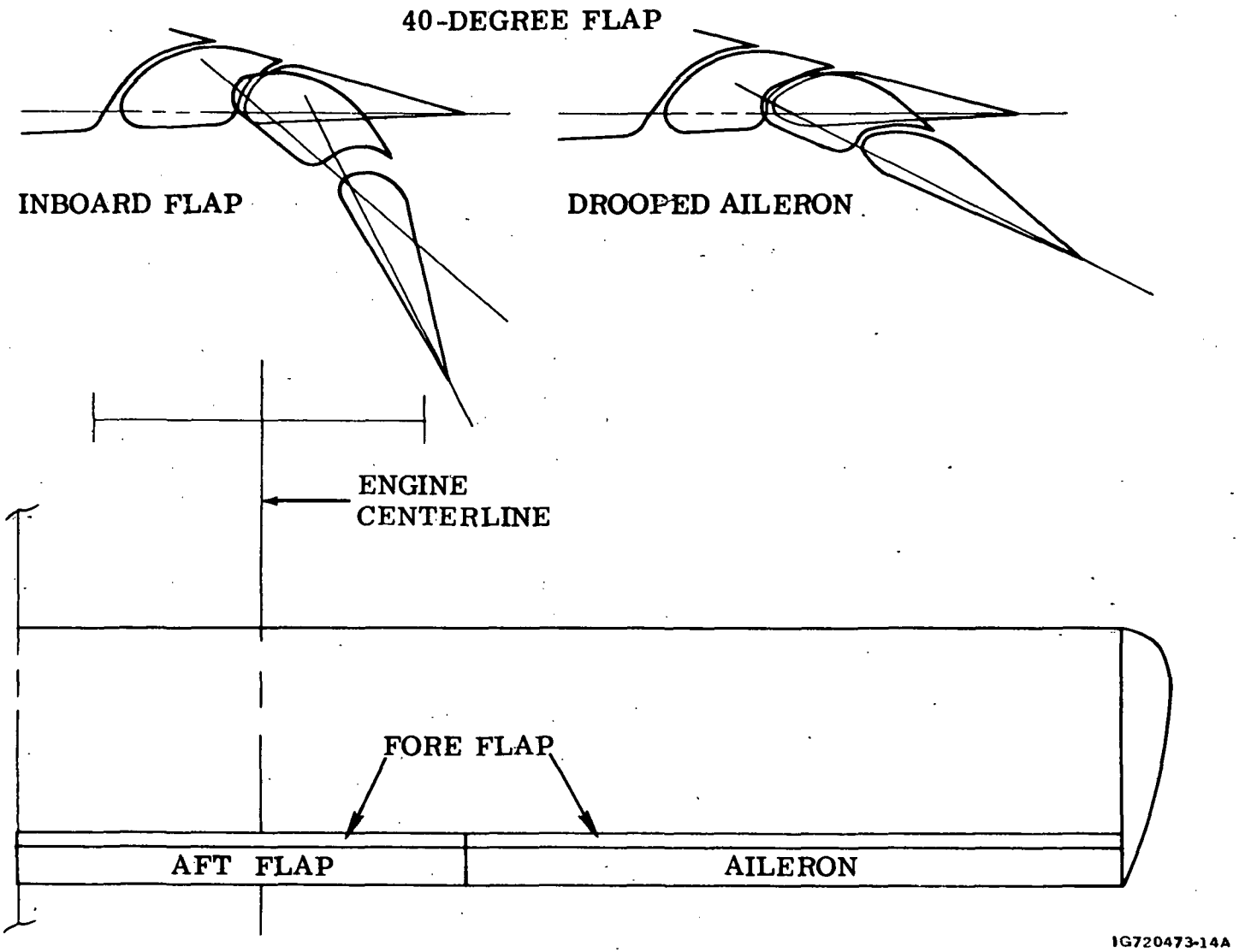

Figure 37: Present flap configuration

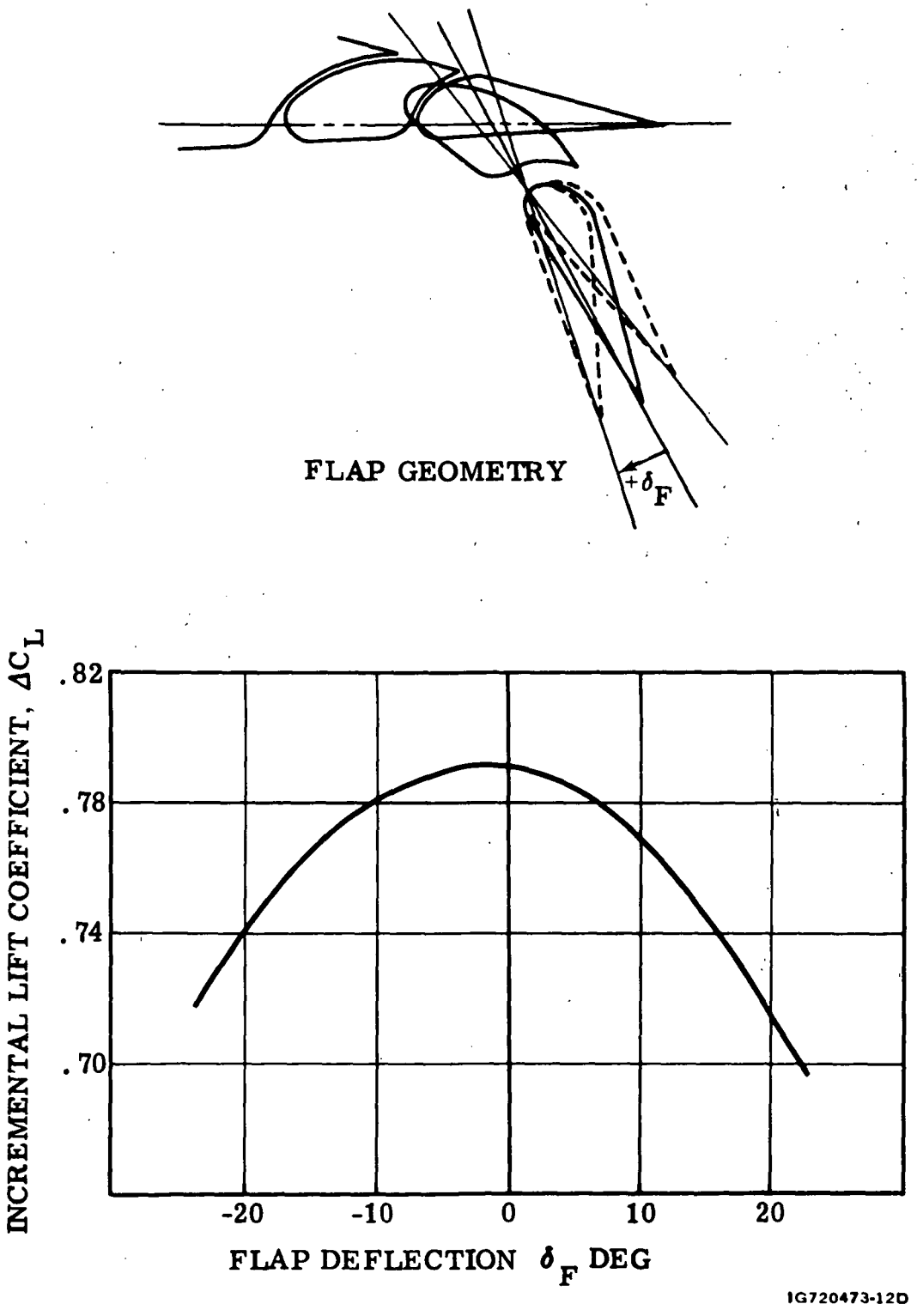

Figure 38: Inboard aft flap effectiveness - 40° flap

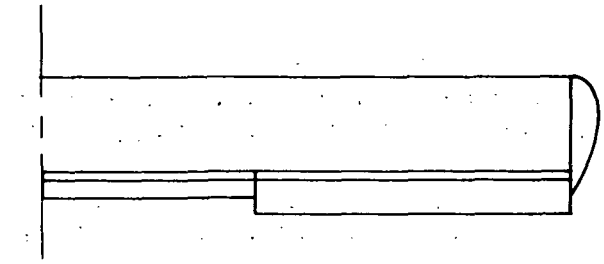

PROPOSED AILERON EXTENSION

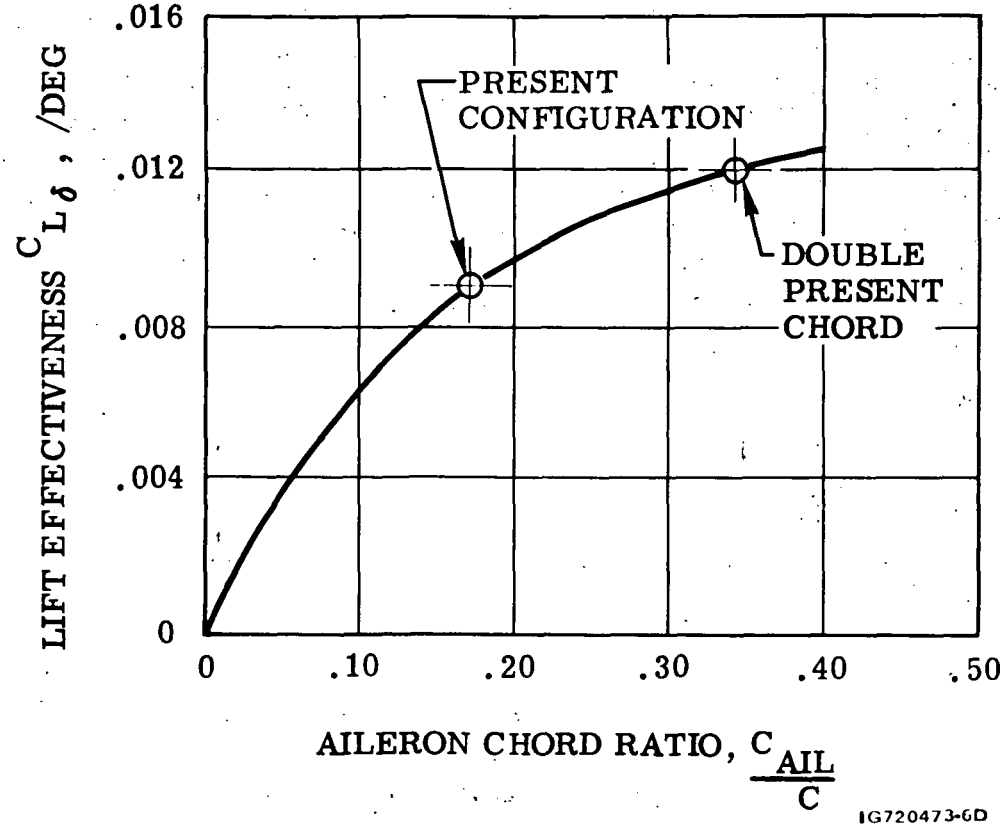

Figure 39: Aileron chord extension effectiveness - 40° flap

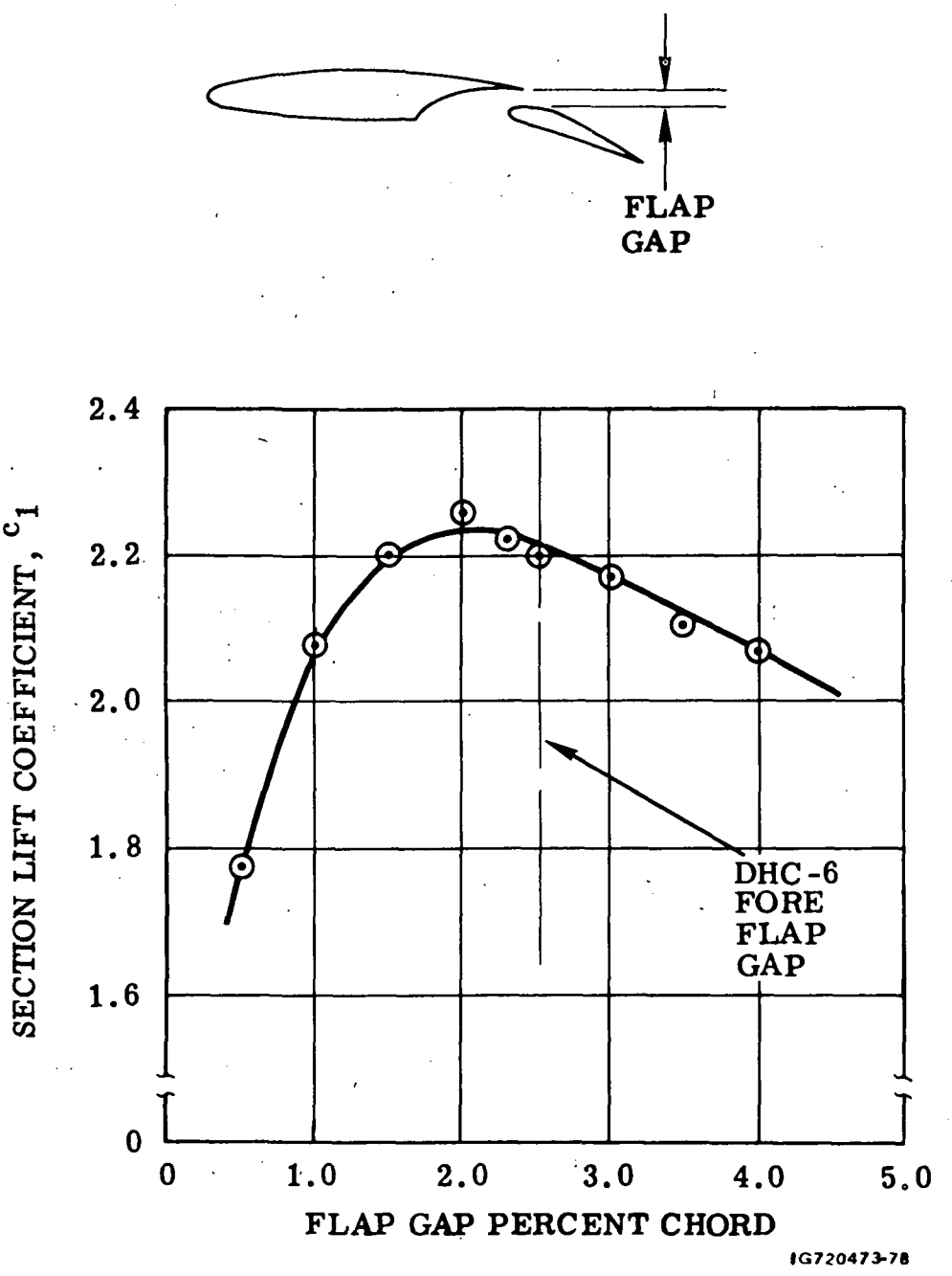

Figure 40: Flap gap effectiveness

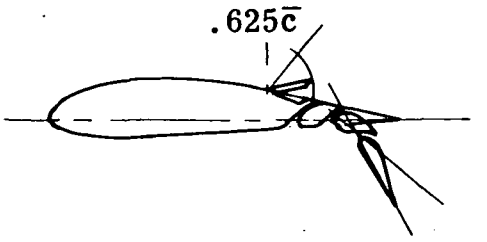

HINGED FLAP
SPOILER CONFIGURATION

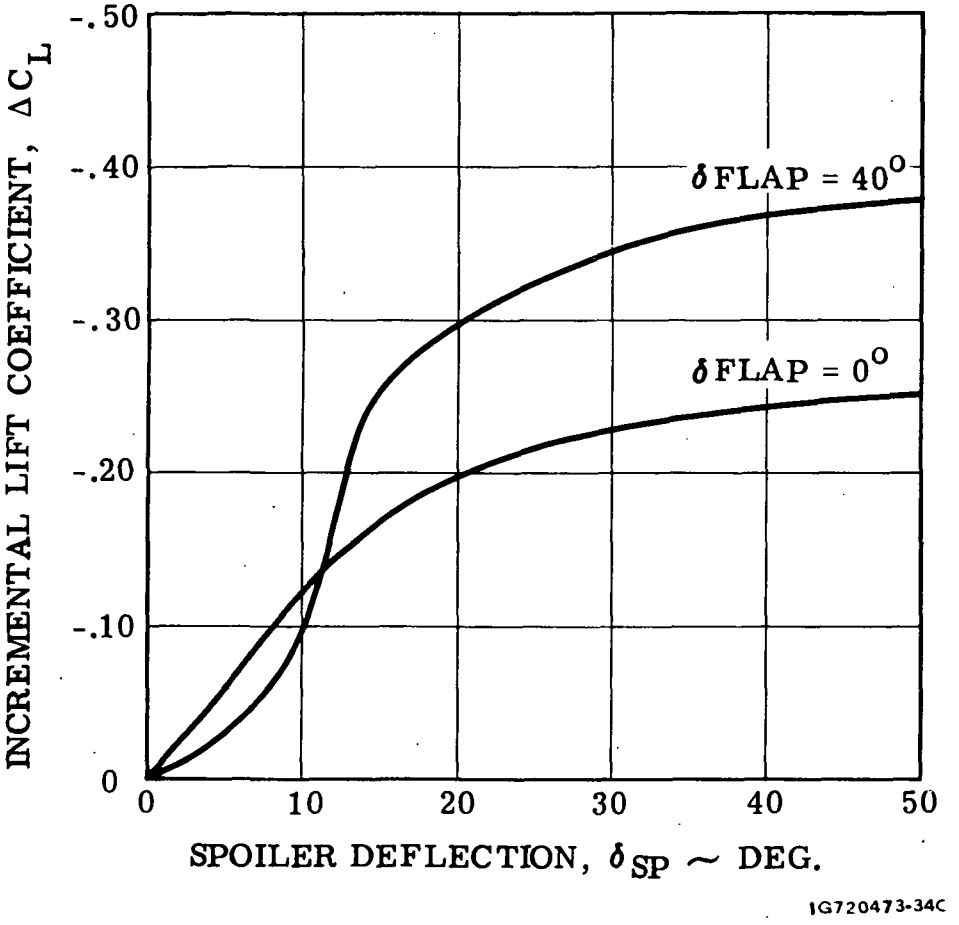

Figure 41: Three dimensional lift effectiveness for a .17 semispan, .10 chord spoiler

The spoiler incremental lift and moment characteristics on the Twin Otter wing were estimated using the technique in Reference 12 and wind tunnel data from Reference 13. The two-dimensional spoiler characteristics with zero degree flap were estimated using the method established by Barnes[12]. The two-dimensional lift characteristics with 40 degree flap were then obtained by using wind tunnel data in Reference 13, and correcting the zero flap estimate. The three-dimensional data was obtained by strip integration of the two-dimensional data over the spoiler span. Propeller slipstream effects on the spoiler were not considered due to the very low thrust setting during the landing approach condition.

The location of the outboard edge of the spoiler was limited by the inboard edge of the aileron so that the aileron effectiveness would not be disturbed. The inboard edge of the spoiler was determined from buffet and pitch trim effects due to the spoiler wake affecting the flow over the horizontal tail. Location of the spoiler on the Twin Otter wing is shown in Figure 42.

The elevator required to trim symmetrical spoiler deflection is presented in Figure 43. Data are presented for the forward cg limit (0.2$\bar{c}$), the aft cg limit (0.36$\bar{c}$) and the cg for the three study conditions. The pitching moment due to the spoiler deflection was determined from the spoiler incremental lift center of pressure and drag estimates. For the extreme cg conditions, 0.5 to 0.6 degrees of elevator will be required to trim the pitching moment due to the symmetrical spoiler deflection at the bias position.

The effect of the 12 degree spoiler bias on the Twin Otter stall speed will be from zero to a 3.5 percent increase in stall speed, depending on how the biased spoiler affects the stall characteristics of the Twin Otter wing. At most, the $C_{L_{max}}$ will be decreased by the incremental C_L at the bias position in Figure 41. This corresponds to a 3.5 percent increase in stall speed for the 40 degree flap landing condition.

The aileron authority required for manual backup was determined using MIL-F-8785B[7] as a guide. This reference specifies roll authority requirements in terms of time of bank. Using the Twin Otter roll time constant at the landing condition, the Level 1, 2 and 3 requirements were converted to roll helix requirements. These levels are shown in the plot in Figure 44.

For the landing flight condition the present Twin Otter aileron meets the Level 1 roll helix requirement. Roll authority data were not available for a portion of the present aileron span, thus the partial span control authority was estimated. Although the calculated roll helix for the total aileron does not coincide with the actual value (analysis data substantiated with flight test data), the computed roll helix is conservative. To meet a Level 3 requirement, the outboard 60 percent of the present aileron span is required for manual backup.

The amount of elevator authority required for manual backup was determined from trim requirements at the critical flight conditions. The elevator required to trim an aft cg (0.36$\bar{c}$), 40 degrees flap, power off condition and a forward cg (0.2$\bar{c}$) flaps up power off condition is shown in Figure 45.

The present elevator required to trim the flaps up, forward cg, power off, $C_{L_{max}}$ is about -20 degrees, trailing edge up. The critical condition for the the trailing edge down deflection is 40 degree flap, aft cg, power off, and minimun C_L. This requires about 15 degrees trailing edge down. The present elevator deflection limits are -25 degrees trailing edge up and 16 degrees trailing edge down. Increasing the maximum trailing edge down deflection to 20 degrees allows 80 percent of the present elevator for manual backup.

A rudder structure assembly break and the ride control system lateral acceleration requirements determined the percentage of present rudder span to be used for manual backup. Following a hydraulics failure the reduced rudder authority will decrease crosswind capability from 12.35 m/second (24 knots) to about 8.75 m/second (17 knots) for the 40 degree flap, 35.68 m/second (70 knots) landing approach condition.

The minimum directional control speed for the total rudder is 33.64 m/second (66 knots) and 39.63 m/second (77 knots) for the manual portion of the split rudder as shown in Figure 46. Takeoff speed with 10 degree flap maximum gross weight is 41.69 m.second (81 knots). However, a double failure (hydraulic power and engine) would have to occur to increase the minimum control speed from 33.64 m/second (66 knots) to 39.63 m/second (77 knots).

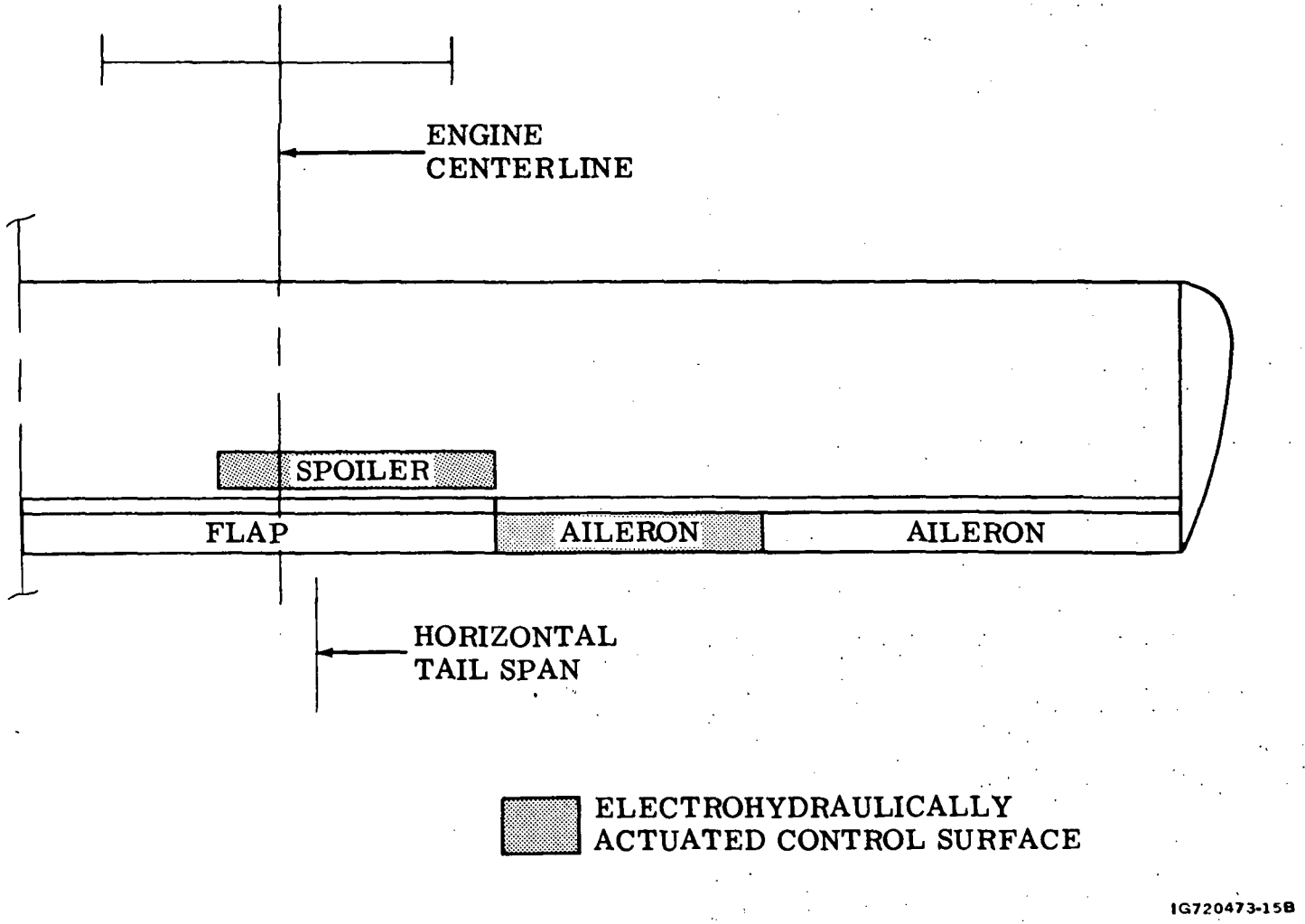

Figure 42: Aileron and spoiler locations

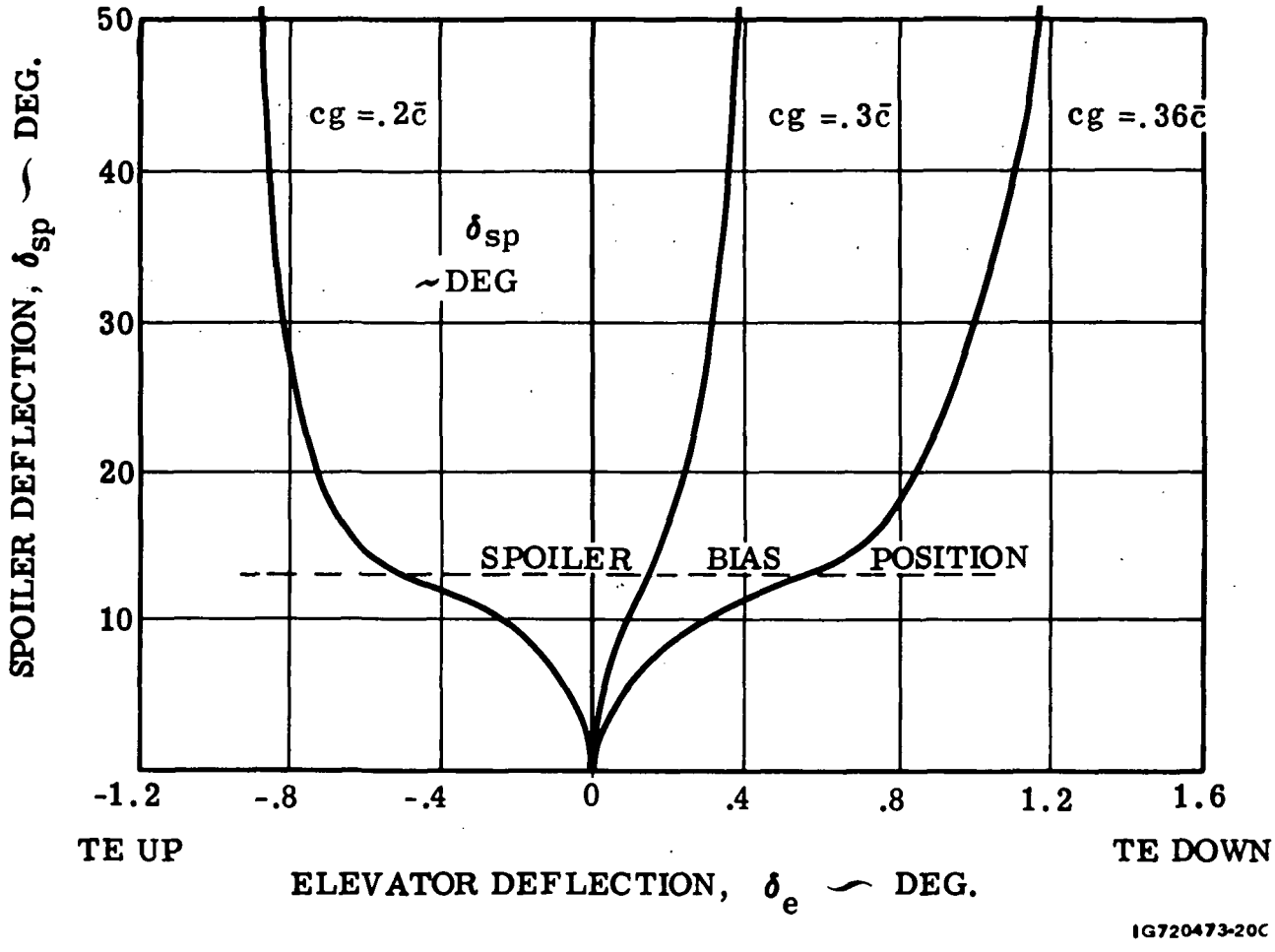

Figure 43: Elevator required to trim symmetrical spoiler

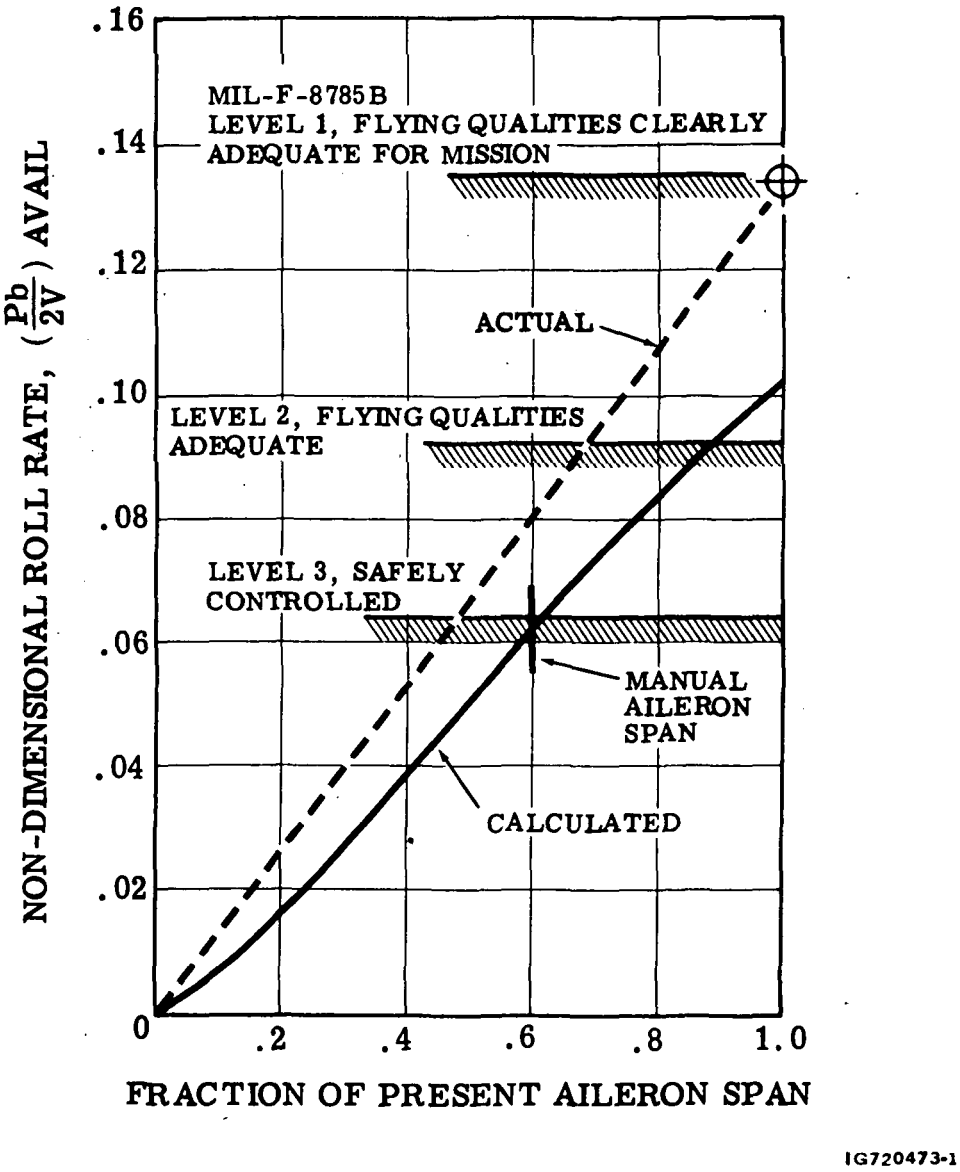

Figure 44: Aileron required for manual backup - landing condition

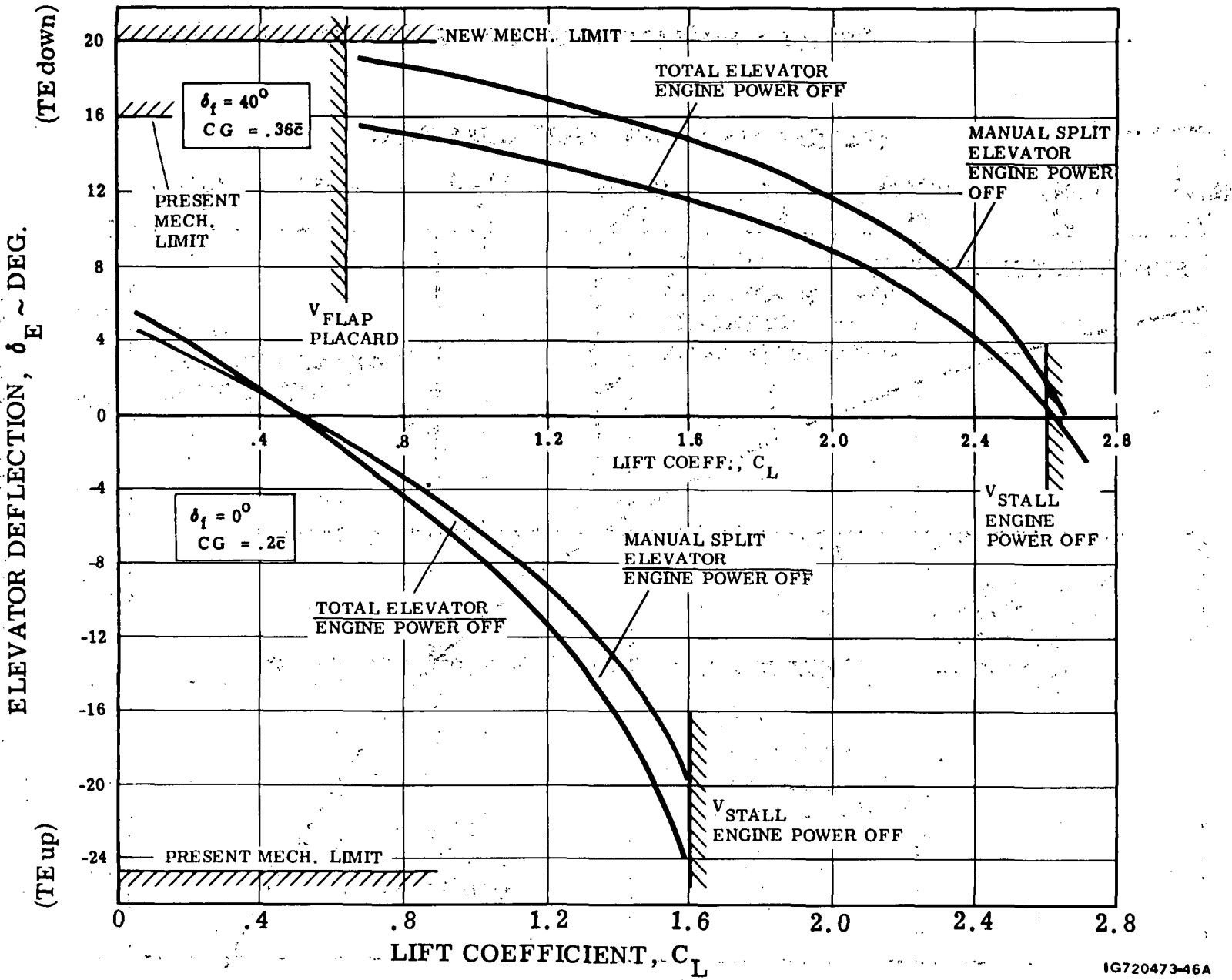

Figure 45: Elevator required to trim - critical flight condition

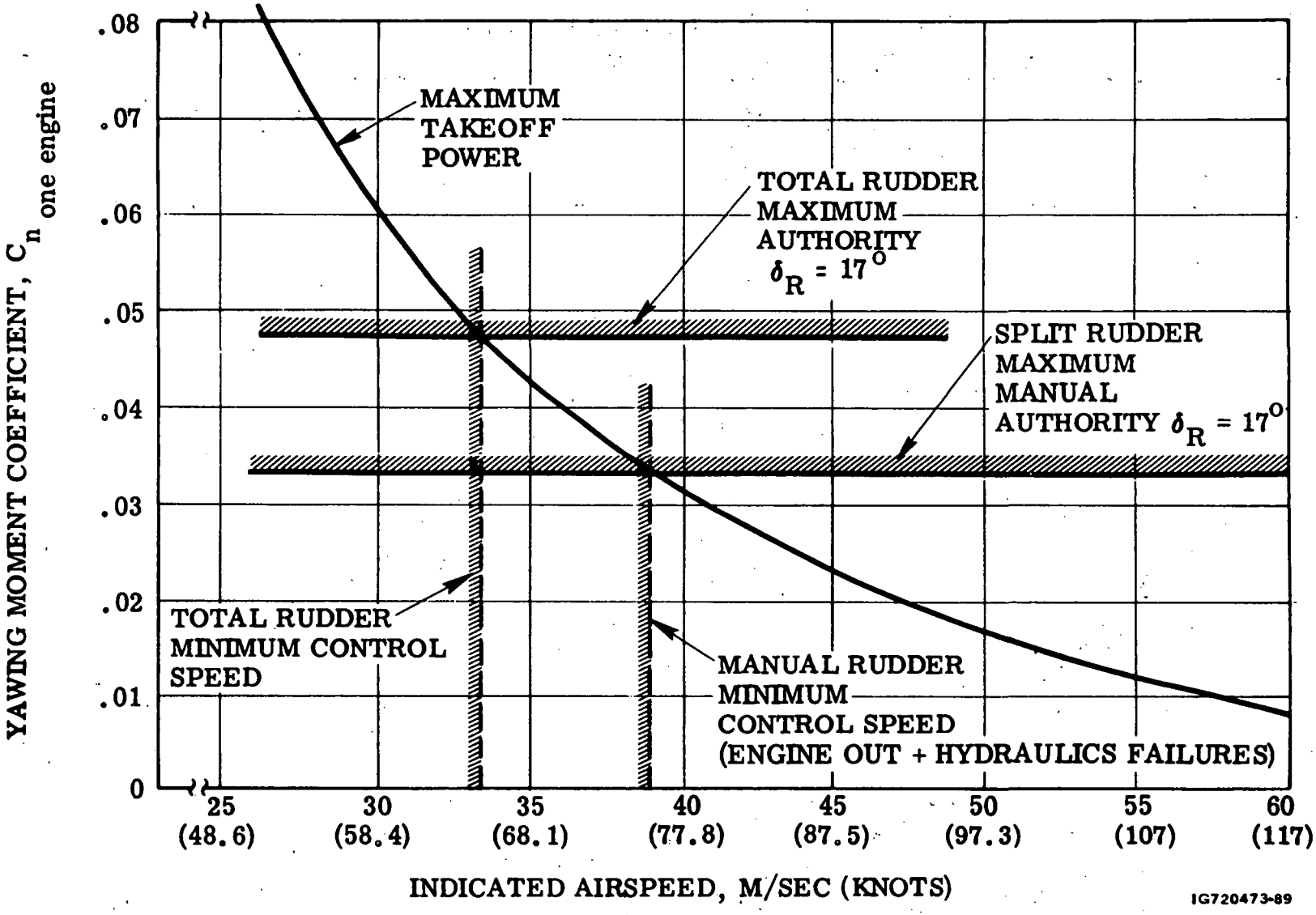

Figure 46: Minimum directional control speed - 10^o flap

8.0 CONCLUDING REMARKS

Results of the feasibility study indicate that an acceptable ride control system can be practically implemented on a DHC-6 Twin Otter with minimum airplane performance degradation. Vertical and lateral accelerations can be significantly reduced using split aileron and split rudder control surfaces. In addition, a split elevator may be required to provide adequate handling qualities. Further, spoiler control surfaces must be added if significant acceleration reductions are desired during landing approach conditions.

Primary data for the various design options are shown for direct comparison in Table VIII. Design goals for the vertical and lateral accelerations are 0.03 and 0.015 RMS g's respectively for a 7 fps RMS turbulence. Vertical acceleration varies with system complexity. The weight penalty is modest for all configurations and airplane range performance penalty is minimal.

During Phase II design a major effort should be made to use the full aileron span for both ride control and manual control. Increasing aileron authority would reduce the aileron actuator rate in direct proportion to the aileron area increase, and would provide sufficient direct lift control force to achieve the acceleration reduction goal at most flight conditions and stations.

Studies should be conducted during Phase II design to investigate reducing, or possibly eliminating the elevator segment. The feasibility study has shown that the elevator may not be required. Data also indicates that the area of the rudder ride control segment can be reduced.

The scope of this program did not include implementation trade studies. Further, design criteria have a strong impact on system complexity. Trade studies should be conducted to define the most practical combination of design turbulence conditions, airplane acceleration criteria, and ride control system implementation.

Although the ride control system was designed to endure failures of the powered segments, dual channel electronics were included in the preliminary design configuration to provide fail-soft capability. Trade studies of safety, system reliability, performance, and cost should be conducted during Phase II to define the most efficient implementation method.

TABLE VIII: RESULTS SUMMARY

OPTION	I	II	III	IV	V
DESCRIPTION	AILERON ELEVATOR RUDDER SPOILER	SAME AS I WITH α SENSOR	AILERON ELEVATOR RUDDER	AILERON ELEVATOR	AILERON
CG VERTICAL ACCEL. • CLIMB • CRUISE • LAND APP	 .031 .035 .055	 .041	 .031 .035 .076	 .031 .035 .076	 .044 .050 .077
CG LATERAL ACCEL. • CLIMB • CRUISE • LAND APP	←	.019 .027 .032	→	NO CHANGE	NO CHANGE
WEIGHT PENALTY NEWTONS (POUNDS)	1,029 (231)	1,094 (246)	835 (188)	695 (156)	530 (119)
PERFORMANCE PENALTY	← LESS THAN 0.5% ALL CONFIGURATIONS →				

IG720473-47B

APPENDIX A

PERFORMANCE POLARS

Figures 47 and 48 present performance polars for a flaps up and flaps down 40^{o} DHC-6 Twin Otter configuration. The data were obtained from an internal de Havilland Report Number 71-6. The longitudinal force coefficient, C_X, is given by

$$C_X = C_T - C_D \tag{7}$$

where the thrust coefficient, C_T, is normalized with respect to the freestream dynamic pressure and wing area.

Data for three flight conditions, cruise, climb and landing approach, are indicated on these polars. Note that at the landing condition the thrust coefficient is negative. During approach conditions negative thrust coefficients of the order -.1 to -.2 are encountered, due to the propeller pitch control drag being larger than thrust during these conditions.

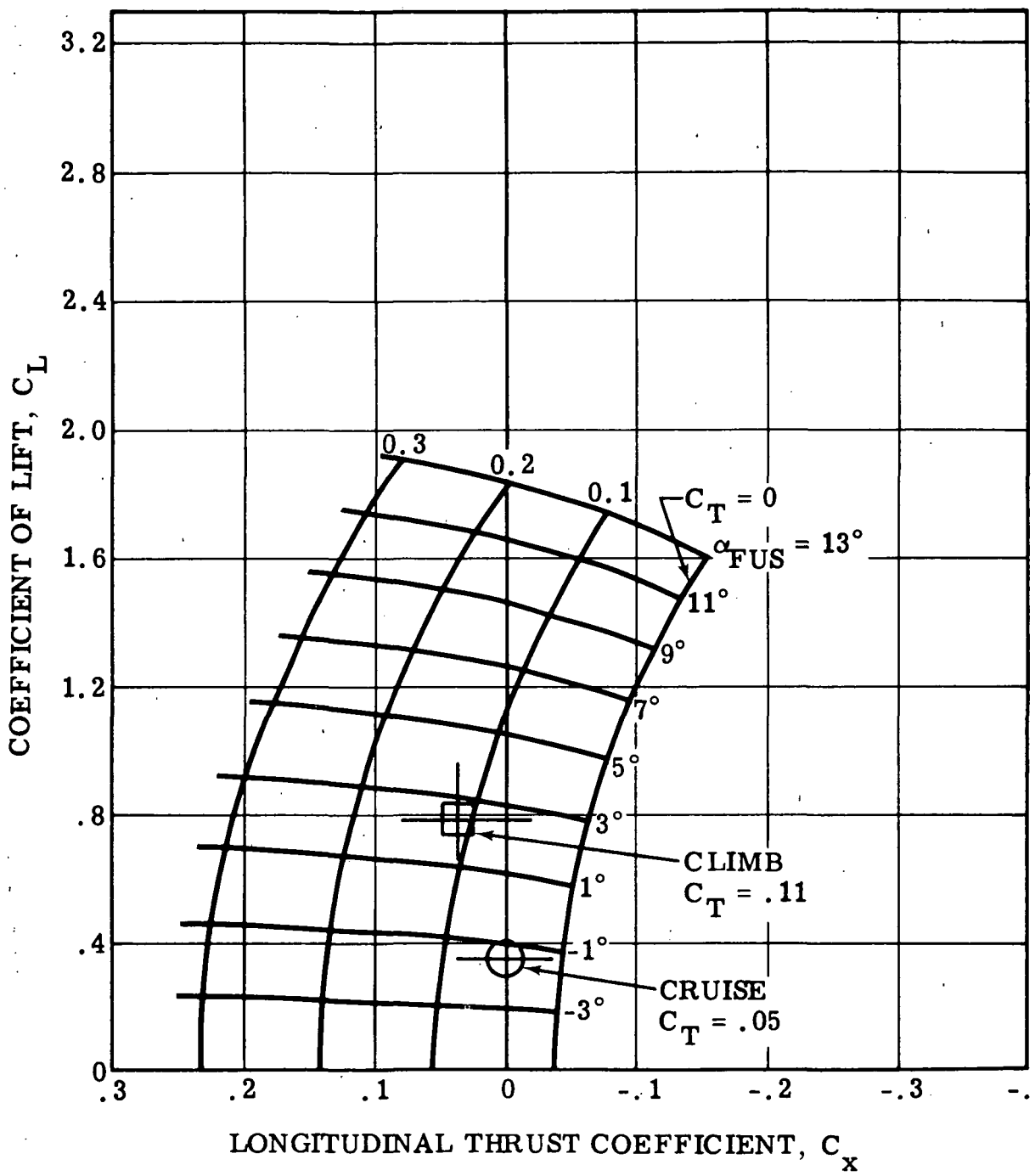

Figure 47: DHC-6 Twin Otter performance polars - 0° flaps

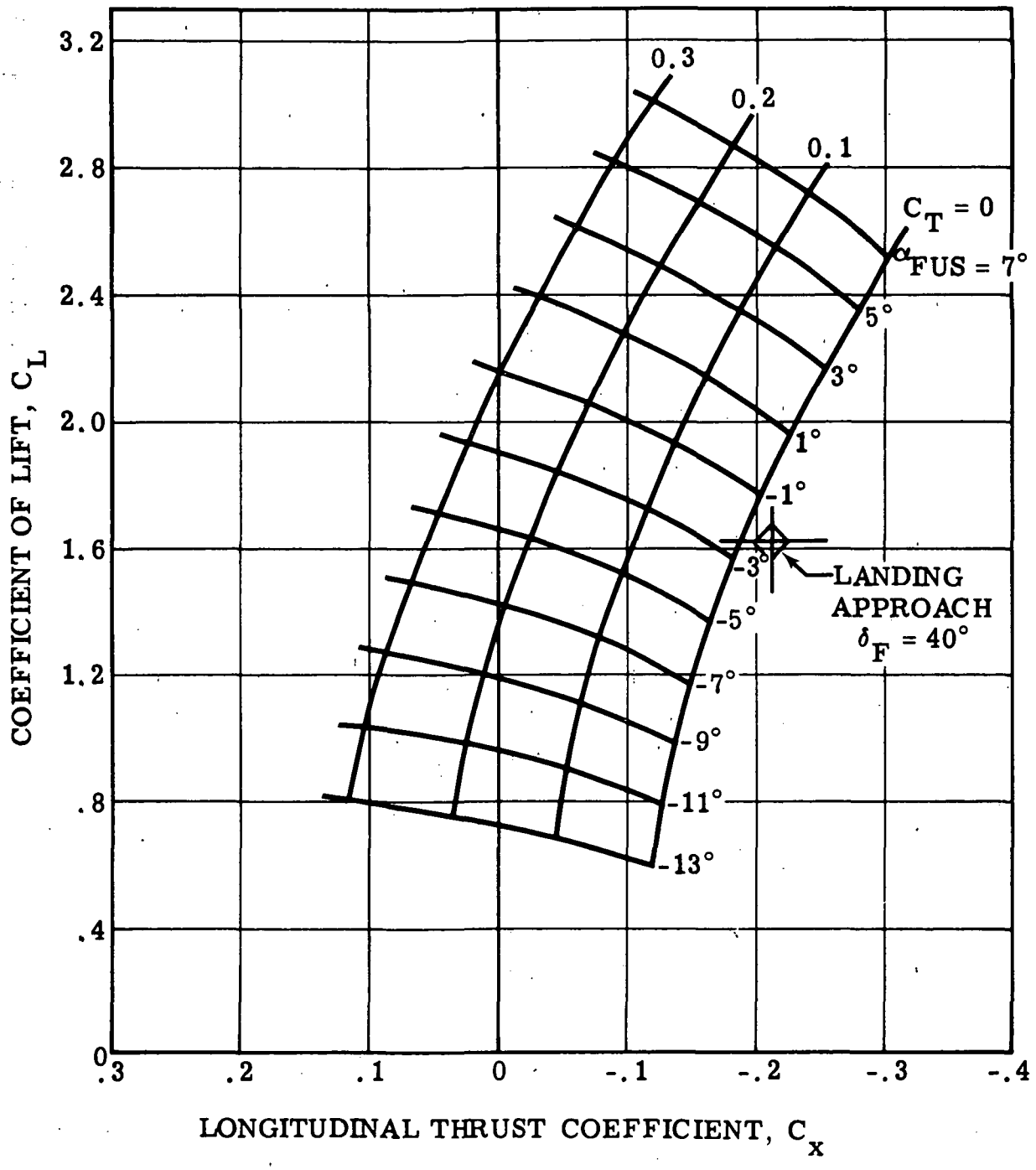

Figure 48: DHC-6 Twin Otter performance polar - 40° flaps

APPENDIX B

LONGITUDINAL EQUATIONS

The LaPlace transformed longitudinal equation are presented below in matrix form:

$$\begin{bmatrix} S + X_u & X_w & g \\ Z_u\,(1 + Z_{\dot{w}})\,S + Z_w & (Zq - U_o)S & \\ M_u & M_{\dot{w}} + M_w\,(S^2 + Mq)S & \end{bmatrix} \begin{bmatrix} u(S) \\ w(S) \\ \theta(S) \end{bmatrix} = \begin{bmatrix} X_{\delta_E} \\ Z_{\delta_E} \\ M_{\delta_E} \end{bmatrix} \delta_E(S) + \begin{bmatrix} X_{\delta_{S_P}} \\ Z_{\delta_{S_P}} \\ M_{\delta_{S_P}} \end{bmatrix} \delta_{S_P}(S) + \begin{bmatrix} X_{\delta_A} \\ Z_{\delta_A} \\ M_{\delta_A} \end{bmatrix} W(S) - \delta_A(S) + \begin{bmatrix} X_{w_g} \\ Z_{w_g} \\ M_{w_g} \end{bmatrix} \psi(S) Wg(S)$$

Definition of longitudinal equation coefficients:

$$W_w = -\frac{\bar{q}\bar{S}}{m}\left(C_{L_O} - C_{D_\alpha}\right)\left(\frac{1}{U_o}\right)$$

$$X_u = \frac{\bar{q}\bar{S}}{m}\left(\frac{2C_\alpha}{U_o} + \frac{C_{D_u}}{U_o}\right)$$

$$X_{\delta_E} = -\frac{\bar{q}\bar{S}}{m}\left(C_{D_{\delta_E}}\right)$$

$$X_{\delta_{S_P}} = -\frac{\bar{q}\bar{S}}{m}\left(C_{D_{\delta_{S_P}}}\right)$$

$$X_{\delta_A} = -\frac{\bar{q}\bar{S}}{m}\left(C_{D_{\delta_A}}\right)$$

$$X_{w_g} = X_w$$

$$Z_w = \frac{\bar{q}\bar{S}}{m}\left(C_{L_\alpha} + C_{D_O}\right)\left(\frac{1}{U_o}\right)$$

$$Z_{\dot{w}} = \frac{\bar{q}\bar{S}}{m}\left(\frac{\bar{c}}{2U_o} \cdot C_{L_{\dot{\alpha}}}\right)\left(\frac{1}{U_o}\right)$$

$$Z_u = \frac{\bar{q}\bar{S}}{m}\left(\frac{2C_{L_o}}{U_o} + \frac{C_{L_u}}{U_o}\right)$$

$$Z_q = -\frac{\bar{q}\bar{S}}{m}\left(\frac{\bar{c}}{2U_o} C_{L_q}\right)$$

$$Z_{\delta_E} = -\frac{\bar{q}\bar{S}}{m}\left(C_{L_{\delta_E}}\right)$$

$$Z_{\delta_{Sp}} = -\frac{\bar{q}\bar{S}}{m}\left(C_{L_{\delta_{Sp}}}\right)$$

$$Z_{\delta_A} = -\frac{\bar{q}\bar{S}}{m}\left(C_{L_{\delta_A}}\right)$$

$$Z_{w_g} = Z_w$$

$$M_w = -\frac{\bar{q}\bar{S}\bar{c}}{I_{yy}}\left(C_{M_\alpha}\right)\left(\frac{1}{U_o}\right)$$

$$M_{\dot{w}} = -\frac{\bar{q}\bar{S}\bar{c}}{I_{yy}}\left(\frac{\bar{c}}{2U_o} C_{M_{\dot{\alpha}}}\right)\left(\frac{1}{U_o}\right)$$

$$M_u = -\frac{\bar{q}\bar{S}\bar{c}}{I_{yy}}\left(\frac{C_{M_u}}{U_o}\right)$$

$$M_q = -\frac{\bar{q}\bar{S}\bar{c}}{I_{yy}}\left(\frac{\bar{c}}{2U_o} C_{M_q}\right)$$

$$M_{\delta_E} = \frac{\bar{q}\bar{S}\bar{c}}{I_{yy}}\left(C_{M_{\delta_E}}\right)$$

$$M_{\delta_{Sp}} = \frac{\bar{q}\bar{S}\bar{c}}{I_{yy}}\left(C_{M_{\delta_{Sp}}}\right)$$

$$M_{\delta_A} = \frac{\bar{q}\bar{S}\bar{c}}{I_{yy}}\left(C_{M_{\delta_A}}\right)$$

$$M_{w_g} = M_w$$

APPENDIX B

Definition of stability derivatives, longitudinal equations:

$$C_{L_o} = \frac{w}{\bar{q}\bar{S}}$$

$$C_{D_\alpha} = \frac{\partial C_D}{\partial \alpha}$$

$$C_{D_o} = \frac{D}{qS}$$

$$C_{D_u} = u_o \frac{\partial C_D}{\partial u}$$

$$C_{D_{\delta_E}} = \frac{\partial C_D}{\partial \delta_E}$$

$$C_{D_{\delta_{S_P}}} = \frac{\partial C_D}{\partial \delta_{S_P}}$$

$$C_{D_{\delta_A}} = \frac{\partial C_D}{\partial \delta_A}$$

$$C_{L_\alpha} = \frac{\partial C_L}{\partial \alpha}$$

$$C_{L_{\dot{\alpha}}} = \frac{\partial C_L}{\partial \left(\frac{\dot{\alpha}\,\bar{c}}{2U_o}\right)}$$

$$C_{L_u} = \frac{u_o \partial C_L}{\partial u}$$

$$C_{L_q} = \frac{\partial C_L}{\partial \left(\frac{q\bar{c}}{2U_o}\right)}$$

$$C_{L_{\delta_E}} = \frac{\partial C_L}{\partial \delta_E}$$

$$C_{L_{\delta_{S_P}}} = \frac{\partial C_L}{\partial \delta_{S_P}}$$

$$C_{L_{\delta_A}} = \frac{\partial C_L}{\partial \delta_A}$$

$$C_{M_\alpha} = \frac{\partial C_M}{\partial \alpha}$$

$$C_{M_{\dot{\alpha}}} = \frac{\partial C_M}{\partial \left(\frac{\dot{\alpha}\,\bar{c}}{2U_o}\right)}$$

$$C_{M_u} = \frac{u_o \partial C_M}{\partial u}$$

$$C_{M_q} = \frac{\partial C_M}{\partial \left(\frac{q\bar{c}}{2U_o}\right)}$$

$$C_{M_{\delta_E}} = \frac{\partial C_M}{\partial \delta_E}$$

$$C_{M_{\delta_{S_P}}} = \frac{\partial C_M}{\partial \delta_{S_P}}$$

$$C_{M_{\delta_A}} = \frac{\partial C_M}{\partial \delta_A}$$

Page Intentionally Left Blank

APPENDIX C

LATERAL-DIRECTIONAL EQUATIONS

The LaPlace transformed lateral-directional equations are presented below in matrix form:

$$\begin{bmatrix} S + Y_v & SY_p - g & (Y_r + U_o)S \\ L_v & S^2 + L_pS & -\frac{I_{xz}}{I_{xx}} S^2 + L_rS \\ N_v & -\frac{I_{xz}}{I_{zz}} S^2 + N_pS & S^2 + N_rS \end{bmatrix} \begin{bmatrix} v(S) \\ \phi(S) \\ \psi(S) \end{bmatrix} = \begin{bmatrix} Y_{\delta_R} \\ L_{\delta_R} \\ N_{\delta_R} \end{bmatrix} \delta_R + \begin{bmatrix} Y_{v_g} \\ L_{v_g} \\ N_{v_g} \end{bmatrix} \psi'(S) \cdot v_g(S)$$

Definition of lateral-directional equation coefficients:

$$Y_v = -\frac{\bar{q}\bar{S}}{m}\left(C_{Y_\beta}\right)\left(\frac{1}{U_o}\right)$$

$$Y_p = -\frac{\bar{q}\bar{S}}{m}\left(\frac{b}{2U_o} C_{Y_p}\right)$$

$$Y_r = -\frac{\bar{q}\bar{S}}{m}\left(\frac{b}{2U_o} C_{Y_r}\right)$$

$$Y_{\delta_R} = \frac{\bar{q}\bar{S}}{m}\left(C_{Y_{\delta_R}}\right)$$

$$Y_{v_g} = Y_v$$

$$L_v = -\frac{\bar{q}\bar{S}b}{I_{xx}}\left(C_{\ell_\beta}\right)\left(\frac{1}{U_o}\right)$$

$$L_p = -\frac{\bar{q}\bar{S}b}{I_{xx}}\left(\frac{b}{2U_o} C_{\ell_p}\right)$$

$$L_r = -\frac{\bar{q}\bar{S}b}{I_{xx}}\left(\frac{b}{2U_o} C_{\ell_r}\right)$$

$$L_{\delta_R} = \frac{\bar{q}\bar{S}b}{I_{xx}}\left(C_{\ell_{\delta_R}}\right)$$

$$L_{v_g} = L_v$$

$$N_v = -\frac{\bar{q}\bar{S}b}{I_{zz}}\left(C_{N_\beta}\right)\left(\frac{1}{2U_o}\right)$$

$$N_p = -\frac{\bar{q}\bar{S}b}{I_{zz}}\left(\frac{b}{2U_o} C_{N_p}\right)$$

$$N_r = \frac{\bar{q}\bar{S}b}{I_{zz}}\left(\frac{b}{2U_o} C_{N_r}\right)$$

$$N_{\delta_R} = \frac{\bar{q}\bar{S}b}{I_{zz}}\left(C_{N_{\delta_R}}\right)$$

$$N_{v_g} = N_v$$

APPENDIX C

Definition of stability derivatives, lateral-directional equations:

$$C_{Y_\beta} = \frac{\partial C_Y}{\partial \beta}$$

$$C_{Y_p} = \frac{\partial C_Y}{\partial \left(\frac{Pb}{2U_o}\right)}$$

$$C_{Y_r} = \frac{\partial C_Y}{\partial \left(\frac{rb}{2U_o}\right)}$$

$$C_{Y_{\delta_R}} = \frac{\partial C_Y}{\partial \delta_R}$$

$$C_{N_\beta} = \frac{\partial C_N}{\beta}$$

$$C_{N_p} = \frac{\partial C_N}{\partial \left(\frac{Pb}{2U_o}\right)}$$

$$C_{N_r} = \frac{\partial C_N}{\partial \left(\frac{rb}{2U_o}\right)}$$

$$C_{N_{\delta_R}} = \frac{\partial C_N}{\partial \delta_R}$$

$$C_{\ell_\beta} = \frac{\partial C_\ell}{\partial \beta}$$

$$C_{\ell_p} = \frac{\partial C_\ell}{\partial \left(\frac{Pb}{2U_o}\right)}$$

$$C_{\ell_r} = \frac{\partial C_\ell}{\partial \left(\frac{rb}{2U_o}\right)}$$

$$C_{\ell_{\delta_R}} = \frac{\partial C_\ell}{\partial \delta_R}$$

APPENDIX D

STABILITY AND CONTROL DERIVATIVES

Longitudinal and lateral-directional stability and primary control derivatives were estabished for the cruise, climb and landing flight conditions. The derivatives were obtained from an internal de Havilland Report Number 71-6. The data were presented as a function of angle of attack, thrust coefficient and flap position. Airplane stability derivatives are tabulated in Table IX, and control surface derivatives are listed for both manual and powered surfaces in Table X.

APPENDIX D

TABLE IX
AIRPLANE STABILITY DERIVATIVES

Derivative		Flight Condition		
		Cruise	Climb	Landing
C_{L_o} ,	nondim.	.35	.788	1.61
C_{D_o} ,	nondim.	.047	.076	.191
C_{D_α} ,	/rad.	.16	.435	1.20
C_{D_u} ,	nondim.	.139	.228	.57
C_{L_α} ,	/rad.	5.9	6.13	5.62
$C_{L_{\dot{\alpha}}}$,	/rad.	1.72	1.93	1.64
C_{L_u} ,	nondim.	0	0	0
C_{L_q} ,	/rad.	5.50	5.50	5.50
C_{M_α} ,	/rad.	-1.16	-1.61	-1.34
$C_{M_{\dot{\alpha}}}$,	/rad.	-6.62	-7.45	-6.49
C_{M_u} ,	nondim.	0	0	0
C_{M_q} ,	/rad.	-22.75	-22.75	-22.75
C_{Y_β} ,	/rad.	-.85	-.87	-1.03
C_{Y_p} ,	/rad.	-.10	-.10	-.10
C_{Y_r} ,	/rad.	.50	.50	.50
C_{ℓ_β} ,	/rad.	-.12	-.11	-.07
C_{ℓ_p} ,	/rad.	.55	-.55	-.55
C_{ℓ_r} ,	/rad.	.13	.185	.446
C_{N_β} ,	/rad.	.122	.124	.140
C_{N_p} ,	/rad.	.007	-.006	-.002
C_{N_r} ,	/rad.	-.185	.19	-.21

APPENDIX D

TABLE X

CONTROL SURFACE DERIVATIVES

Derivative		Flight Condition		
		Cruise	Climb	Landing
$C_{L_{\delta_E}}$ (RCS),	/rad.	.063	.0688	.063
$C_{L_{\delta_E}}$ (Man),	/rad.	.401	.435	.39
$C_{L_{\delta_A}}$ (RCS)	/rad.	.464	.464	.241
$C_{L_{\delta_{sp}}}$,	/rad.	—	—	-.974
$C_{M_{\delta_E}}$ (RCS)	/rad.	-.246	-.269	-.241
$C_{M_{\delta_E}}$ (Man)	/rad.	-1.587	-1.73	-1.53
$C_{M_{\delta_A}}$ (RCS),	/rad.	-.074	-.074	-.0367
$C_{M_{\delta_{sp}}}$,	/rad.	—	—	.0106
$C_{Y_{\delta_R}}$ (RCS)	/rad.	.117	.117	.117
$C_{Y_{\delta_R}}$ (Man),	/rad.	.273	.273	.273
$C_{N_{\delta_R}}$ (RCS),	/rad.	-.047	-.407	-.047
$C_{N_{\delta_R}}$ (Man),	/rad.	-.105	-.105	-.105
$C_{l_{\delta_R}}$ (RCS)	/rad.	.017	.014	.017
$C_{l_{\delta_R}}$ (Man),	/rad.	.023	.015	.025
$C_{l_{\delta_A}}$ (RCS),	/rad.	.086	.086	.083
$C_{l_{\delta_A}}$ (Man),	/rad.	.12	.12	.117

APPENDIX E

AIRPLANE INERTIA AND GEOMETRY

Airplane dimensional and inertial properties used in the equations of motion are listed in Table XI below. All other data required is listed in, or can be derived from Table I.

TABLE XI
DHC-6 DIMENSIONAL AND INERTIAL PROPERTIES

Airplane Property	Flight Conditions		
	Cruise	Climb	Landing
I_{xx}, kg – m^2 (slug – ft^2)	22 370 (16 500)	22 370 (16 500)	22 370 (16 500)
I_{yy}, kg – m^2 (slug – ft^2)	36 060 (26 600)	36 060 (26 600)	36 060 (26 600)
I_{zz}, kg – m^2 (slug – ft^2)	53 960 (39 800)	53 960 (39 800)	53 960 (39 800)
I_{xz}, kg – m^2 (slug – ft^2)	1630 (1200)	1630 (1200)	1630 (1200)
$\bar{s}$, m^2 (ft^2)	39 (420)	39 (420)	39 (420)
b, m (ft)	19.8 (65)	19.8 (65)	19.8 (65)
$\bar{c}$,m m (ft)	1.98 (6.5)	1.98 (6.5)	1.98 (6.5)

APPENDIX F

SIGN CONVENTIONS

Sign conventions for forces, moments, angular rates, and linear velocities are shown in the sketch below. The positive sense of each variable is shown.

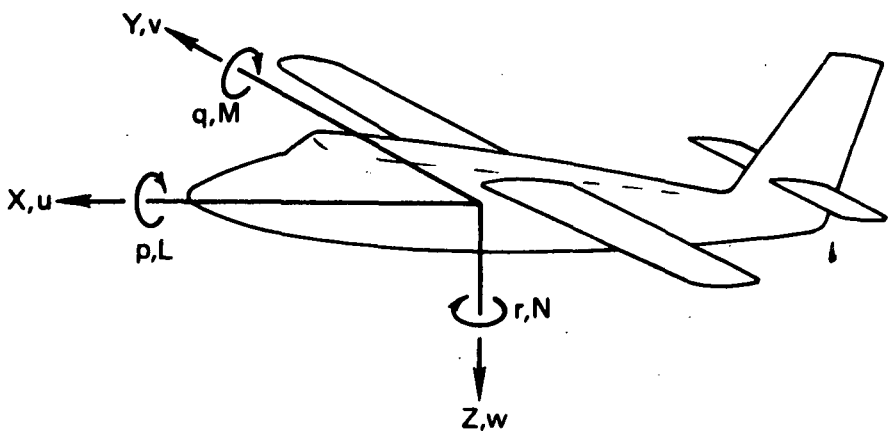

Sign conventions for control deflections are listed below:

Control Surface	Positive Deflection
Elevators	trailing edge down
Ailerons (symmetrical)	trailing edge down
Spoilers (symmetrical)	trailing edge up
Rudder	trailing edge left

REFERENCES

1. Hunsaker, J. C. and Wilson, E. B., "Report on Behavior of Aeroplanes in Gust Turbulence," NACA TR-1 (MIT), dated October 1915.

2. Phillips, W. H., Kraft, Christopher C., "Theoretical Study of Some Methods for increasing the Smoothness of Flight Through Rough Air," NACA TN-2416, dated July 1951.

3. NASA TN-4332, "An Approach to the Problem of Esimating Severe and Repeated Gust Loads for Missile Operations," September 1958.

4. ASD-TR-61-235, "Optimum Fatigue Spectra," April 1962.

5. MIL-A-8861A(USAF), "Airplane Strength and Rigidity, Flight Loads," March 1971.

6. NASA TM-X-2620, "Symposium on Vehicle Ride Quality," October 1972, pages 107, 108, 113, 193.

7. MIL-F-8785B, "Flying Qualities of Piloted Airplanes," August 1969.

8. BuAer Flight Controls Systems Manual, Volume II, "Dynamics of the Airframe," September 1952.

9. Fung, Y. C., "The Theory of Aeroelasticity", John Wiley and Sons, Inc., 1955.

10. Bisplinghoff, R. L., Ashley, H., and Halfman, R. L., "Aeroelasticity," Addison-Wesley Publishing Co., 1957.

11. Foster, D. N., "Flow Around Wing Sections with High-Lift Devices," Journal of Aircraft, Vol. 9, No. 3, March 1972.

12. Barnes, C. S., "A Developed Theory of Spoilers on Airfoils," Aeronautical Research Council, C. P. No. 887, 1966.

13. Fischel, J., and Ivey, M. F., "Collection of Test Data for Lateral Control with Full-Span Flaps," NACA TN-1404, 1948.

*U.S. GOVERNMENT PRINTING OFFICE: 1973-739-029/60

"The aeronautical and space activities of the United States shall be conducted so as to contribute . . . to the expansion of human knowledge of phenomena in the atmosphere and space. The Administration shall provide for the widest practicable and appropriate dissemination of information concerning its activities and the results thereof."

—NATIONAL AERONAUTICS AND SPACE ACT OF 1958

NASA SCIENTIFIC AND TECHNICAL PUBLICATIONS

TECHNICAL REPORTS: Scientific and technical information considered important, complete, and a lasting contribution to existing knowledge.

TECHNICAL NOTES: Information less broad in scope but nevertheless of importance as a contribution to existing knowledge.

TECHNICAL MEMORANDUMS: Information receiving limited distribution because of preliminary data, security classification, or other reasons. Also includes conference proceedings with either limited or unlimited distribution.

CONTRACTOR REPORTS: Scientific and technical information generated under a NASA contract or grant and considered an important contribution to existing knowledge.

TECHNICAL TRANSLATIONS: Information published in a foreign language considered to merit NASA distribution in English.

SPECIAL PUBLICATIONS: Information derived from or of value to NASA activities. Publications include final reports of major projects, monographs, data compilations, handbooks, sourcebooks, and special bibliographies.

TECHNOLOGY UTILIZATION PUBLICATIONS: Information on technology used by NASA that may be of particular interest in commercial and other non-aerospace applications. Publications include Tech Briefs, Technology Utilization Reports and Technology Surveys.

Details on the availability of these publications may be obtained from:

SCIENTIFIC AND TECHNICAL INFORMATION OFFICE

NATIONAL AERONAUTICS AND SPACE ADMINISTRATION

Washington, D.C. 20546